

UNIVERSITÄTSKLINIKUM HAMBURG-EPPENDORF

Zentrum für Experimentelle Medizin, Institut für Experimentelle Pharmakologie und
Toxikologie

Direktor: Professor T. Eschenhagen

Thrombus-Targeted Theranostic Microbubbles for Simultaneous Ultrasound Diagnosis and Therapy of Thrombosis.

Dissertation

zur Erlangung des Grades eines Doktors der Medizin
an der Medizinischen Fakultät der Universität Hamburg.

vorgelegt von:

Yannik Andreas Gkanatsas
aus Bremen

Hamburg 2017

**Angenommen von der
Medizinischen Fakultät der Universität Hamburg am: 13.12.2017**

**Veröffentlicht mit Genehmigung der
Medizinischen Fakultät der Universität Hamburg.**

Prüfungsausschuss, der Vorsitzende: Prof. Dr. Thomas Eschenhagen

Prüfungsausschuss, zweite Gutachterin: Prof. Dr. Renate Bonin-Schnabel

Prüfungsausschuss, dritter Gutachter: PD Dr. Florian Langer

Table of contents

Title page.....	1
Table of contents.....	3
List of Figures:.....	6
List of Tables:.....	7
Chapter 1. Introduction.....	8
1.1 Cardiovascular Disease (CVD).....	8
1.1.1 <i>Epidemiology and Importance of CVD</i>	8
1.1.2 <i>Atherosclerosis</i>	8
1.1.3 <i>The role of platelets in atherosclerosis and atherothrombosis</i>	9
1.2 Haemostatic System.....	10
1.2.1 <i>Platelets</i>	10
1.2.2 <i>Coagulation cascade</i>	13
1.2.3 <i>Fibrinolysis and thrombolytic therapy</i>	15
1.3 Antibodies.....	18
1.3.1 <i>Single chain antibodies</i>	18
1.4 Ultrasound.....	20
1.4.1 <i>Basic physics</i>	20
1.4.2 <i>Ultrasound contrast agents – Microbubbles (MB)</i>	21
1.4.3 <i>Clinical indications for the use of MBs</i>	23
1.5 Molecular ultrasound imaging:.....	24
1.5.1 <i>Molecular ultrasound imaging in cancer</i>	25
1.5.2 <i>Molecular ultrasound imaging in inflammation and thrombosis</i>	25
1.6 Theranostics:.....	27
Chapter 2. Material and Methods.....	29
2.1 Material.....	29
2.1.1 <i>List of chemicals</i>	29
2.1.2 <i>List of equipment</i>	30
2.1.3 <i>List of software</i>	32
2.1.4 <i>List of enzymes and reaction kits</i>	33
2.1.5 <i>Buffers and media</i>	34
2.1.6 <i>Primers and plasmids</i>	37
2.1.7 <i>Antibodies</i>	38
2.3 Molecular biology methods.....	39
2.3.1 <i>DNA Isolation</i>	39
2.3.2 <i>Separation of DNA by agarose gel electrophoresis</i>	39
2.3.3 <i>Nano Drop® – Concentration and Purity of DNA</i>	40
2.3.4 <i>Preparation of competent cells</i>	40
2.3.5 <i>Amplification of DNA</i>	40
2.3.6 <i>Vectors</i>	41
2.3.7 <i>Restriction enzyme digest</i>	42
2.3.8 <i>Ligation</i>	42
2.3.9 <i>DNA introduction into cells</i>	43
2.3.10 <i>Screening for positive clones after transformation</i>	43
2.3.11 <i>DNA sequencing</i>	44
2.4 Protein chemical methods:.....	44

2.4.1 Protein expression and production in <i>E. coli</i> strains.....	44
2.4.2 Production of proteins in mammalian cells: Human embryonic kidney (HEK) cells 293F	45
2.4.3 Small scale purification (SCP) of proteins	46
2.4.4 Large scale purification of proteins.....	46
2.4.5 Dialysis of protein samples.....	47
2.4.6 Bicinchoninic Acid (BCA) Protein assay.....	47
2.4.7 Analysis of protein samples using sodium dodecyl sulfate polyacrylamide gel electrophoresis (SDS-PAGE)	47
2.4.8 Analysis of protein samples with Coomassie brilliant blue G250 staining	49
2.4.9 Analysis of protein using western blotting	49
2.4.10 Immunoreactions	50
2.4.11 Sortase-A reaction.....	50
2.4.12 Negative purification after Sortase A reaction	50
2.5 Blood collection	51
2.5.1 Generation of platelet rich plasma (PRP).....	51
2.6 Flow cytometry	51
2.6.1 Parameters for analysis in flow cytometry.....	51
2.6.2 Gating of cells on flow cytometry.....	52
2.6.3 Data analysis with histograms on flow cytometry.....	52
2.6.4 Flow cytometry of platelets with scFv _{anti-LIBS}	52
2.7 Conjugation of proteins to microbubbles	53
2.7.1 Conjugation of biotinylated scFv-AviTag and biotinylated scuPa construct to commercial streptavidin coated lipid microbubbles via biotin-streptavidin coupling.....	53
2.7.2 Calculations of protein need for conjugation	54
2.8 In vitro assays	55
2.8.1 Urokinase activity assay with 2444X substrate	55
2.8.2 Urokinase activity assay with S2251 substrate	55
2.8.3 Fibrinolysis assay	55
2.8.4 Flow chamber adhesion assay.....	56
2.9 Ultrasound	57
2.9.1 VisualSonics Vevo2100 – high frequency scanner for small animals	57
2.9.2 Imaging of the carotid artery with Vevo 2100	58
2.10 In vivo animal models.....	58
2.10.1 Femoral vein catheterisation	58
2.10.2 Ultrasound imaging of thrombolysis using the ferric chloride injury model.....	58
2.10.3 Assessment of bleeding time.....	59
2.11 Statistical analysis	59
2.11.1 S2251 assay:.....	59
2.11.2 Flow cytometry:	60
2.11.3 In vivo thrombolysis:.....	60
2.11.4 In vivo bleeding time:.....	60
Chapter 3. Results	61
3.1 In vitro analysis of scFv _{anti-LIBS} :.....	61
3.1.1 Production and purification	61
3.1.2 Evaluation of functionality by FACS-assay.....	62
3.2 In vitro analysis of scuPA constructs:.....	66
3.2.1 Production and purification of scuPA (with LPETG tag) and biotinylated scuPA	66

3.2.2 Evaluation of functionality with S2251 substrate assay.....	68
3.2.3 Evaluation of fibrinolysis in microthrombi	70
3.3 Testing of targeted theranostic microbubbles in vitro and in vivo:.....	71
3.3.1 Evaluation of adhesion in flow chamber	71
3.3.2 Molecular ultrasound imaging of thrombolysis	72
3.3.3 Assessment of bleeding time.....	73
Chapter 4. Discussion.....	74
4.1 Limitations	77
Chapter 5. Summary	78
5.1 Zusammenfassung.....	80
Chapter 6. List of abbreviations.....	82
Chapter 7. Bibliography	85
Chapter 8. Acknowledgment	96
Chapter 9. Curriculum vitae	97
Chapter 10. Eidesstattliche Erklärung.....	99
Chapter 11. Supplements	100
A. List of publications	100
B. Thrombus-Targeted Theranostic Microbubbles: A New Technology towards Concurrent Rapid Ultrasound Diagnosis and Bleeding-free Fibrinolytic Treatment of Thrombosis	101

List of Figures:

Figure 1-1: Global death ranks..... 8

Figure 1-2: Fibrinogen binding to GPIIb/IIIa on platelet membrane. 12

Figure 1-3: The fibrinolytic system. 15

Figure 1-4: MB response to the ultrasound wave..... 21

Figure 2-1: Vevo 2100 – high frequency scanner for small animals. 57

Figure 3-1: Successful production and purification of scFv_{anti-LIBS}. 61

Figure 3-2: Binding of scFv_{anti-LIBS} to activated platelets. 62

Figure 3-3: Binding of scFv_{anti-LIBS} to activated platelets. 63

Figure 3-4: Proving platelet activation with PAC-1. 64

Figure 3-5: Histograms demonstrating binding of scFv_{anti-LIBS}. 65

Figure 3-6: Vector map and gene work of scuPA as well as indication of successful biotinylation. 67

Figure 3-7: Assessment of amidolytic activity of the scuPA/biotinylated scuPA in light transmission assay (96 well plate). 69

Figure 3-8: Fibrinolysis assay in a 96-well plate demonstrating successful thrombolysis with biotinylated scuPA. 70

Figure 3-9: TT-MB adhesion to platelet aggregate..... 71

Figure 3-10: In vivo thrombolysis under ultrasound control..... 72

Figure 3-11: Assessment of bleeding risk of TT-MBs. 73

List of Tables:

Table 1-1: Summary of important platelet agonists.....	11
Table 1-2: Different forms of urokinase plasminogen activators (uPA).....	17
Table 1-3: Indications of MBs in different organ systems.....	24
Table 2-1: List of chemicals used in this thesis.	29
Table 2-2: Equipement used in this thesis.	30
Table 2-3: Reaction kits and enzymes used for this thesis.	33
Table 2-4: The THY media for E.coli protein production with the Avi-tag.....	34
Table 2-5: Buffers used in the thesis.....	35
Table 2-6: Forward and reverse Primers that were used for this thesis.....	37
Table 2-7: Plasmid-construct that were used in this thesis.	37
Table 2-8: Antibodies that were used for this thesis.....	38
Table 2-9: Example for PCR reaction mix with the GoTaq® polymerase.	41
Table 2-10: Example for PCR protocol.....	41
Table 2-11: 4% stacking gel reaction mix.....	48
Table 2-12: 12% SDS Gel reaction mix.....	49
Table 6-1: List of abbreviations.	82

Chapter 1. Introduction

1.1 Cardiovascular Disease (CVD)

1.1.1 Epidemiology and Importance of CVD

Acute events in the circulatory system caused by thrombosis, such as myocardial infarction and stroke, remain the leading causes of death and disability in the western world (Go et al., 2014) (see figure 1-1). 12.9 million people died from ischaemic heart disease and stroke alone in 2010. That stands for one in four deaths worldwide. Years of life lost to premature mortality increased by 17-28%, according to data of ischaemic heart disease and stroke from 1990 to 2010. To put these values into perspective, heart and circulatory diseases killed more people in 2010 than communicable (infectious), maternal, neonatal and nutritional disorders combined, and almost double the number from cancer. The underlying pathophysiology for these CVDs is atherosclerosis.

1990		2010		
Mean rank (95% UI)	Disorder	Disorder	Mean rank (95% UI)	% change (95% UI)
1.0 (1 to 2)	1 Ischaemic heart disease	1 Ischaemic heart disease	1.0 (1 to 1)	35 (29 to 39)
2.0 (1 to 2)	2 Stroke	2 Stroke	2.0 (2 to 2)	26 (14 to 32)
3.0 (3 to 4)	3 Lower respiratory infections	3 COPD	3.4 (3 to 4)	-7 (-12 to 0)
4.0 (3 to 4)	4 COPD	4 Lower respiratory infections	3.6 (3 to 4)	-18 (-24 to -11)

Figure 1-1: Global death ranks.

Global death ranks with 95% UIs for the top 4 causes in 1990 and 2010, and the percentage change with 95% UIs between 1990 and 2010. Uncertainty interval (UI), chronic obstructive pulmonary disease (COPD). Adapted from Go et al., 2014.

1.1.2 Atherosclerosis

Atherosclerosis is the chronic inflammation of the arteries or, more precisely, the vascular subintima. It is an advancing disease, initially characterised by the accumulation of cholesterol derivatives and oxidised fatty acid-engorged macrophages, followed by necrotic lipid filled areas (e.g. remnants of dead macrophages) and a progressively increasing number of smooth muscle cells. A fibrous cap, mainly composed of extracellular matrix components, forms the boundary between the plaque and the lumen. Very good reviews have been published on this subject (Libby, 2002), (Weber and Noels, 2011), (Hansson and Libby, 2006). Platelets play a role in this inflammatory process; it is, of course, mainly their adherence and aggregation which leads to vessel occlusion upon plaque rupture.

1.1.3 The role of platelets in atherosclerosis and atherothrombosis

It is known that platelets secrete proinflammatory cytokines for many hours after their entrapment in a fibrin network (Lindemann et al., 2001). *In vitro* studies also show that platelets maintain their secretory capabilities after disaggregation (Owen et al., 1995). The platelets contain a number of inflammatory mediators which play a role in atherosclerotic lesion and the subsequent atherothrombosis, varying from CD40L, interleukin 1 β , RANTES to growth factors like Platelet derived factor 4 (PF-4). PF-4, operates as a leukocyte attractant and enhances the binding of oxidised LDLs (oxLDL) to endothelial cells (Nassar et al., 2003). RANTES activates, via an intracellular cascade, a genetic pathway in monocytes, which in turn produces inflammatory cytokines like interleukin 8 (IL-8) or Tumour necrosis factor α (TNF α) (Weyrich et al., 1995).

It has become apparent that platelet contribution to inflammation is mediated through their interaction with leukocytes. The reintroduction of platelets to a neutrophil solution stimulates, for example, the oxidant production of neutrophils (Del Maschio et al., 1989). On the other hand, activated neutrophils result in increased agonist sensibility in platelets (Del Maschio et al., 1990). These interactions and modulation mechanisms rely on several factors, namely, the release of soluble mediators and their subsequent metabolism, the presentation of surface bound mediators and direct cell adhesion (Bhatt 2008). The exposure of P-selectin on adherent platelets enables, for example, leukocyte rolling and finally diapedesis in atherosclerotic lesions (McEver, 2001).

Huo et al. and Massberg et al. published important original articles concerning the role of platelets in atherosclerosis in early 2000 editions of *Nature* and the *Journal of Experimental Medicine* (Huo et al., 2003), (Massberg et al., 2002). Hue et al. showed with epifluorescent intravital microscopy and electron microscopy that perfusion of an atherosclerotic carotid artery with activated platelets prior to leukocyte perfusion substantially increased leukocyte interaction to the lesion. Injection of platelets to increase the circulating amount of platelets by two or three fold even lead to a 39% gain of the lesions in comparison to the controls, suggesting an exacerbation of atherosclerosis due to higher amounts of activated, circulating platelets. Not only the exacerbation, but the initiation of the atherosclerotic lesion is critically influenced by platelets, according to Massberg et al. In 10 week old Apo E deficient mice without any visible atherosclerotic lesions, transient and firm platelet adhesions on areas of subsequent atherosclerotic lesions were increased 12- and 24-fold, as compared with

wild type mice. At this time point, leukocyte adhesion was not elevated in APO E deficient mice in comparison with wild type mice. In subsequent experiments, the inhibition of glycoprotein 1 α (GP1 α) on platelets, mediating adhesion without endothelial cell denudation under high shear rates, caused a significant reduction in cross-sectional carotid plaque area (by 81%, 18 week old mice).

To conclude, platelets contribute to atherosclerosis and do so mainly through leucocyte interactions. They also play an undeniable role in acute events, like atherothrombosis, where the exposure of tissue factor and lipid deposits under a ruptured fibrinous plaque lead to platelet activation and haemostasis.

1.2 Haemostatic System

The elaborate balance between activation, in- and hyperactivation in this difficult system is fascinating. An array of different factors play an important role, namely platelets, coagulation factors and fibrinolytic proteins. The commonly accepted stages describing the haemostatic system comprise, firstly, of an initial vasoconstriction that limits blood flow over the injured endothelium. Secondly, a loose platelet plug forms over the site of injury (mainly collagen binding) and the coagulation cascade is activated through the exposure of tissue factor on the collection of negatively charged surfaces, specifically from platelets. Conversion from fibrinogen to fibrin is the last step of the common pathway of the coagulation, leading to platelet stabilisation. The white clot is formed, which is renamed as the red clot when erythrocytes get entangled in the 'mesh'. The fourth step implies the reconstitution of normal blood flow following tissue damage repair. Plasmin, as the fibrinolytic agent, must be added in this context. The important cell derived response in haemostasis is mediated through Platelet aggregation.

1.2.1 Platelets

Adhesion and platelet aggregation

Upon exposure to the subendothelial matrix, platelets mainly bind to collagen. This binding process - *adhesion* - is mediated most importantly through von Willebrand factor (vWf) and platelet glycoprotein 1b (GP1b) receptors (Savage et al., 1996). Adhesion is followed by a stimulation process, leading to further platelet *aggregation* (clustering). The Adhesion can also occur on dysfunctional endothelium and on exposed lipid deposits, as is often the case after atherosclerotic plaque rupture (Bhatt 2008). Unique is the adhesion dependence on shear forces, as platelets only begin to

adhere to the damaged site at minimum $600\text{--}3000 \text{ A}^{-1}$ (Turitto et al., 1977), (Roth, 1991). The aggregation relies immensely on one of the 9 integrin receptors on the platelet surface: glycoprotein IIb/IIIa (GPIIb/IIIa) (further discussed in section below). Its substrate is collagen. An overview over important platelet agonists for this thesis are given in table 1-1.

Platelet agonists

Table 1-1: Summary of important platelet agonists.

Agonist	Source	Receptor
Thrombin	Coagulation cascade	PAR-1, PAR-4, GPIIb α
Adenosine Diphosphate (ADP)	Platelet dense bodies	P2Y ₁ , P2Y ₁₂
Collagen	Subendothelium	GPIa/IIa, GPIIb/IIIa, GPIV, GPVI
Serotonin	Platelet dense bodies	5-HT ₂ receptor
Thromboxane A ₂ (TXA ₂)	Produced by other cells	PGH ₂ , TXA ₂ receptor
Platelet activating factor	Lipid mediator produced by other cells	PAF receptor

Proteinase-activated receptor (PAR), purinergic G protein-coupled (P2Y), glycoprotein (GP), serotonin (5-HT), prostaglandin H₂ (PGH₂), platelet activating factor (PAF). Adapted from Platelets in CVD (Bhatt 2008).

At the site of injury, platelets become activated by several biochemical stimuli, many of which are secreted by the platelets themselves, resulting in the activation of a forward feedback loop (auto-stimulation). The effects are signaled into the cell by glycoprotein receptor binding, G-protein activation and, thus, a phospholipase C or phospholipase A₂ pathway. Thrombin is a highly potent platelet activator, as it activates both pathways simultaneously. Platelets expose different thrombin receptors of varying affinity, including protease activated receptors (PAR) (Greco and Jamieson, 1991). These PARs are cleaved by thrombin. The new N-terminus undergoes a conformational change and attaches to the receptor, such that auto-stimulation occurs. Interestingly, the thrombin remains free to cleave other receptors (Alberelli and De Candia, 2014), supporting rapid and strong platelet activation. The effects of adenosine diphosphate (ADP) on platelets were used in this research, e.g. in the flow cytometry experiments. In a physiological environment, ADP leads to platelet activation and

further platelet recruitment through purinergic G protein-coupled Y_1 (P2Y₁) or P2Y₁₂ receptors on the platelet membrane (Bhatt 2008). Inherited ADP binding abnormalities is a cause of bleeding complications, supporting the important role of ADP in the hemostatic system (Nurden and Nurden, 2014).

Glycoprotein IIb/IIIa receptor

As mentioned before, platelet activation is strongly associated with the GPIIb/IIIa membrane receptor, as its presentation on the platelet surface, firstly increases with activation and secondly mediates activation (so called outside-in signalling). The main purpose of this abundant receptor (50,000/platelet) from the integrin family remains the binding of fibrinogen to enable the subsequent platelet cross linking and aggregation (Bhatt 2008) as seen in figure 1-2. The heterodimeric receptor (with subunits IIb and IIIa) undergoes a Ca^{2+} -dependent conformational change upon platelet activation, enabling high affinity binding only in the activated state (Shattil et al., 1985).

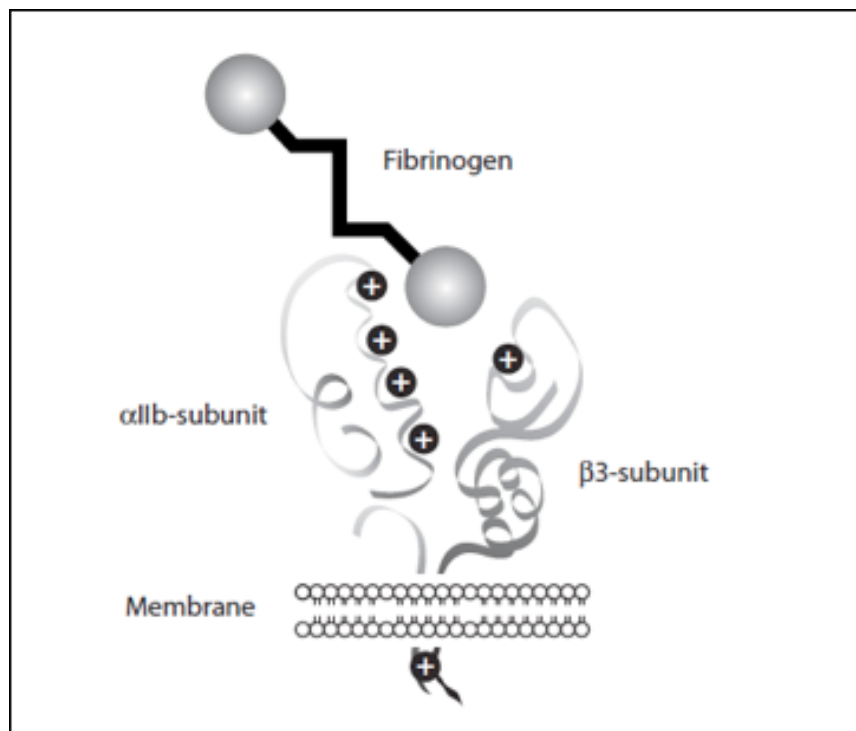


Figure 1-2: Fibrinogen binding to GPIIb/IIIa on platelet membrane.

Adapted from Platelets in CVD (Bhatt 2008)

GPIIb/IIIa antagonists have therefore become an attractive target in medicine, causing 95% platelet aggregation inhibition, 5 minutes following intravenous (Roffi and Mukherjee, 2008). A number of clinical trials have reviewed the benefit of the GPIIb/IIIa

receptor inhibitors, arriving at very heterogenic results. Oral GPIIb/IIIa blockers and long infusions (in contrast to bolus application) entail increased mortality in acute coronary syndrome (ACS) treatment in a meta-analysis (Quinn, Plow and Topol, 2002). The authors propose an insufficient platelet inhibition (<80%) and/or a paradoxical outside-in signalling of the antagonist, suggesting platelet activation, rather than inhibition, as a potential explanation. Other clinical trials stand in contrast to these findings - in the context of a percutaneous coronary intervention (PCI) on high risk ACS patients without ST- elevations and an optimal loading dosage of clopidogrel and ASS. The ISAR-REACT-2 study, with a primary endpoint composite of death, myocardial infarction (MI) or urgent target vessel revascularisation (TVR) at 30 days, was significantly reduced by abciximab (by 25%) compared to the placebo group (Kastrati A et al. 2006). Whereas a similar ISAR REACT study (Kastrati et al., 2004) with low risk ACS patients, as well as the CADILLAC study (Stone et al., 2002) on patients with ST-Elevation MI, displayed no benefit of abciximab over the placebo control. A meta-analysis (Labinaz et al., 2007) summarising a great extent of the trials on GPIIb/IIIa blockers on patients undergoing PCI shows a positive mortality reduction of 28% and 20% at 30 days and 1 year, respectively. Minor bleeding risks were associated with the active treatment group.

In their editorial, Roffi and Mukherjee (Roffi and Mukherjee 2008) attest a confined future usage of conventional GPIIb/IIIa blockers for peri-procedural complications of PCI and for the treatment of high-risk ACS patients, with or without ST-segment elevation. Due to the rise in alternative antithrombotic regimens, such as prasugrel, the broad application of GPIIb/IIIa will be restricted. Clinical advancements are equally made for the complementary part in hemostasis, concerning the coagulation factors (development of direct oral anticoagulants, like apixaban, rivaroxaban, dabigatran), interfering with the coagulation cascade.

1.2.2 Coagulation cascade

Although coagulation factors and platelets are constantly present in the vessel lumen, the coagulation cascade will generally not be activated in intact arteries or veins. Coagulation factors continue to circulate in inactive states as long as the endothelium is healthy and does not expose collagen, tissue factor or negatively charged phospholipids. Conversely, when these substances are present, the coagulation cascade is initiated. Constant vascular flow ensures that any activated coagulation factors are briskly removed. Laminar flow in an undisturbed vessel causes a thin layer

of plasma to cover the endothelium, inhibiting direct platelet contact with it. The following factors further ensure the absence of clotting in intact vessels: the expression of antiplatelet and anti-coagulant factors on the endothelium, the circulation of proteases which degrade activated factors and multiple-stimuli-dependent activation, e.g. of platelets (Adams and Bird, 2009).

Most modern-day clinicians separate the haemostatic system into an intrinsic and an extrinsic pathway. The understanding and evaluation of clinical tests, such as the activated partial thromboplastin time (aPTT) and the international normalized ratio (INR), can be deduced. However, knowledge of the interplay between coagulation factors and cellular membranes, e.g. on platelets (Pérez-Gomez and Bover, 2007), changed the picture. The exposure of tissue factor (TF) in the subendothelium causes factor VII activation and the subsequent activation of factor X is believed to be the key basis of haemostasis initiation. Only small amounts of thrombin are formed. The second activation phase includes an amplification process on phosphatidylserine membrane surface of platelets, leading to the third phase - propagation - where a 'thrombin burst' forms the adequate amount of fibrin required for a clot stabilisation (Adam and Bird, 2009).

The amplification phase implies an 'intrinsic Xenase'. The TF:VIIa complex of the initiation phase (extrinsic Xenase) leads to conversion of IX to IXa. In combination with factor XIIIa, the production of activated factor Xa is 50-100 times increased (Mann et al., 2006). The localisation on platelet membranes increases the reaction efficiency of Xenase and Prothrombase (Xa:Va) further (Mann et al., 2003). The generated thrombin not only cleaves fibrinogen, but also p is a central player in determining the activity of clot protecting factors, such as thrombin activation fibrinolysis inhibitor (TAFI), thus hindering simultaneous fibrinolysis through plasmin.

1.2.3 Fibrinolysis and thrombolytic therapy

The fibrinolytic system itself is balanced by multiple activating and inhibiting factors as displayed in figure 1-3.

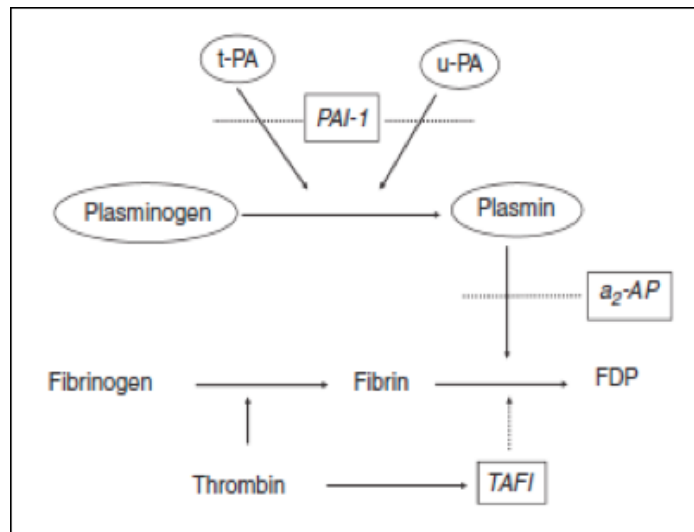


Figure 1-3: The fibrinolytic system.

Tissue plasminogen activator (t-PA), urokinase plasminogen activator (uPA), plasminogen activator inhibitor -1 (PAI-1), α₂-antiplasmin (α₂-AP), thrombin activation fibrinolysis inhibitor (TAFI). Adapted from Rijken and Lijnen, 2008

Following aggregation and fibrin formation, the equilibrium between the three major components of the fibrinolytic system is crucial for the velocity and extent of fibrin deposit removal. Firstly, there is plasminogen, the inactive zymogen of the proteolytic enzyme plasmin. Plasminogen is itself activated by limited proteolysis. Plasmin inhibitors and activators are crucial to the second and third parts of the fibrinolytic system (Wiman and Collen, 1978). The interactions between fibrin, plasminogen, plasmin and its inhibitors and activators are mainly mediated by lysine and lysine binding sites in the respective proteins. Some are discussed below:

Thrombin activatable fibrinolysis inhibitor (TAFI)

The TAFI is a Zn-dependent carboxypeptidase. It has a high specificity for lysine residues, inhibiting the binding site of plasminogen and tissue plasminogen activator (t-PA) on fibrin. High concentrations of plasmin lead to its activation. TAFI is produced in liver cells and can be found in platelets (Cesarman-Maus and Hajjar, 2005).

Plasminogen activator inhibitor (PAI)

PAIs play a key role in inhibiting urokinase plasminogen activator (uPA) and (t-PA) activity (Kruithof et al., 1984). They are present in endothelial cells, monocytes,

macrophages, hepatocytes, adipocytes and platelets, and are released under increased cytokine and growth factors concentrations. Moderate to severe bleeding complications are consequential when absent in humans (Cesarman-Maus and Hajjar, 2005).

α 2-antiplasmin

The α 2-antiplasmin molecule forms complexes with plasmin to inhibit plasmin's function, therefore protecting clots. It is the main physiological inhibitor of plasmin and can be directly attached to an alpha chain of fibrin when XIII and Ca^{2+} are present (Lijnen, 2001). When plasmin is bound to fibrin it is protected from antiplasmin.

Plasmin

Plasminogen is activated by t-PA and uPA. Kallikrein, factor XIa and XIIa can account for activation as well, even if only to a minor extent. When cross linked fibrin is degraded by plasmin, D-dimers develop, which can be measured in clinical settings. A positive feedback mechanism leads, in turn, to the cleavage and transformation of t-PA and uPA from single chain to more active two-chain polypeptides (Cesarman-Maus and Hajjar, 2005).

t-PA.

The differences between uPA (see below) and t-PA are not enormous. A main difference, however, is that t-PA, in contrast to uPA, is more often co-localised with plasminogen on fibrin, as both are exhibiting high lysine binding affinity (Rijken and Lijnen, 2009).

(Low molecular weight) single chain urokinase plasminogen-activator (scuPA)

Urokinase plasminogen activators are used as thrombolytic drugs for the lysis of blood clots. They cleave plasminogen, converting it into its active form, plasmin (Rijken et al., 2008). Plasmin in turn degrades fibrin-based thrombi, thereby resulting in the breakdown of blood clots.

Table 1-2: Different forms of urokinase plasminogen activators (uPA).

Name	Size	State of activation	Feature
Single chain urokinase plasminogen activator	54 kD	low	Physiological
Two chain urokinase plasminogen-activator	54 kD	high	Activated through plasmin
Low molecular mass two chain urokinase plasminogen activator	33 kD	high	High plasmin concentrations lead to further hydrolysis of above
Low molecular weight single-chain urokinase plasminogen activator (scuPA)	32kD	low	Used in this project.
Low molecular weight two chain urokinase plasminogen activator	32kD	high	Activated through plasmin

In the literature, the nomenclature of varying subtypes is partly inconsistent. Importantly, there are two different characterisations or attributes to the protein and its state. Firstly, one differentiates between the size (low molecular weight/low molecular mass/high molecular weight) and, secondly, between low and high activity level. Thus, urokinase, a 54kD glycoprotein, is a zymogen which not only activates plasmin, however is also in turn activated by plasmin in a forward feedback loop (Spraggon et al., 1995). Apart from its catalytic domain, like many other serine proteases, the

urokinase has an N-terminal extension, commonly referred to as the A-chain. This particular A-chain contains kringle domains and epidermal growth factor domains. It remains attached through disulfide bonds after zymogen activation (Behrens et al., 2011). The incurred form of the protein is highly active and is called two chain urokinase. This plasmin-mediated proteolysis occurs between lysine (Lys) 158-Isoleucine (Ile) 159, yielding residues A1-158 and B159-411, when considering the high molecular weight urokinase (Spraggon et al., 1995).

The low molecular weight scuPA consists of residues 144-411 and can be generated with hydrolysis by specific metalloproteases (Rijken et al., 2008) but retains its zymogen character (Yan et al., 2007). Its reduced size (32kD) is advantageous for clinical and experimental setups, for example by enabling better plaque infiltration. A second, low molecular mass urokinase (33kD) can be generated by very high concentrations of plasmin. In this case, the Lys135-Lys136 bond is also hydrolysed following the previous cleavage of the Lys158-Ile159 (Rijken et al., 2008). For this project, a low molecular weight single-chain urokinase (scuPA) was employed; a small (32kD) zymogen protein.

The urokinase plasminogen activator receptor (u-PAR) should be mentioned shortly. It is expressed on an array of different cells, such as monocytes, macrophages, fibroblasts, endothelial cells and a variety of tumour cells (Cesarman-Maus and Hajjar, 2005). uPA/u-PAR interactions lead to cell/cell and cell/extra cellular membrane (ECM) proteolysis. Other reactions apart from proteolysis like the promotion of cell invasion through activation of several migration-associated signalling molecules, such as extracellular signal-regulated kinases, can occur (Killeen et al., 2009). uPA/u-PAR pairing thus plays an important role in tumour invasion of e.g. the colorectal carcinoma (Berger, 2002). As part of the final targeted theranostic microbubble (TT-MB) construct of this thesis, the scuPA and a single chain antibody were attached to the microbubble.

1.3 Antibodies

1.3.1 Single chain antibodies

The variable fragment (Fv) is the smallest unit of an immunoglobulin, functioning as antigen-recognition and binding site. An antibody in scFv (single chain fragment variable) format consists of variable regions of heavy (VH) and light (VL) chains, which are joined together by a flexible peptide linker that can be easily expressed in functional form in *E. coli* (Ahmad et al., 2012). There are numerous advantages of using single chain antibodies, rather than monoclonal antibodies, in various applications, for

example superior tumour penetration (due to its smaller size) and a much more rapid clearance from the circulatory system and normal tissue, enabling an earlier imaging time (Batra et al., 2002). Two main advantages supporting single chain antibody use in our project are the dramatically reduced production costs, as production can occur in *E. coli*, and the desirable decrease in immunogenicity. The antibody lacks the constant fragment (Fc) which modulates the immunogenic response. Since the development of the phage-display technology in 1985 (Smith, 1985), many different usages have been established, foremost in molecular imaging.

Application of single chain antibodies (molecular imaging)

The scFv antibodies are employed in different research areas. Fibroblast growth factor-1 was successfully targeted in innovative preclinical breast cancer therapies; scFv1C9 arrests the cell cycle in breast cancer cells and its over expression leads to reduced tumor size and metastasis (Shi et al., 2014)). Hu et al. show targeting of a scFv fusion construct against carcinoembryonic antigen (CEA) and were able to image the rapid uptake due to radiolabeling (Hu et al., 1996).

The first antibody fragment to undergo clinical trials was Pexelizumab (Alexion Pharmaceuticals, USA) (Hagemeyer et al., 2009). It appears to reduce cardiac enzyme release and possibly mortality in patients with acute myocardial infarction and coronary bypass surgery (Th  roux et al., 2005), (Mahaffey et al., 2006). It was designed to inhibit complement-mediated tissue damage associated with inflammation and reperfusion. Inflammatory receptors such as E- and P-selectin, which mediate leukocyte adherence and transmigration, have been successfully blocked (Swers et al., 2006), (Friedman et al., 1996).

The blood coagulation system, with its receptor abundance, has naturally become a target for scFv antibodies alone or in fusion constructs. For example, scFv Y₁ binds to the GP1b receptor on platelets, hindering vWF factor from binding, thus restricting platelet adhesion (Hagay et al., 2006). Fibrin-targeted serine protease inhibitor, tick anticoagulant peptide (TAP) (effective factor Xa inhibitor) delivery has displayed strong anti-coagulative effects at concentrations where TAP itself was not effective (Hagemeyer et al., 2004). Ligand-induced binding sites binding scFv (scFv_{anti-LIBS}) antibodies used in this project are recombinant, small single-chain antibody fragments, which bind exclusively to *activated* platelets via their ligand-induced binding sites (LIBS). LIBS are exposed on the platelet integrin receptor GPIIb/IIIa upon platelet activation. Data concerning the scFv_{anti-LIBS} was first published in 2004 and again in

2006 (Schwarz et al., 2004), (Schwarz et al., 2006) after it was created through phage display technology. It has been used for the positron emission tomography – computed tomography (PET-CT) (Alt et al., 2014), magnetic resonance imaging (MRI) (von Elverfeldt et al., 2014) and already for ultrasound microbubble targeting (Wang et al., 2012).

1.4 Ultrasound

Ultrasound is a valuable, non-invasive tool in medical diagnostics for assessment of anatomical structures, as well as the circulatory system. Longitudinal waves, where wave propagation and wave oscillation are carried out in the same direction, at frequencies higher than the audible range (20-20,000Hz) >20kHz, are used for medical ultrasound.

1.4.1 Basic physics

The transducer releases soundwaves (converting electro-potentials with piezoelectric crystals into mechanic waves) at different intensities which propagate through the tissue. Three main phenomena of the waves' physical interaction with the medium are combined under the term attenuation. *Absorption*: This term describes the loss, or rather transformation, of energy from (mechanical) wave energy to heat. The amount of transferred energy is dependent on the traversed medium, its viscosity and the frequency. *Refraction*: Refraction describes the bending of the wave at an interface between different media. It is described by Snell's equation and depends on the angle, as well as the velocity, of the sound in different media. *Reflection*: The reflection of sound waves is the basis for ultrasound. It incorporates changes of direction of sound energy in a way that at least a part of the energy returns to the source of energy release.

The traditional ultrasound uses transducers to produce ultrasound waves that propagate through the tissue. Due to characteristic impedance differences (meaning differences in viscosity, compressibility), waves are scattered and partly reflected at interfaces. The reflected waves are received by the transducer. An image can be formed by processing information, such as intensity and time delay, which correspond with tissue attributes and depth (Gessner and Dayton, 2010). Spatial resolution of ultrasound is determined by the frequency. Higher frequencies correlate with higher resolution. However, the incremental increase in picture quality is acquired at the expense of depth penetration (Shung, 2010). In clinical practice 1-10MHz frequencies

render a submillimetre to millimetre range resolution, whereas 20-50MHz (High frequency ultrasound) increase resolution to the tens of micrometre (Klibanov, 2005) but are rather used in preclinical settings.

The mechanical index (Mi) is an indication of the mechanical effects on the tissue during insonification. Importantly, it is a factor which can be used to in regards to possible side effects of ultrasound. The index is proportional to the peak negative pressure. A Mi above 0.7 indicates a theoretical risk of cavitation if gas filled ultrasound enhancing contrast agents are being used (see section bio effects microbubbles).

1.4.2 Ultrasound contrast agents – Microbubbles (MB)

Ultrasound contrast enhancing microbubbles were first introduced in 1968 when they were administered into the aortic root and were described as 'clouds of echoes probably arisen from mini bubbles' by Gramiak and Shah (Gramiak and Shah, 1968). From that point onward, microbubbles with different shell types, gas cores, sizes, charges and thus ever evolving characteristics have been produced. The basic physics behind the contrast enhancing capabilities remain identical. MBs mainly consist of a gaseous core, which is impacted by the ultrasound waves. The waves make the MBs compress, expand and backscatter an immense signal. They are hence extremely echogenic.

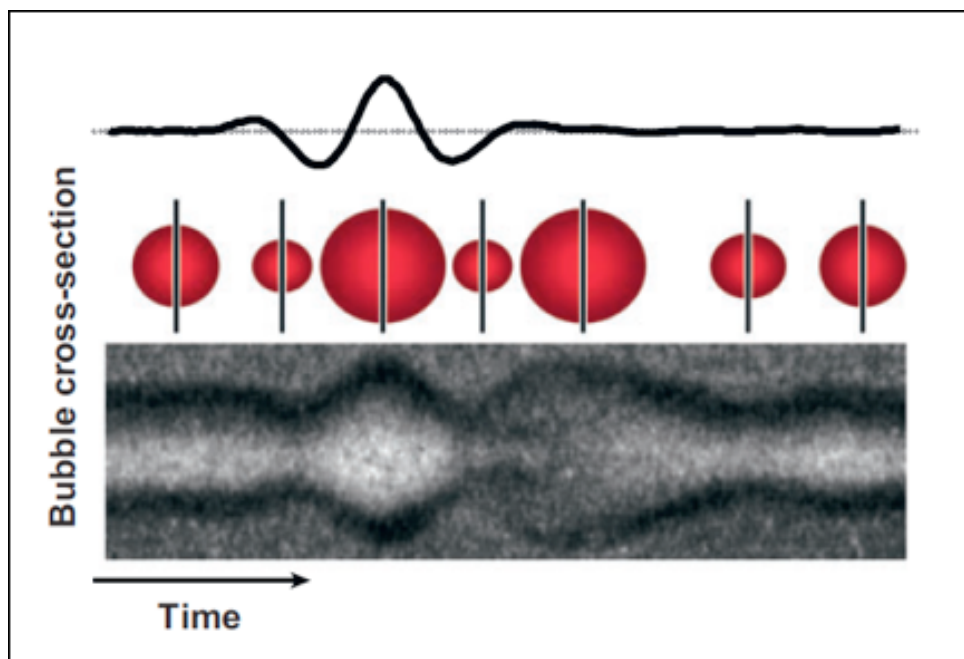


Figure 1-4: MB response to the ultrasound wave.

MBs respond to ultrasound waves by an oscillating movement owing to the extremely compressible gas core. Adapted from Ferrara, Pollard, and Borden 2007.

Current microbubbles are between 2 and 6 μm in diameter (Alzaraa et al., 2012). As such, they are in the same order of magnitude as erythrocytes. Furthermore, they even exhibit similar behaviour (microvascular rheology) to red blood cells (Lindner et al., 2002). Entrapment in capillary beds is mainly transient and alleviated through shape changes into bullet-form microbubbles (Lindner et al., 2002). Microbubble stability has been of pivotal importance for the development and improvement of the reagents for clinical practice. According to Laplace law, at an interface of gaseous bubble and a liquid state, the surface tension of the bare bubbles leads to a pressure drop and an almost immediate dissolution, making an encapsulation indispensable (Ferrara et al., 2007). Another factor that comes into play is the entrapped gas core, where low soluble, gas-like perfluorocarbons are commonly employed to improve stability (Szijjártó et al., 2012). PEG brushes and the introduction of charge have overcome the problem of quickly fusing bubbles with lipid monolayers (Klibanov, 2005).

Shell material

The first approved microbubbles consisted of an albumin coated shell (Ferrara et al., 2007) and had one main disadvantage in common with the 1st generation MBs composed of surfactant and galactose; a poor half-life of a few seconds (Alzaraa et al., 2012). For this thesis, the MBs shells were made out of a monolayer of lipid (micelle), a widely used approach. They were acquired through VisualSonics (VisualSonics Inc., Canada). A comparatively easy in production and a good echogenicity (Ferrara et al., 2007), combined with a satisfying stability, has led to their predominance in the MB field. The lipid chain length had an especially important impact on many physical properties, including stability (Duncan and Needham, 2004). Aside from the physical properties and stability, bio effects and safety play an important role with any infusible medication.

Bio effects and safety

Of late, the safety of ultrasound itself has been extensively studied, leading to the creation of guidelines intended to minimise mechanical and thermal effects (Barnett et al., 2000). Thermal effects are created by high frequency ultrasound waves which cause a temperature rise in the adjacent tissues, whereas mechanical effects, like cavitation (formation of tiny gas bubbles due to ultrasound vibration), are owing to high acoustic focused US (Alzaraa et al., 2012). Cavitation can lead to or is used for

sonoporation (transient cell permeability increase), permanent cell permeabilisation, microvessel rupture (Skyba et al., 1998) and necrosis (Alzaraa et al., 2012). Ultrasound is nonetheless widely appreciated as a safe diagnostic procedure. Safety concerns regarding MBs as a contrast agent have, however been expressed, especially the obstruction ('air-embolism') of cardiac and pulmonary microcirculation. The use of untargeted MBs has been Food and Drug Administration (FDA) approved for products of several companies, such as Optison (Molecular Biosystems, Inc., San Diego, CA.). European approval was also granted to Sonovue (Bracco Diagnostics, Milan, Italy) (Alzaraa et al., 2012). A research group from the US looked into the concern in detail (Lindner et al., 2002). MB entrapment was observed with intra-vital microscopy. It was, however, predominantly transient, with dislodgement (>80% after 10 minutes) coinciding with MB conformational changes (bullet form), much like erythrocytes in microcirculation. Signs of neither platelet nor leukocyte adhesion were found, nor did the entrapped MBs expand. Negligible distortion (<1 µm) was detected in the vessel wall adjacent to the entrapped MBs. Clinical routine practice stated the occurrence of only very few allergic reactions, like hypotension over time (Cosgrove and Harvey, 2009).

Targeted MBs have not been tested in clinical settings. The targeting agent, as well as coupling chemistry, potentially trigger immunogenic responses. Enhanced complement activation and mediated nonspecific adhesion (Lindner, 2009), (Borden et al., 2006) were found in preclinical studies.

1.4.3 Clinical indications for the use of MBs

Today, untargeted MBs are approved for clinical application and are employed in many medical fields, including cardiology and gastroenterology (Alzaraa et al., 2012). Beaton, Cochlin and Kumar suggested to use contrast enhanced ultrasound for a primary investigation to characterise focal liver disease. They back up their claim, with excellent sensitivity (92%) and specificity (100%) to find malignant focal lesions and discriminate from benign lesions (Beaton et al., 2010). Another example is MB attachment to cardiac heart chambers, resulting in increased accuracy of echocardiography in assessing left ventricular size and systolic performance at rest or during stress (Lindner, 2004).

Table 1-3: Indications of MBs in different organ systems.

Organ	Current application	Potential application
Head	Quantitative analysis of cerebral blood flow	—
Heart	Improves detection of endocardial border	Detection of myocardial perfusion
Aorta	Surveillance of endoleak after abdominal aortic endograft	—
Liver	Detection of focal liver lesions	Evaluate angiogenesis in tumors
Liver	Intraoperative evaluation of the adequacy of ablation	—
Liver	Identification of arteriovenous shunt (eg, cirrhosis, metastases, post-transplant)	—
Liver	Intraoperative guidance for resection of metastases	—
Spleen	Infarction and ischemia	—
Kidney	Infarction and ischemia	—
Ovary	Assessment of lesions vascularization	—
Uterus	Check tubal patency	Identify neovascularization of aggressive inflammation
Joint	—	Detection of inflammation
Urinary Bladder	Detection of ureteric reflux	—
Breast	Assessment of lesions	Detect sentinel nodes
Breast	—	—
Prostate	Enhancement of malignant tissue	Assessment of lesions vascularization
Parathyroid	—	Identify adenoma
Abdominal trauma	Evaluation of blunt hepatic trauma	Define the extent of devitalized tissues
Bowel	Determine disease activity in inflammatory bowel disease by the assessment of bowel wall vascularization	Monitoring therapeutic response to antiangiogenic therapy
Abdominal malignancies	—	Monitoring therapeutic response to antiangiogenic therapy

Adapted from Alzaraa et al., 2012

Recent scientific focus lies on the development of targeted MBs; MBs tethered to ligands with specificity for, for example, thrombosis, Inflammation or Angiogenesis. With the ability of targeting comes the growing potential of localised gene delivery (Yan et al., 2014) and drug delivery in this sector.

1.5 Molecular ultrasound imaging:

To be able to pursue a targeting approach, coupling chemistry is required to bind the ligands to the bubbles. Generally, four different strategies are employed. Firstly, the ligand can be added to an element of the membrane. The membrane will then be assembled in a second step (Tardy et al., 2002). The rigidity of this direct attachment leads to further development and an introduction of a spacer molecule e.g. polyethylene glycol (PEG) for increased flexibility (Wu et al., 1998). This approach is not suitable for proteins (e.g. antibodies) that cannot resist high temperatures or shear stress, as the second step the formation of the MBs, requires this. (Chiang et al., 1986). Therefore, covalent and non-covalent strategies have been successfully tested, where the ligand is attached to intact microbubble. A common approach is a 'biotin-

streptavidin coupling sandwich'. Biotin MBs are produced as previously explained. Streptavidin is then added and finally a biotinylated protein can be conjugated onto the streptavidin. Respective excess is removed by low speed centrifugations (Klibanov, 2005). The remaining two alternatives are covalent binding strategies. Carboxylated lipid derivatives in the MB membrane could lead to amide bond formation via activation of carboxylated derivative in form of transitional ester products. Mostly used for liposomes with higher lipid concentration, this method is not efficient enough in monolayers and a lot of excess protein is wasted. The fourth approach consists of thioether conjugation which is stable and specific, as thiol groups can be added into the protein in a specific place and are not as abundant as amino groups, which react in the approach previously (Klibanov, 2005). With a specific antibody on the surface of the MB various clinical applications, e.g. in inflammation, thrombosis or in cancer were tested.

1.5.1 Molecular ultrasound imaging in cancer

Ultrasound contrast enhancement is mainly restricted to the circulatory lumen, which excellently facilitates the study of tumour angiogenesis. The targets are integrin molecules which are over expressed by the tumour's endothelial cells. With Alpha-v beta-3 (Avb3) targeted MB, a research group was able to study angiogenesis on glioblastoma in mice (Ellegala et al., 2003). The strongest signal was obtained at the outer margins of the tumour. In spite of an increase in microvascular blood volume over the studied period, the mean blood flow progressively decreased. According to the authors, this is due to a reduction overtime in red blood cell velocity in the glioma microcirculation. Pysz et al. used microbubbles with molecules directed against human kinase insert domain receptor and cross reactivity to the vascular endothelial growth factor receptor 2 (VEGFR2) (Pysz et al., 2010). This enabled them to study angiogenesis, even longitudinally, *in vivo* on human colon cancer xenografts.

1.5.2 Molecular ultrasound imaging in inflammation and thrombosis

The overexpression and up-regulation of receptors and vascular adhesion molecules as a secondary response to inflammation on endothelial cells is well known. Vascular cell adhesion molecule-1 (VCAM-1), P-selectin and other leukocyte adhesion molecules on endothelial cells have therefore become a target for molecular ultrasound. The accumulation of targeted microbubbles to VCAM in an atherosclerotic mouse *in vivo* showed considerable contrast-enhancement at very early stages of the disease (10 week old mice). This signal increased by 3-fold at 10 weeks, between 4-

and 6-fold at 20 weeks, and 9-to 10-fold at 40 weeks, as compared to wild-type mice (Kaufmann et al., 2010). Basic *in vitro* work concerning P-selectin was performed by Takalkar et al. where, in flow chamber experiments, shear stress was important for binding dynamics. Other findings showed increased MB retention at higher P-selectin site densities (Takalkar et al., 2004). Acoustic radiation can further increase P-selectin binding as it presses the bubbles to the edges of the lumen (Rychak et al., 2007). Early endothelial activation associated with a high fat diet and insulin resistance was proved with targeted MBs against VCAM-1 and P-selectin in non-human primates before intimal wall thickening. This interestingly offered a more consistent picture than a soluble inflammatory marker (like IL-18) in blood over a one-year time period (Chadderdon et al., 2014).

Molecular ultrasound has great potential in the field of diagnostics and in its application as a tool for real-time monitoring of treatments and decision making in thrombus formation. The GPIIb/IIIa receptor, a key player in aggregation on platelets, has been studied as an attractive target (Culp et al., 2004), (Martin et al., 2007), (Xie et al., 2009b), (Wang et al., 2012). Schumann et al. were one of the first to show the higher affinity of GPIIb/IIIa targeted microbubbles to thrombi (Schumann et al., 2002). The results from Martin et al. demonstrated that targeted MB bind to thromboemboli under pulsatile flow conditions. They were able to enhance the detection of this phenomena using contrast-enhancing bubbles under transcranial Doppler measurements ((Martin et al., 2007). This finding suggests a field other than cardiovascular disease for the use of MBs: stroke. Sonoporation, where a destruction of the bubbles probably leads to lysis and the enhanced penetration of thrombolytic and anti-thrombotic drugs, is frequently employed in this area. It was shown that intravascular thrombolysis with transcutaneous, low frequency ultrasound was capable of reopening cranial (Xie et al., 2009b) thrombosis in swine with Eptifibatide (GPIIb/IIIa blocker) coupled microbubbles and a good safety profile (Culp et al., 2004). Concerning myocardial infarction, Xie et al. published an excellent paper, with pigs receiving platelet-targeted MBs. They showed a more rapid replenishment of the central affected area and higher epicardial recanalisation rates when treated with MBs and half dose recombinant prourokinase, heparin and aspirin, as compared with only prourokinase etc. (Xie et al., 2009). Wang et al. came forward with a novel strategy combining low cost production of scFv_{anti-LIBS} antibodies, straight forward coupling and the high affinity against the GPIIb/IIIa target

(Wang et al., 2012). It was that approach, that was refined to a theranostic ultrasound approach.

1.6 Theranostics:

Theranostics in general is a modern development in line with the recent progressing approach in medicine: 'personalised medicine'. Targeted therapy is compiled in accordance to the individual 'molecular profile' and thus the prediction of individualised benefits from the treatment is in focus (Kelkar and Reineke, 2011). Basically, two main approaches to theranostics have emerged: I) the biomarker approach - *in vitro* (e.g. blood) or *ex vitro* (e.g. histopathology) data is scanned for at risk profiles, used for early diagnosis of recurring events. II) Imaging-based guidance – e.g. imaging guided intervention procedures, cell therapy or imaging controlled drug delivery (Idee et al., 2013). Theranostic approaches have attracted major attention in the recent years as the lead to the development of single agents with diagnostic and therapeutic capabilities promising individualized therapy with fewer side-effects.

In recent advancements, a journal for theranostics has been created. Interesting published results include MB use for blood brain barrier (BBB) opening (Chiang et al., 1986). First Burst-tone focused ultrasound (0.5/0.7 MPa) entails widening of tight junctions in consequence of endothelial cell deformation. With MB destruction (0.6 MPa) and replenishment, Chiang-Hsiang et al. were able to approximate the mean blood flow velocity. Another attractive development in the field of theranostics involved multicompartmentalised drug carriers, as Ranhua Xiong from Belgium discusses (Xiong et al., 2013). Outer compartments could be used as diagnostic sensors. Ions could lead to e.g. change in fluorescence which can be observed. A second mechanism is needed to release a drug in the inner compartment. Laser rays in the near infrared range induce transient permeability of the shell due to a transient temperature rise (Xiong et al., 2013). As mentioned earlier in the section urokinase plasminogen activator, UPA and its receptor (u-PAR) play a role in invasive tumour progress. Image-guided murine surgery targeting the u-PAR was performed by Yang et al. The u-PAR is expressed in the external region of the tumour, in this study breast and pancreatic tumours. Small peptide fragments directed against u-PAR and labelled with a dye were visualised after injection and represented the tumour margin. These findings might improve R0 resections and thus reduce tumour recurrence (Yang et al., 2013).

An example of theranostics applied in today's clinics, is the transcatheter arterial chemoembolisation (TACE) of the unresectable, asymptomatic, hepatocellular carcinoma (HCC) (European Association For The Study Of The Liver and European Organisation For Research And Treatment Of Cancer, 2012). A cytotoxic drug emulsified in the contrast agent Lipiodol is percutaneously administered. This procedure is pursued by an embolisation of the tumour feeding arteries, whereby in general Lipiodol combines three major properties: transient embolisation, radio opacity and drug delivery (Idée and Guiu, 2013).

Chapter 2. Material and Methods

2.1 Material

2.1.1 List of chemicals

Table 2-1: List of chemicals used in this thesis.

Abbreviation of chemicals	Chemicals
APS	Ammonium Persulfate
Ca ²⁺	Calcium
CaCl ₂	Calcium chloride
Cu ²⁺	Copper
DTT	Dithiothreitol
EDTA	Ethylene diamine tetracetic acid
HCl	Hydrogen chloride
HEPES	Hydroxyethyl piperazineethanesulfonic acid
IPTG	Isopropyl β-D-1-thiogalactopyranoside
KCl	Potassium chloride
KH ₂ PO ₄	Potassium di-hydrogen phosphate
Mg	Magnesium
MgCl ₂	Magnesium chloride
MgSO ₄	Magnesium sulfate
Na	Sodium

2.1.2 List of equipment

Table 2-2: Equipement used in this thesis.

Product	Company
Biological safety cabinets class II: BH2000 Series	Clyde-Apac, Wodddville, SA, Australia
F-VIEW II Digital Camera	Olympus Australia, Mt Waverley, VIC, Australia
Centrifuge Eppendorf 5810	Eppendorf, NY, USA
Microfuge 18 Centrifuge	Beckman Coulter, Krefeld, Germany
Alegra X15 R Centrifuge	Beckman Coulter, Gladesville, NSW, Australia
Avanti™ j-25I Centrifuge	Beckman Coulter, Gladesville, NSW, Australia
DNA gel electrophoresis apparatus: wide mini and mini cells for DNA electrophoresis and power supplies of iMupid	Helixx Technologies, Toronto, Ontario, Canada
FACS Calibur	BD Bioscience, Heidelberg, Germany
FPLC System	GE Healthcare Bio-Science, Rydalmere, NSW, Australia
Biologic DuoFlow System	Bio-Rad, Gladesville, NSW, Australia
DRY Block Heater	Ratek, Boronia, VIC, Australia
CO2-Incubator: Function Line BB15	Heraeus Holding GMB, Hanau, Germany
Certomat CT Plus	Sartorius Stedim Biotech, SA, Australia
Imager: Universal HOOD II	BioRad, Hercules, CA, USA
Gyro Rocker	Stuart, Staffordshire, UK
BR-2000 Vortexer	Hercules, CA, USA
Microscope: Olympus IX81	Olympus, USA
Syringe pump	PhD 200, Harvard Apparatus, Holliston, USA
Gyratory Mixer	Ratek, Boronia, VIC, Australia
Gyro Rocker	Stuart, Staffordshire, UK

Product	Company
BR-2000 Vortexer	Hercules, CA, USA
PCR-Express Gradient Thermocycler	Hybaid Ltd, Hameshire, UK
SDS and Western gel electrophoresis apparatus: PowerPac Basic	BioRad, Hercules, CA, USA
Orbital Mixer Incubator	Ratek, Boronia, VIC, Australia
Spectrophotometer: DU®-640	Beckman Coulter, Gladesville, NSW, Australia
Victor Multilabel Counter 1420	PerkinElmer, USA
Benchmark plus Microplate reader	BioRad, Hercules, CA, USA
Nanodrop ND-1000	Biolab, Clayton, VIC, Australia
Ultrasound imaging machine: IE33	Philips, Netherlands
Ultrasound imaging machine: Vevo2100	VisualSonics Inc, Canada
Monovette Coagulation 9NC 10ml tubes	Sarstedt AG&Co
Vacutainer® Safety-Lok™ Blood Collection Set	Becton Dickinson

2.1.3 List of software

Adobe Photoshop 6.01

Cell Quest Pro, 4.0.2

Graph Pad Prism 6.0

ImageJ 1.43

Image Pro Plus 6.0

QuantityONE (Version 4.5.2 Bio-RAD)

Microsoft Office

Philips QLAB software

VisualSonics imaging software

2.1.4 List of enzymes and reaction kits

Table 2-3: Reaction kits and enzymes used for this thesis.

Kits	Company
QIAquick® PCR Purification Kit (50/250)	Qiagen, Doncaster, VIC, Australia
QIAquick® Gel Extraction Kit (250)	Qiagen, Doncaster, VIC, Australia
QIAGEN Plasmid Maxi Kit (25)	Qiagen, Doncaster, VIC, Australia
QIAGEN Plasmid Mega Kit (5)	Qiagen, Doncaster, VIC, Australia
LiquiChip Ni-NTA beads (500)	Qiagen, Doncaster, VIC, Australia
QIAGEN Ni-NTA Superflow Cartridge (5)	Qiagen, Doncaster, VIC, Australia
GoTaq® Green Polermase Master-Mix	Promega, Melbourne, VIC, Australia
Wizard® Plus Minipreps DNA Purification System	Promega, Melbourne, VIC, Australia
Wizard® SV Gel and PCR CleanUp System	Promega, Melbourne, VIC, Australia
BugBuster™ Protein Extraction Reagent	Novagen, Darmstadt, Germany
SuperSignal® West Pico Chemoluminescent Substrate	PIERCE, Murarrie, QLD, Australia
BCA™ Protein Assay Kit	PIERCE, Murarrie, QLD, Australia
Zyppy™ Plasmid Maxiprep Kit	Zymo Research Corporation, Irvine, CA, USA
Enzymes	Company
Restriction enzymes	New England Biolabs®, USA
T4 Ligation mix	New England Biolabs®, USA
Rapid DNA Ligation Kit	Roche, Penzberg, Germany

2.1.5 Buffers and media

Table 2-4: The THY media for *E.coli* protein production with the Avi-tag.

THY media (tryptone, HEPES, yeast)	
Tryptone	20g
HEPES	10g
Yeast extract	11g
NaCl	5g
MgSO ₄	1g

THY media, luria broth (LB), super optimal broth (SOB) and super optimal broth with catabolite repression (SOC), were prepared as described by Maniatis et al., 1982. Standard autoclaving conditions (20 minutes, 121 °C) were performed for sterilisation of the bacterial culture media, as well as glassware. When required, thermo labile components such as ampicillin (100 µg/ml) were added to the autoclaved media after they were cooled down to 50° C.

Table 2-5: Buffers used in the thesis.

1x Lysis buffer, pH 8.0	
NaH ₂ PO ₄	50 mM
NaCl	300 mM
Imidazole	10 mM
1x Washing buffer, pH 8.0	
NaH ₂ PO ₄	50 mM
NaCl	300 mM
Imidazole	20 mM
1x Elution buffer, pH 8.0	
NaH ₂ PO ₄	50 mM
NaCl	300 mM
Imidazole	250 mM
5x SDS Running Buffer	
Tris	25 mM
Glycine	192 mM
SDS	1%
Transfer buffer	
Methanol	10%
5x Towbin	20%
ddH ₂ O	70%
5x Towbin	
Tris	125 mM
Glycine	950 mM
SDS	10%

Table 2-5: Buffers used in the thesis.

5x Reducing Loading Buffer	
Tris pH 6.8	250 mM
Dithiothreitol (DTT)	500 mM
Glycerol	50%
SDS	10%
Bromophenol blue	0.5%
FPLC Washing buffer, pH 8.0	
NaH ₂ PO ₄	50 mM
NaCl	300 mM
Imidazole	20 mM
Elution buffer, pH 8.0	
NaH ₂ PO ₄	50 mM
NaCl	300 mM
Imidazole	250 mM
Talon bead wash buffer (negative purification after the Sortase A reaction), pH 7.0	
NaCl	300mM
NaH ₂ PO ₄	30mM

2.1.6 Primers and plasmids

Table 2-6: Forward and reverse Primers that were used for this thesis.

Primer name	Plasmid	Sequence
pAC6-F	pAC6	5'-CCGGCTCGTATAATGTGTGG-3'
pAC6-R	pAC6	5'-ATCAGACCGCTTCTGCGTTC-3'
pSectag2A-F	pSectag2A	5'-TAATACGACTCACTATAGGG-3'
pSectag2A-R	pSectag2A	5'-TAGAAGGCACAGTCGAGG-3'
Primer name	Restriction enzyme	Sequence
ScuPA-LPETG-F	EcoRI	5'-CTGAGAATTCTCCTGAAGTTCCAGTGC GGCCAGA-3'
Scupa-LPETG-R	NotI	5'-TCATCACCACCACTGATGAGAGGCGG CCGCCTCG-3'

Table 2-7: Plasmid-construct that were used in this thesis.

Plasmid	Properties	Source of reference
pAC6-anti-LIBS	amp, BiP signal, V5, 6X-HIS, MT promoter, pUC ori	Wang et al., 2012 (This work)
Psectag2A-scuPA	amp, Ig κ signal, c-myc, 6X-HIS, CMV promoter, pUC ori	This work

2.1.7 Antibodies

Table 2-8: Antibodies that were used for this thesis.

Antibody	Property	Source of reference
scFv _{anti-LIBS_Avitag}	LIBS specific, V5 tag, Histag, Biotin, produced in <i>E. coli</i>	Wang et al., 2012 (This work)
AlexaFlour®488	anti-penta-His, FITC-labelled	QUIAGENTM
anti-CD62P-PE	rat, anti-mouse P-selectin, PE-labelled	BD PhrarmingenTM
anti-His-HRP	anti-penta-His, HRP-labelled	Jackson IR®
anti-mouse-FITC	goat, anti-mouse IgG, PE-labelled	Jackson IR®
anti-mouse-PE	goat, anti-mouse IgG, FITC-labelled	Jackson IR®
anti-mouse-HRP	goat, anti-mouse IgG, HRP-labelled	Jackson IR®
anti-rat-FITC	goat, anti-rat IgG, FITC labelled	Jackson IR®
Biotin-PE	PE-labelled	Sigma-Aldrich®
PAC-1-FITC	rat, anti-mouse GPIIb/IIIa, FITC-labelled	BD PhrarmingenTM
Streptavidin-PE	PE-labelled	Jackson IR®
Abciximab (Repro®)	GPIIb/IIIa receptor antagonist	Eli Lilly
Fibrinogen-FITC	Fibrinogen From Human Plasma, Alexa Fluor® 488 Conjugate	Life technologies

2.3 Molecular biology methods

2.3.1 DNA Isolation

To isolate DNA-Plasmids, a Miniprep Kit from the company Promega (Promega, Australia) was employed. A 10ml Luria broth (LB) of overnight culture (37°C) with vigorous shaking of 220 rotations per minute (rpm) from a glycerol stock (*E. coli* with plasmid of interest) containing 100 µg/ml ampicillin was pelleted at 4800xg for 20 minutes, the supernatant discarded. The following steps were conducted according to the kit supplier's manual. When larger amounts of isolated DNA were needed for a large scale transient transfection, the QIAprep® Plasmid Maxiprep Kit (Qiagen, Australia), as well as the Zyppy™ Plasmid Maxiprep Kit (Zymo Research Corporation, USA) were used. Here, the 10ml LB with *E. coli* plasmids of interest containing 100 µg/ml ampicillin were shaken for 8 hours at 37°C with 220 rpm. 2 ml of the 8 hour culture were transferred into 400 ml of LB media containing 100 µg/ml ampicillin in a non-baffled Erlenmeyer flask and the cells were grown overnight at 37°C with vigorous shaking at 220 rpm. The following steps were conducted according to the kit supplier's manual. The purity and concentration of DNA was measured with the NanoDrop® ND-1000 device.

2.3.2 Separation of DNA by agarose gel electrophoresis

The DNA samples were combined with 6x electrophoresis loading buffer (NEB, USA) in a ratio of 5:1. Samples were separated in an agarose gel [0.7% to 1.0% (w/v) agarose in 1x TAE buffer (40mM Tris-acetate, 1 mM EDTA, pH8), containing 0.0001% (v/v) SYBR® Safe DNA gel stain (Invitrogen™, California, USA) to a concentration of 0.1 µg/ml] for 30 minutes. The electrophoresis was performed in 1x TAE buffer at 100 V. Following electrophoresis, the agarose gel was visualized on an UV transilluminator at a wavelength of 320nm. Molecular masses were determined using a high 1kb PLUS GBICO-BRL® ladder (Life Technologies, Rockville, MD, USA, which also allowed for quantitation of DNA bands. Subsequently, the desired fragments were excised with a scalpel under UV light and extracted with the QIAquick® Gel Extraction Kit (250, Qiagen, Australia), following manufacturer's instruction. Both the concentration and the purity of products were measured using NanoDrop® ND-1000 device (paragraph adapted from Dr. Xiaowei Wang's PhD thesis).

2.3.3 Nano Drop® – Concentration and Purity of DNA

The NanoDrop® ND-1000 device is a compact, modern UV-spectrophotometer where even minute amounts of dissolved DNA are sufficient to identify the concentration of the DNA. 1 µl of DNA was pipetted on the reader which measured at a wavelength of 260 nm. An absorbance of 1 correlates with a concentration of 50 µg/µl double stranded DNA. A DNA solvent was used beforehand to calibrate the device. The ratio of absorbance at 260 nm and 280 nm can be used to assess the purity of DNA. A ratio of approximately 1.8 indicates pure DNA. If the ratio is appreciably lower, it may indicate the presence of protein, phenol or other contaminants, which absorb strongly at or near 280 nm.

2.3.4 Preparation of competent cells

BL21 (star) competent cells were cultured overnight in 5 ml of LB media, at 37°C with vigorous shaking of 220 rpm. After culturing overnight, 2 ml of the overnight culture were transferred into 1L of LB media in a non-baffled Erlenmeyer flask. The cells were grown at 37°C with vigorous shaking of 220 rpm until the absorbance at 600 nm (A_{600}) reached 0.6. The cells were chilled on ice for 30 minutes and centrifuged at 4000 g for 10 minutes at 4°C. Supernatant was discarded and pellet was resuspended in 40 ml of ice-cold sterile-filtered 0.75 M calcium chloride (CaCl_2) solution. The cells were incubated on ice for 10 minute and centrifuged as mentioned above. The pellet was resuspended in 20 ml of ice-cold sterile-filtered 0.75 M (CaCl_2) solution on ice for 30 minute. Centrifugation was repeated and pellet was resuspended in 4 ml of ice-cold sterile-filtered 0.75 M (CaCl_2) solution. Cells (100 µl) were aliquoted into pre-chilled Eppendorf tubes, snap frozen with liquid nitrogen, and store in -80°C (adapted from Dr. Xiaowei Wang's PhD thesis).

2.3.5 Amplification of DNA

The polymerase chain reaction (PCR) is an important tool in molecular biology, enabling the amplification and modification of even minute amounts of DNA (1pg) e.g. the introduction of additional Tags or restriction sites with the appropriate primer pairs. PCR is a stepwise procedure involving repetitive cycles of three main steps; denaturing, annealing and extension, which are preceded by an initial denaturation of the DNA strands at 95 °C for 2 minutes. This step is also needed to heat activate the Taq polymerase enzyme (here GoTaq®). The melting temperature (T_m) was calculated for both primers with the NEB T_m calculator and the lower temperature was chosen as the annealing, and thus amplification, temperature. In case of an

unsuccessful PCR annealing, a gradient PCR with various temperatures could be used to optimise the conditions. As described in the separation of DNA section, the DNA was further analysed with an agarose gel and consequently extracted with a Gel extraction Kit (Promega, Australia) following the instructor's manual. The purity and concentration of DNA was measured with the NanoDrop® ND-1000 device.

Table 2-9: Example for PCR reaction mix with the GoTaq® polymerase.

Component	Volume	Final concentration
Template DNA	1 µl	1-50 ng/µl
100 µM downstream primer	1 µl	1 µM
100 µM upstream primer	1 µl	1 µM
GoTaq® Master Mix 2x	25 µl	1 X
Nuclease free water	22 µl	
Final volume	50 µl	

Table 2-10: Example for PCR protocol.

Reaction cycle		Time	Temperature
Step 1	Initial Denaturation	2 min	95°C
Step 2	Denaturation	30 sec	95°C
	Annealing	30 sec	T _m -5°C or gradient
	Extension	1 min/1000bp	72°C
Repeat step 2: e.g. 35 times			
Step 3	Final Extension	5 min	72°C
End	Storage	-	4°C

2.3.6 Vectors

Psectag2A vector

A 5.2kB long vector (Invitrogen™, California, USA) was engineered for the stable or transient expression in mammalian cells. In addition to a Zeocin resistance gene for the potential creation of a stable cell line and selection in *E.coli*, the Psectag2A vector includes an immunoglobulin K (IgK) leader sequence transferred from an antibody sequence. The leader sequence guarantees the secretion of proteins into the supernatant. Moreover, it contains a c-myc tag, as well as a 6x Hexahistidyl-tag (His tag) for purification purposes behind the multiple cloning site. This vector was used for the production of the scuPA with a LPETG tag.

Pac6 Avitag™ vector

The pAC6 vector was purchased from Avidity (Avidity Biosciences, USA). It incorporates the Avitag, which allows a C-terminal peptide conjugation of the biotin in *E. coli* strains EVB 100 or EVB 101 (Avidity Biosciences, USA). The first describer was Schatz et al 1993. The biotinylation occurs as an enzymatic conjugation of a single biotin on a unique 15 amino acid peptide tag using the biotin ligase (BirA) from *E. coli*. The amino acid sequence of the AviTag™ is GLNDIFEAQKIEWHE. The vector is Isopropyl β-D-1-thiogalactopyranoside (IPTG) inducible and confers an Ampicillin resistance.

2.3.7 Restriction enzyme digest

The DNA was digested with the appropriate restriction enzymes following the producer's manual (NEB, USA) at 37°C for at least 2 hours. Generally, 2 to 3 units per 1µg DNA were employed. 1 unit is defined as the amount of enzymes required to cut 1µg of DNA in 1h at 37°C in a 50ul reaction volume. The reaction was performed in HF buffer (NEB, USA) and the volume was kept small (50µl to 100µl) to ensure appropriate enzyme activity. If not otherwise stated, the digestion was undertaken as a double digest after checking the manufactures double digest finder to ensure 100% activity for both enzymes. The fragments were separated with the agarose gel electrophoresis and the ones at the appropriate sizes were excised under the UV Transluminator. The restricted DNA was then extracted with Wizard® SV Gel CleanUp System (Promega Australia), following the instructor's manual. Both the concentration and the purity of products were measured using NanoDrop® ND-1000 device. The DNA was stored at -20°C.

2.3.8 Ligation

The digested insert was ligated into the digested vector following the NEB recommendations for the T4 Ligase (NEB, USA). The standard molar working ratios of Insert 3:1 vector or 5:1 were used for a single insertion. 1µl of NEB T4 ligase was employed in a total reaction volume of 10ul consisting of 1 µl 10x T4 DNA ligase reaction buffer (NEB, USA), vector and insert (not exceeding 200ng together) and nuclease free water. The ligation was either performed at RT for 2 hours or at 4°C overnight (16 hours). As a negative control, the restricted vector was incubated with 0mol of the insert, using the highest amount of vector in case of trying different insert-vector ratios simultaneously.

2.3.9 DNA introduction into cells

The ligated DNA was transformed into NEB Turbo competent cells as follows. Bacterial cell aliquots were thawed on ice and 100µl was added to the ligation mixture. After another 30 minutes of incubation on ice, the bacteria were heat shocked for 50 seconds at 42°C to ensure the uptake of DNA into the cells. Subsequently, 900µl of SOC media (20% (w/v) tryptone, 5% (w/v) yeast extract, 0.5% (w/v) NaCl, 10mM mgCl₂, 10mM MgSO₄ and 2 % (v/v) glucose) was added and the tube was incubated in a 37°C incubator for 1 hour, vigorously shaken at 220 rpm. 40µl and 200µl were plated on an agar plate containing LB media supplemented with an appropriate selective antibiotic, ampicillin. The plate was kept in an incubator at 37°C overnight (12-16 hours). The colonies were screened by PCR colony screening to identify positive clones. The DNA of positive clones was amplified and transformed (using the same procedure described above, but instead of 100µl, extracted DNA from the clones was used) into EVB100 or EVB101 to allow for high protein expression. Before expressing the proteins, the DNA was sequenced to confirm intact, non-mutated DNA.

2.3.10 Screening for positive clones after transformation

Selection of positive clones incorporating the vector with the insert was achieved with the PCR colony screening (See PCR, here template DNA is replaced by colony of interest and the initial denature time was prolonged to 10 minutes to assure destruction of bacterial cell membranes). If the vectors contained the insert, it would be possible to amplify the DNA fragment with the appropriate primers and visualise them at the appropriate height on an agarose gel electrophoresis. Clones with refused vector backbones or uncut vectors, for example from imprecise excision from the gel after restriction digest, were excluded and not sent to sequencing. The clones on the agar plate were numbered and parts of each clone scraped with a sterile pipette tip. The tips were placed in respective tubes containing 15ul, made up from 2x GoTaq® Polymerase dye, 1:50 of 100µM of forward, respectively reverse primer and nuclease-free water to adapt the volume. Following the PCR, the mixture was loaded into an agarose gel and run for 30 minutes at 110V. The bands were visualised with the UV transilluminator. Upon identification of a positive colony, the clone was used to inoculate 10ml of LB media containing 100µg/ml ampicillin. The cells were grown overnight at 37°C with vigorous shaking at 220 rpm. Glycerol stocks were prepared with an aliquot of the overnight culture and stored at -80°C.

2.3.11 DNA sequencing:

DNA sequencing was performed with help from the Australian Genome Research Facility. Sequence results were used to verify DNA inserts in plasmids and the absence of mutations. DNA sample concentrations were previously determined using a NanoDrop® ND-1000 device and adjusted prior sequencing according to facility requirements (forward and reverse primers with 0.8pmol/μl, at least 600 to 1500μg of DNA and a final volume of 15μl). Sequence alignment was performed using EMBOSS Pairwise Alignment Tool for Global or Local Sequence Alignment EBI at the European Bioinformatics Institute (<http://www.ebi.ac.uk/Tools/emboss/align/>) (Emboss).

2.4 Protein chemical methods:

Proteins were produced using bacterial strains of *E. coli* or mammalian cells. After the production of protein, Immobilised Metal Chelate Affinity Chromatography (IMAC) was executed, using FPLC with a Nickel column or Ni-NTA agarose resin beads (Invitrogen, USA) and TALON® Metal Affinity Resin (Clontech Laboratories, Inc, USA). The protein concentration was determined using Bicinchoninic Acid (BCA) Protein Assay (PIERCE, USA). The purification content was further analysed using coomassie stained sodium dodecyl sulphate polyacrylamide gel electrophoresis (SDS-PAGE) and Western blotting.

2.4.1 Protein expression and production in *E. coli* strains

Proteins were for this thesis partly expressed in an *E. coli* strain, namely AVB101 engineered by the company Avidity (Avidity Biosciences, USA). The strain is lacking the OmpT and Lon proteases which degrade peptides around the bacteria and is characterised by sturdy growth. It contains a specific IPTG inducible plasmid with the BirA and a chloramphenicol resistance gene. BirA is also known as Biotin-Protein ligase. The ligase activates the biotin using ATP as its second substrate, thus enabling the conjugation to the proteins, precisely the Avi-Tag. The induction procedure was executed according to the company's (Avidity Biosciences, USA) manual: Firstly, a 10ml overnight culture from a glycerol stock in LB broth was supplemented with 10ug/ml Chloramphenicol and 100ug/ml Ampicillin vigorously shaking at 220 rpm at 37°C. 5ml of the overnight culture was added to 1L of TYH media in a baffled flask with 100ug/ml ampicillin. 20ml of 20% sterile glucose solution was supplemented and the culture was shaken vigorously at 37°C. When the optical density₆₀₀ (OD₆₀₀) mixture reached 0.7, 10ml of 5mM biotin solution (12mg d-biotin to 10ml of warm 10mM bicine buffer(pH8.3) and filter sterilised), as well as 15ml of 100mM IPTG, was added to

induce in vivo biotinylation for 3 hours. Cells were pelleted in 4x 250ml at 5800x g for 10 minutes at 4°C. The media was poured off and the bacteria pellet was frozen in -20°C freezer overnight. The pellet was resuspended in BugBuster™ Master Mix (Novagen, Germany), 5ml per 1g cell pellet and 1 tablet protease inhibitor for 10 to 15 minutes on a rotary shaker. The mixture was centrifuged at 16 250 g for 15 minutes. The supernatant, as well as the final pellet, were kept for the ensuing purification procedures.

2.4.2 Production of proteins in mammalian cells: Human embryonic kidney (HEK) cells 293F

The HEK cells were derived from an epithelial cell line and are popularly used for the expression of recombinant proteins for a transient expression (Graham et al., 1977). It is known that the cellular compartments generally generate functional proteins through correct post-translational folding and processing (Thomas and Smart, 2005). The cells were maintained in FreeStyle™ 293 Expression Medium (Invitrogen, USA) without addition of antibiotics in a 37°C, 8% CO₂ humidified incubator, under constant shaking at 110 rpm.

Large scale transient transfection with polyethylenimine (PEI) (Polyscience Inc., Germany)

By neutralising and overcoming the charge of the anionic phosphate backbone of the DNA, the reagent, PEI, enables DNA to crossing the membrane phospholipid bilayer. It condenses DNA in positive particles which are taken up into the cell through endocytosis. The method was established by the Commonwealth Scientific and Industrial Research Organisation (CSIRO) and performed according to protocol. The DNA plasmids for transfection were diluted to a ratio of 1:4 with PEI. 24 hours prior to transfection, *H293F* cells were diluted with Freestyle 293 expression medium (Invitrogen, USA) to a concentration of 1×10^6 cells/ml. Transfection was performed when the cell density was approximately 2×10^6 cells/ml and the viability was 95% or greater. The ratio of Freestyle 293 expression medium to PBS (with diluted DNA and PEI) was 9:1. An appropriate amount of cell culture medium was transferred into a shaker flask and placed in the incubator at 37°C, shaking at 110 rpm. 1µg/ml of DNA plasmid was added to pre-warmed (37°C) PBS and vortexed gently. PEI was added to the concentration of 3µg/ml, and vortexed three times at three seconds each time. The mixture was incubated for 15 minutes at RT. The cell culture medium was removed

from the incubator. The DNA-PEI mixture was added to the medium while swirling gently. Glucose was added to a final concentration of 6g/L. The flask was returned to the incubation and cultured at 37°C, with 5% CO₂, shaking at 110 – 140 rpm. The culture was supplemented with 5g/L lupin and 0.2 mM butyric acid after one day. At day 3, 5 and 7 after transfection, the culture was supplemented with 2mM Glutamine. At day 5, the culture was again supplemented with 5g/L lupin. The glucose level was maintained at a final concentration of 5 – 6g/L. The cells were harvested when viability reached 40 – 50%. The cells were centrifuged at 3000 g for 15 minutes at 4°C, and the supernatant was collected for protein purification (paragraph adapted from Dr. Xiaowei Wang's PhD thesis).

2.4.3 Small scale purification (SCP) of proteins

Ni-NTA agarose resin beads (Qiagen, Germany) and TALON® Metal Affinity Resin (Clontech Laboratories, Inc, USA) were used for small scale bench top purification. The beads bind to the proteins' 6x His-tag. The pre-washed Ni-NTA resin beads (0.5ml per 10 ml sample) were incubated with supernatant overnight at 4°C. The mixture was subsequently filled in a disposable 5ml polypropylene column with a bottom filter (Thermo Fisher Scientific Inc., USA). 5ml of wash buffer (50mM NaH₂PO₄, 300mM NaCl, 20mM imidazole, pH 8.0) was added to the Ni-NTA beads and incubated for 10 minutes. The washing step was carried out three times to remove unspecific or weakly bound proteins. The protein was finally eluted after incubation of 250-500µl elution buffer (50mM NaH₂PO₄, 300mM NaCl, 250mM imidazole, pH 8.0) for 15 minutes. Five to eight elution fractions were collected. Before further analysis was possible, the eluting buffer was removed with dialysis. In the case of SCP under urea, the elution buffer was supplemented with 8mmol urea.

2.4.4 Large scale purification of proteins

A large scale purification of proteins was performed with the BioLogic DuoFlow Systems (BioRad, USA) and the Ni-NTA Superflow Column (Qiagen, Germany). This fast protein liquid chromatography (FPLC) procedure used a Ni²⁺-column for ion-chromatography. The system was equilibrated with 20ml of 20mM imidazole wash buffer at 5ml/min. The supernatant, collected from the production of bacterial or mammalian cells, was then loaded on to the column at a flow rate of 1ml/min. The flow through was collected as a control. After the loading, the column was washed with 20ml of 10mM imidazole washing buffer and 20ml of 12.5mM and sometimes with 5ml imidazole washing buffer to remove weakly or unspecificly bound proteins respectively.

The washes were collected as a control. The column was eventually eluted with 20ml or more of 250mM imidazole elution buffer and individual 2ml fractions were collected. With the help of a UV absorbance graph chart where the fraction numbers were displayed, only the promising fractions were kept for dialysis.

2.4.5 Dialysis of protein samples

Imidazole was employed to elute the protein from the column. It interferes with ensuing experiments (such as those that use BCA) and potentially causes immunogenic reactions. For these reasons, it had to be removed by dialysis. In general, the dialysis was performed against PBS without $\text{Ca}^{2+}/\text{Mg}^{2+}$ in SnakeSkin® Pleated Dialysis Tubing (Thermo Fisher Scientific Inc., USA) for 24 hours at 4°C. The molecular weight cut off (MWCO) is 10K. At least one buffer change was carried out to achieve higher imidazole removal.

2.4.6 Bicinchoninic Acid (BCA) Protein assay

The concentration of purified proteins was determined with the BCA™ Protein Assay Kit (PIERCE, USA), according to manufacturer's manual. A reduction in copper ions by proteins resulting in color change of the reaction mixture, is the principle behind the assay. 200µl of bicinchoninic acid and Cu^{2+} ions were incubated with 25µl of protein samples at 37°C for 30 minutes. For comparison purposes, 7 standard dilutions of bovine serum albumin supplied with the kit were incubated at the same time. The absorbance of the solutions was measured at a wavelength of 560nm in the Victor 3V Multi-label counter (Perkin Elmer, USA) or the Benchmark plus Microplate reader (BioRad, USA). The concentration of the protein was calculated with Microsoft Office Excel by comparing the absorbance of the samples with those of the standards.

2.4.7 Analysis of protein samples using sodium dodecyl sulfate polyacrylamide gel electrophoresis (SDS-PAGE)

The SDS-PAGE is used to separate charged molecules such as proteins or DNA, mainly according to their size. SDS binds in a constant ratio per g protein and is highly negatively charged. In other words, the amount of SDS that can bind, and therefore the intensity of the negative charge developed by the protein, depends on its size, thus allowing a separation according to size, rather than charge.

All gels consist of a 4% acrylamide stacking gel on top of a 12% acrylamide separating gel (table 2-9, table 2-10). Both gels contain 0.1% (w/v) SDS. This composition causes a change in the running velocity of proteins. The stacking gel has a higher pore size and a pH-value of 6.8, while the separation gel has smaller pores with a pH-value of

8.8. The samples run faster through the stacking gel and get compressed by glycine molecules in the buffer, which causes the proteins to enter the separation gel in a sharp, tight packaged band, resulting in a higher separation resolution. The SDS-PAGE gels were set using the PROTEAN® 3 electrophoresis system (Bio-RAD, Germany) for 80 mm x 50 mm x 0.75 – 1.5 mm (height x length x width) gels. The protein samples were combined with 5x SDS sample loading buffer (300mM Tris-Cl, pH 6.8, 12% (w/v) SDS, 0.6% (w/v) bromophenol blue, 60% (v/v) glycerol, 600mM dithiothreitol) in a 4:1 ratio and incubated at 96°C for 5 minutes. The SDS-PAGE was carried out using the PowerPac Basic (BioRad, USA), filled with Tris-Glycine-SDS running buffer (25mM Tris, 192mM Glycine, 0.1% (w/v) SDS, pH 8.3). The samples were loaded into the wells of the stacking gel and subjected to 20mA. When the samples reached the separating gel, the current was increased to 30mA. 10µl of dual colour Precision Plus Protein™ standard (BioRad, USA) was added to mark protein sizes on the gel (paragraph adapted from Dr. Xiaowei Wang's PhD thesis).

Table 2-11: 4% stacking gel reaction mix.

Components	4 % gel
ddH ₂ O	3645 µl
1 M Tris-HCl (pH 8.8)	625 µl
acrylamide: Bis/Acrylamide (40 %)	650 µl
SDS 10 % (v/v)	50 µl
APS	25 µl
TEMED	5 µl
final volume	5 ml

Table 2-12: 12% SDS Gel reaction mix.

Components	12 % gel
ddH ₂ O	4290 µl
1 M Tris-HCl (pH 8.8)	2500 µl
acrylamide: Bis/Acrylamide (40 %)	3000 µl
SDS 10 % (v/v)	100 µl
APS	100 µl
TEMED	10 µl
final volume	10 ml

2.4.8 Analysis of protein samples with Coomassie brilliant blue G250 staining

SDS-PAGE gels were immersed in Coomassie stain (0.2% (w/v) Coomassie brilliant blue G250, 40% (v/v) ethanol, 10% (v/v) acetic acid for 1 hour. The Coomassie molecule attaches particularly to the hydrophobic regions of proteins and cause an absorption change leading to the blue staining of the proteins. Gels were destained in destaining solution (40 % (v/v) methanol, 10 % (v/v) acetic acid) until protein bands were easily distinguished. All images of SDS-PAGE gels were taken with the BioRad Universal HOOD II Gel-Doc system (BioRad, USA) analysed with the help of Quantity ONE software, version 4.5. (Paragraph adapted from Dr. Xiaowei Wang's PhD thesis)

2.4.9 Analysis of protein using western blotting

Proteins from SDS-PAGE (section 2.4.7) were transferred to a nitrocellulose membrane ImmobilonTM (Millipore, Bedford, MA, USA), 0.45µm pore size, using the tank blot device from Bio-Rad (BioRad, USA). Previous to blotting, the membrane was washed for 20 seconds in methanol and 5 minutes in ddH₂O. The membranes and gels were also equilibrated in transfer buffer for 15 minutes to provide shrinking since the transfer buffer contained methyl alcohol. Assembly of the transfer sandwich started with a pre-wetted fibre pad, which was placed on the transfer cassette. Onto that a pre-wetted filter paper was placed, over which the equilibrated gel was laid. A pre-wetted membrane covered the gel and another filter paper was put on top. Any air bubbles were removed gently by rolling them out with a glass tube. Finally, two fibre pads were placed on top before the cassette was closed. The tank was then filled with transfer buffer and a cooling unit (ice block) was placed in it. Transfer conditions were 110 Volts for 120 minutes to ensure a complete transfer (Paragraph adapted from Dr. Xiaowei Wang's PhD thesis).

2.4.10 Immunoreactions

Immunoreactions were used to detect specific proteins on a membrane. The membranes were first blocked to prevent unspecific binding of the antibodies. This was done by placing the membrane in solutions containing 1 % (w/v) BSA or non-fat dry milk, dissolved in PBS and 1% (v/v) Tween 20 (Sigma-Aldrich, USA) (PBS-Tween). The membranes were blocked overnight at 4°C under gentle shaking. Afterwards, the membranes were washed twice in the previously mentioned PBS-Tween mixture. They were then incubated with a specific horseradish peroxidase (HRP) and diluted to between 1:5,000 and 1:10,000 in PBS-Tween. Anti-6x His-tag antibody HRP was used to detect the protein construct, and streptavidin-HRP (BD Bioscience, USA) was used to determine the success of *in vivo* biotinylation of the protein construct. Subsequently, the membranes were washed three times for 10 minutes in PBS-Tween before incubation with the secondary antibody or final washing with PBS-Tween. The detection of the HRP coupled antibody was done using the SuperSignal West Pico Chemiluminescent Substrate (Thermo Fisher Scientific Inc., USA), an enhanced chemiluminescent (ECL) substrate for the HRP enzyme, according to the manufacturer's instructions, before imaging. HRP enzymes catalyse the reaction of H₂O₂ to H₂O by oxidation of luminol. The reaction emits a chemiluminescence light signal that can be detected. All Western blots were visualised on a light sensitive film or with the BioRad Universal HOOD II Gel-Doc system (BioRad, USA) (Paragraph adapted from Dr. Xiaowei Wang's PhD thesis).

2.4.11 Sortase-A reaction

The staphylococcus sortase-A enzyme recognises a LPXTG motive on a protein and effectively conjugates it to a nucleophile (polyglycininc). For the sortase reaction, the protein (scuPA with LPETG): peptide (Biotin): sortase ratio is 1:3:3 calculated to mols (molarity) respectively. CaCl²⁺ is added to a final concentration of 0.5mMol. Finally, a sortase assay buffer was used to top the final reaction volume up to 500µl. The mixture was incubated for 5 hours at 37°C, shaking at 750rpm.

2.4.12 Negative purification after Sortase A reaction

The scuPA with LPETG carries a His-Tag behind its LPETG motif. If the enzyme reaction is successful, everything behind the LPET is replaced by the peptide substrate (biotin). Therefore, only the unreacted protein still carries a His tag after the reaction. The sortase also possesses a His tag. Talon® beads (Clontech, USA) interact with the His tags and 'catch' those reagents leaving the supernatant merely with reacted

protein. For 1mg of protein, 500µl of Talon® beads were employed. The beads were equilibrated with the Talon® bead wash buffer (300mM NaCl; 30mM NaH₂PO₄; pH 7.0). Secondly, the composition was centrifuged for 5 minutes at 12000rpm and the supernatant was discarded. The wash steps were repeated at least 3 times before the protein was added onto the beads and incubated rolling overnight. The mixture was then spun at 12000rpm for 10 minutes again and the supernatant was collected. The supernatant was dialysed against PBS without Ca²⁺ and Mg²⁺ overnight using a 10 K MWCO membrane (Thermo Fisher Scientific, USA) to remove all unreacted biotin.

2.5 Blood collection

Blood was collected from healthy volunteers who had not taken any anticoagulant medication in the last 14 days. Citrate was used in the monovettes (Sarstedt, Germany) to anti-coagulate the blood.

2.5.1 Generation of platelet rich plasma (PRP)

A citrated whole blood sample was centrifuged at 180x g for 10 minutes. Acceleration was set to 4, and deceleration was set to 0, to stop the platelets from being activated in the centrifuge. The supernatant was carefully removed without disturbing the thin buffy coat layer of white blood cells.

2.6 Flow cytometry

Flow cytometry is a versatile method where a large number of cells can be quantified and analysed rapidly. Cell features, including cell surface receptors, cell size and cell granularity, as well as cell interactions and ligand-receptor interactions, can be studied. Flow cytometry is used abundantly in medical research, as well as general medical diagnostics (e.g. in human immunodeficiency virus (HIV) diagnostics, CD4 and CD8 ratio). It improved possibilities of diagnosing rare, inherited platelet disorders (Linden et al., 2004), such as Glanzmann thrombasthenia.

2.6.1 Parameters for analysis in flow cytometry

The two simple parameters in flow cytometry are forward scatter (FSC) and side scatter (SSC), which give information about cellular size and granularity. The FSC detector is aligned with the laser beam. When a cell passes through the beam, it diffracts the light according to its size. The larger the cell, the more photons are diffracted in line of the laser beam (forward) and thus, the more FSC is detected. The SSC detector recognises photons that were refracted in a 90° angle from the laser beam. The higher the granularity within the cell, the more light is scattered perpendicular (or sideways)

to the laser and the SSC value increases. Every cell type has a specific FSC, SSC profile and can thus be sorted with fluorescence-activated cell sorting (FACS). The other analysis parameter is fluorescence. Different flow cytometers vary in their amounts of lasers and therefore in the amount of absorbance they can detect in their channels. For every laser there is one channel. The concentration of photons detected by a photomultiplier tube in one channel is directly proportional to the amount of antibodies labelled with fluorescein isothiocyanate (FITC) or phycoerythrin (PE) on each cell. Hence, the more fluorescence detected, the more antibodies were bound to the cell.

2.6.2 Gating of cells on flow cytometry

In many flow cytometry experiments, the gating strategy is important for analysing subpopulations of interest and to minimise errors in measurements due to unspecific binding. A gate can be set as a numerical or graphical boundary, including, respectively excluding cells, with certain properties (especially used in FSC and SSC). According to the FSC/SSC dot-plots (where every blot represents a cell with a certain size and granularity), one can specifically choose a population. This compromises the advantage that e.g. apoptotic cells or cells with high unspecific binding will not be analysed. For standardisation purposes, the number of events in a gate can be set (in this thesis to 10,000).

2.6.3 Data analysis with histograms on flow cytometry

The histograms display one certain parameter on the x-axis (e.g. fluorescence in FL-1 channel) against the frequency of events on the y-axis. The mean intensity fluorescence (MFI) can be calculated according to the histogram distribution. The MFI was then further analysed with GraphPad Prism in order to test whether the binding of antibodies was significant or occurred by chance alone, and to test the *in vivo* biotinylation of scFv_{anti-LIBS}.

2.6.4 Flow cytometry of platelets with scFv_{anti-LIBS}

PRP was obtained as described earlier. It was diluted to a 1:20 ratio with 20µM PBS with Ca²⁺ and Mg²⁺. Half of the samples were stimulated with ADP, a potent platelet activator and incubated for 5 minutes before the scFv_{anti-LIBS} antibody was added (5µg/ml) to the stimulated and unstimulated PRP. After another 10 minutes of incubation, the secondary antibody Penta-His Alexa Fluor 488 Conjugate (Qiagen, Australia) or R-Phycoerythrin Streptavidin (Jackson ImmunoResearch Laboratories,

Inc., USA), as well as the controls (see below), were pipetted into the PRP samples and further incubated for 15 minutes in the dark. Samples were then fixated with cell-fix (BD Bioscience, USA) and stored for a maximum of 12 hours at 4°C before analysis with the BD FACSCalibur (BD Bioscience, USA).

Common Controls

First procaspase activating compound (PAC-1) (BD Bioscience, USA) (labeled for the FITC channel) recognizes an epitope of the activated GPIIb/IIIa and, in this way, acts as an inhibitor of fibrinogen mediated platelet aggregation. PAC-1 binding serves as a positive control for activated platelets. CD62P (BD Bioscience, USA) (labeled for the PE channel), the membrane glycoprotein P-selectin, is thought to mediate (among others) platelet leukocyte interactions. The protein is stored in alpha vesicles of platelets, is exposed on the membrane after platelet aggregation and can be thus used similarly to PAC-1. Secondary antibodies are commonly directed against usual protein motives employed in bio medical research, such as His tags, biotin, and can also be coupled to flourochromes. They are also tested on their own to show minimal or nonspecific binding. Isotype controls assess unspecific background binding of the antibody, e.g. occurring because of cross species reactions mediated by the constant region (Fc). The Fc region is determined by the species in which the antibody was produced. A murine Fc host might lead to activation of human blood cells and high background staining. The isotypes retain the unspecific properties of the host without being directed against specific fragment antigen-binding (Fab) targets.

2.7 Conjugation of proteins to microbubbles

Commercially available target-ready MBs from VisualSonics with streptavidin coated surface were used for this thesis (VisualSonics Inc., Canada), Perfluorocarbons stabilises the bubbles in the vial so that they can be stored for up to one year at 4°C. Once the vial is punctured and the gas escapes, the MBs must be used within the next 6 hours.

2.7.1 Conjugation of biotinylated scFv-AviTag and biotinylated scuPA construct to commercial streptavidin coated lipid microbubbles via biotin-streptavidin coupling

The microbubbles were mixed gently for 10 seconds, according to the manufacturer's manual. Conjugation of 20µg of biotinylated scFv_{anti-LIBS} and 20ug of scuPA biotin to 1.5×10^9 /ml of microbubbles was carried out at room temperature for 20 minutes. To remove the excess of unbound protein, a gradient purification was performed. The

purification was based on a gradient centrifugation procedure. The tips of 5ml disposable transfer pipettes were cut at the 1 ml mark. In order to use the transfer pipette for gradient centrifugation, they were inverted. The microbubbles are air-filled; therefore, they will float. 4.7ml of 20% (w/v) sucrose were added to the bulb of a transfer pipette. 1ml of microbubbles was added gently onto the top of the sucrose solution. Additional 1ml of PBS with Ca/Mg was added gently onto the top of the microbubbles. Transfer pipettes were centrifuged at 150 g for 5 minutes at 4°C. Whole microbubbles form a thin white layer at the top, while the infranatant would consist of fragments of destroyed microbubbles after gradient centrifugation. Transfer pipettes were clamped approximately 1mm to 2mm below the thin white layer. The cake layer was then resuspended and removed as purified products. scFv_{anti-LIBS}, scuPA conjugated microbubbles were stable for up to 6 hours at 4°C (paragraph adapted from Dr. Xiaowei Wang's PhD thesis).

2.7.2 Calculations of protein need for conjugation

One vial of MBs holds around 1.5×10^9 /ml Bubbles. The amount of protein added was in excess to the actual binding capacity of the MBs. 20µg of scFv_{anti-LIBS} and 20 µg of biotinylated scuPA was added to 1.5×10^9 /ml. The surface density of streptavidin was provided by the manufacturer, in which the microbubbles used throughout our study bear an average of 2700 streptavidin molecules per μm^2 of microbubble determined by ELISA and a functional immunoassay (manufacturer's data). Streptavidin is a tetramer, a binding capacity of 10800 biotinylated scFv molecules per μm^2 of microbubble surface was calculated. Takalkar et al. (Takalkar et al., 2004) found the average radius of a microbubble is 1.75µm, therefore the surface area of a microbubble is $9.6\mu\text{m}^2$. This gives a maximum of 103,908 binding sites per microbubble. This is in accordance with Takalkar et al. (Takalkar et al., 2004) who calculated a binding capacity of around 100,000 antibody molecules per microbubble. The company provided 1.5×10^9 microbubbles per vial and hence 1.6×10^{14} molecules of scFv_{anti-LIBS} will be sufficient to saturate all streptavidin binding sites. This equals to 8.5µg of scFv_{anti-LIBS} or 8.9µg of biotinylated scuPA and is sufficient to saturate all streptavidin binding sites on all the microbubbles in one vial. Therefore, with the 20µg of scFv_{anti-LIBS} and 20µg of biotinylated scuPA biotin used per vial, we are well above the saturating dose. All excess of antibody that was not conjugated could be easily removed by a washing step (paragraph adapted from Dr. Xiaowei Wang's PhD thesis).

2.8 *In vitro* assays

2.8.1 Urokinase activity assay with S2444X substrate

The urokinase activity was determined with a micro titre assay under the utilisation of S2444X (Chromogenix, Italy) chromogenic substrate. S2444X (Chromogenix, Italy) is meant to be specific for urokinase and allows conclusion on amidolytic effect on pyro-Glu-Gly-Arg-pNA (S2444X). According to the manufacturer, amidolytic activity can differ from the fibrinolytic activity of urokinases. Plasmin (0.05U/ml) is needed to convert the single chain into the more active two chain form of urokinase. In a final volume of 200µl, urokinase varying in concentration, 2.5ul to 18ul of plasmin (stock of 1U/ml), and assay buffer (38mmol/L of NaCl, 5 mmol/L of Tris-HCl, 0.1 % bovine serum albumin, pH 8.8) were incubated for 2 hours at room temperature under shaking. Following the incubation, 0.5mmol of chromogenic substrate S2444X (Chromogenix, Italy) was added and measurement began straight after with the Victor Multilabel Counter 1420 (PerkinElmer, Australia) or the Benchmark plus Microplate reader (BioRad, USA) for 1 hour. The activity was compared against a standard of commercially available urokinase (Medac, Hamburg, Germany) with 0 to 20 units in the same volume as the respective scuPA samples. Plasmin activation was not necessary.

2.8.2 Urokinase activity assay with S2251 substrate

The S2251 (Chromogenix, Italy) is a chromogenic substrate for the plasmin and, in turn, plasmin generated by plasminogen activators. Conversion of substrate by plasmin cleavage leads to a product which differs in optical density and hence can be measured with a photometer at 450nm. The conversion of plasminogen to plasmin was measured in a micro titre assay as follows; 400nmol/l of human plasminogen (Sigma-Aldrich, Germany) and 1mmol/l of S2251(Chromogenix, Italy) were incubated with different standard units of commercial urokinase (Medac, Hamburg, Germany) and amounts of urokinase. The samples were measured with the Benchmark plus Microplate reader (BioRad, USA) at 450nm every 60 seconds for 1 hour. The plate was shaking for 2 seconds before each reading and the microplate reader was heated to 37°C.

2.8.3 Fibrinolysis assay

100µl of PRP were pipetted into 96 well plates. A 50µl composition of premixed reagents was added. This mix included CaCl (final concentration 8mM, thromboplastin

(Siemens Healthcare Diagnostics Inc., USA; final dilution 1:50) and 20 μ M Thrombin Receptor Activator Peptide (TRAP, Sigma-Aldrich, Germany), leading to a strong platelet activation, as well as HEPES buffer to top up the volume. The mixture included furthermore either 100U/ml, 200U/ml commercial urokinase, an equivalent of 200U/ml commercial urokinase (calculated from the S2251 assay) of our urokinase construct or HEPES buffer control. Directly after the addition of the reagent composition to the 100 μ l of PRP, the plate was read in the Bio-Rad Benchmark Plus microplate reader at a wavelength of 405nm every minute for 1 hour at 37°C. Before each measurement, the plate was mixed for 2 seconds. Clot formation and its breakdown (% clot remaining) were measured over 60 minutes. Statistical analysis was performed in GraphPad 6. Prism.

2.8.4 Flow chamber adhesion assay

It is important to analyse the constructs additionally under flow conditions, proving its efficacy before the approach into an animal model. Key aspects in flow systems are shear stress and shear rate (which is additionally dependant on viscosity), as well as the coating of the chamber. Fibrin degradation and MB attachment were studied in the experiment. A glass capillary (Vitrotubes, USA) was coated with 100 μ g/ml collagen (Takeda, Austria) at 4 C° overnight; thereafter blocked with 1% BSA for 1 hour at 37°C. Whole blood anticoagulated with 3.2% w/v citrate that was supplemented with 60 μ g/ml Oregon Green Fibrinogen (Invitrogen, USA) was perfused at 500s⁻¹ for 11 minutes to form microthrombi stabilised with a fibrin network on the collagen fibres. The blood was reconstituted with 12mmol/L CaCl₂, 6mmol/L MgCl₂, 600 μ g/ml thromboplastin (Thromborel S; Siemens Healthcare, Germany) resulting in 2mmol/L free calcium through a second channel. Mixing was achieved along a merged end piece/channel owing to diffusion. The reconstituted whole blood perfusion was followed by perfusion of PBS with calcium and magnesium for 10 minutes. Because of the buoyancy of the microbubbles, the capillary was used inverted by placing the microthrombi side of glass capillary on top. A syringe pump (PhD 200, Harvard Apparatus, Holliston, USA) was used to perfuse the TT-MB dispersion or 7812.5U/ml commercial urokinase (as a positive control; 500U/g bodyweight is normally administered if human bolus administration is transferred to the mouse settings) through the flow chamber at defined shear rates. 1-2ml of TT-MBs (1 x 10⁶ /mL) or commercial urokinase were perfused continuously through the flow chamber at low shear rate (50s⁻¹). After initial minutes of low shear rate, the shear rate was decreased to 0s⁻¹ for incubation.

Experiments were visualised with IX81 Olympus microscope (Olympus, USA) and Cell^P 1692 (Analysis Image Processing) software, using brightfield and fluorescence imaging to take photos every minute for at least 15 minutes. Binding of microbubbles was analysed using Image J software.

2.9 Ultrasound

2.9.1 VisualSonics Vevo2100 – high frequency scanner for small animals

High frequency ultrasound images were acquired with a Vevo 2100 (VisualSonics, Toronto, ON, Canada) imaging system, using the 40MHz MS550D (55MHz maximal broadband frequency; 40MHz average frequency; 40µm axial resolution; 90µm lateral resolution; and 7.0 mm geometric focus) scanhead. Aquasonic® blue ultrasound transmission gel (Parker Laboratories, USA) was used in all ultrasound experiments. The imaging platform of the Vevo2100 imaging system allowed both the scanhead and the platform, on which the animal positioned, to be fixed. Therefore, the images were acquired at the exact focal plan. The imaging platform included a microscan transducer adaptor, where transducer was attached. This adaptor is connected to an imaging ball joint which allows movement in different angles. The microscan transducer stand allows adjustments from left to right, as well as movement of the transducer upwards and downwards (paragraph adapted from Dr. Xiaowei Wang's PhD thesis).



Figure 2-1: Vevo 2100 – high frequency scanner for small animals.

2.9.2 Imaging of the carotid artery with Vevo 2100

The 40MHz MS550D scanhead was used for the imaging of the carotid artery in mice. The MS550D is placed in the microscan transducer adaptor with its indicator positioned at 12 o'clock. In many cases, imaging of the carotid artery required the imaging platform where the mouse rested to be positioned flat and the scanhead was placed directly above the neck region of the mouse. Fine tuning of the position of the scanhead using the adjustable microscan transducer stand is required to obtain a clear image of the carotid artery. Both the imaging platform and the MS550D scanhead were locked in position, for the remaining of the study, after a clear image of the artery was available, reducing the chance of changes in the area of interest and eliminating operator error.

2.10 *In vivo* animal models

All experiments involving animals were approved by the Alfred Medical Research and Education Precinct Animal Ethics Committee. The amount of commercial uPA for injection was calculated according to units per gram (U/g) body weight of the animals. The animals were anaesthetised with ketamine (50mg/Kg, Parnell Laboratories, NSW, Australia) and xylazine (10mg/kg, Troy Laboratories, NSW, Australia). Fur was removed by shaving cream (Dove, Australia). Mice were placed on a 37°C heater mat to prevent hypothermia (paragraph adapted from X. Wang, J. Palasubramaniam, Y. Gkanatsas et al.).

2.10.1 Femoral vein catheterisation

An incision was made on the left or right limb of the animal and subcutaneous layers were dissected to expose the femoral vein. A catheter was placed into the femoral vein to facilitate injection (paragraph adapted from X. Wang, J. Palasubramaniam, Y. Gkanatsas et al.).

2.10.2 Ultrasound imaging of thrombolysis using the ferric chloride injury model

Ultrasound of animals was performed with a Vevo2100 high-resolution imaging system (VisualSonics Inc., Canada) using the 40MHz MS550D transducer. Animals were placed on the imaging station after ferric chloride induced injury was performed to induce a thrombus. A small filter paper (2mm x 1mm) saturated with 6% ferric chloride was placed under the left carotid artery of the animal for 3 min. Animals were injected with either LIBS-MBs with commercial uPA, TT-MBs, or LIBS-MBs with saline as vehicle control. Videos and images were acquired before, during and at several time

points after injecting 1.5×10^7 microbubbles in a total volume of 100 μ l. We injected a high dose 500U/g of commercial uPA (Medac, Germany), a low dose 75U/g of commercial uPA or saline as vehicle control. Repetitive ultrasound imaging sequences were performed every 5 min for 45 min after thrombolysis. Analysis was performed using the VisualSonics imaging software (VisualSonics Inc.). All experiments involving animals were approved by the Alfred Medical Research and Education Precinct Animal Ethics Committee (E/1406/2013/B) (adapted from X. Wang, Y. Gkanatsas et al.).

2.10.3 Assessment of bleeding time

An incision is made on the neck of the animal to reveal the left jugular vein. One minute after injecting the therapeutic construct or vehicle control, the tail of the animal was transected 5mm from the tip and submersed immediately into 37°C saline solution. The bleeding time was monitored and recorded as the time needed for the cessation of visible blood stream for 1 minute (paragraph adapted from X. Wang, J. Palasubramaniam, Y. Gkanatsas et al.).

2.11 Statistical analysis

All statistical analysis was performed in Graph Pad Prism, version 6.0. **p values** <0.05 were considerate significant. In general, a normal distribution was assumed. Data of 2 sets was analysed with the t-test. With more than 2 data sets a variance analysis (ANOVA) was employed.

2.11.1 S2251 assay:

The idea was that the straight incline around the iso 50 of the sigmoidal curve depicts the highest enzymatic conversion rate and linear regression could be easily calculated as the slope was linear around the adjacent values. Each experiment used triplicates. The highest value of the triplicate mean and the mean of the adjacent 5 higher values were averaged. The 50% value was searched in the data table. 10 (as opposed to 2) higher and lower values (of the triplicate mean) were chosen to minimise the error, ending with 21 values. The average of each 21 values over 3 experiments was calculated with Graph Prism and a linear slope plotted. From every standard and our construct, a slope value could be determined. The slope values were then plotted, now against the known enzymatic units of the standards in Excel ($R^2=0.97$). The equation of the linear regression could be used to find the units of our construct.

2.11.2 Flow cytometry:

Flow cytometry data were analysed with two-way ANOVA repeated measures, using the Bonferroni's multiple-comparison test. In the cases where only two groups were compared the t-test was employed.

2.11.3 In vivo thrombolysis:

Thrombi areas after thrombolysis were expressed in percentage as compared to initial area and analysis was performed using two-way ANOVA with Bonferroni correction for multiple testing.

2.11.4 In vivo bleeding time:

The assays were analysed with one-way repeated measures ANOVA with the Bonferroni post-test.

Chapter 3. Results

3.1 *In vitro* analysis of scFv_{anti-LIBS}

3.1.1 Production and purification

scFv_{anti-LIBS} was recuperated from the purified supernatant of *E. coli* (pAC6 vector). The western blot visualised the protein band at the expected height (Figure 3-1). The Western blot with streptavidin HRP suggests successful biotinylation of the scFv_{anti-LIBS} construct.

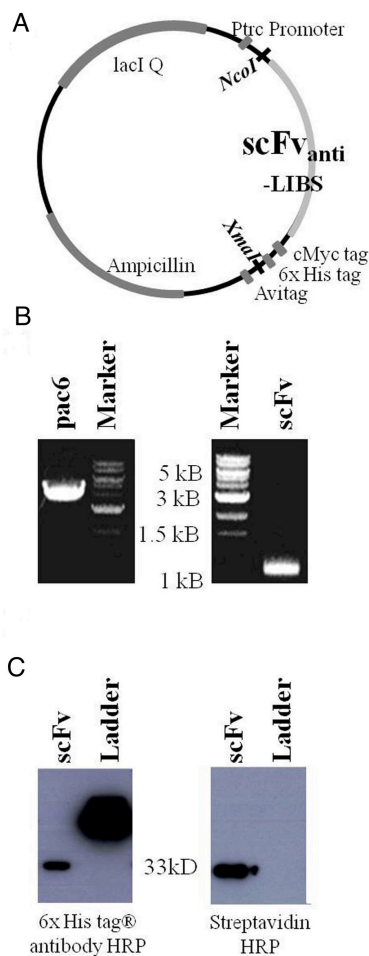


Figure 3-1: Successful production and purification of scFv_{anti-LIBS}.

(A) Vector map of scFv_{anti-LIBS} (B) Agarose Gel indicating heights of the pac6 vector and the scFv_{anti-LIBS} insert (C) On the western blot with streptavidin HRP, the biotinylated scFv_{anti-LIBS} band can be visualised at around 33kD. Anti 6x His-tag antibody HRP was also employed and served as a second control.

3.1.2 Evaluation of functionality by FACS-assay

Platelets were activated with ADP (Figure 3-4). The scFv_{anti-LIBS} exhibits binding to activated platelets in the FACS assay, in figure 3-3. In figure 3-2, the his-tag was targeted, which had allowed for purification of the protein. The successful biotinylation could be assessed with a streptavidin-antibody (similar to the evidence in the Western blot in figure 3-1). An exemplary graph of a single experiment showing exclusive binding of scFv_{anti-LIBS} to activated platelets is shown as a histogram (figure 3-5).

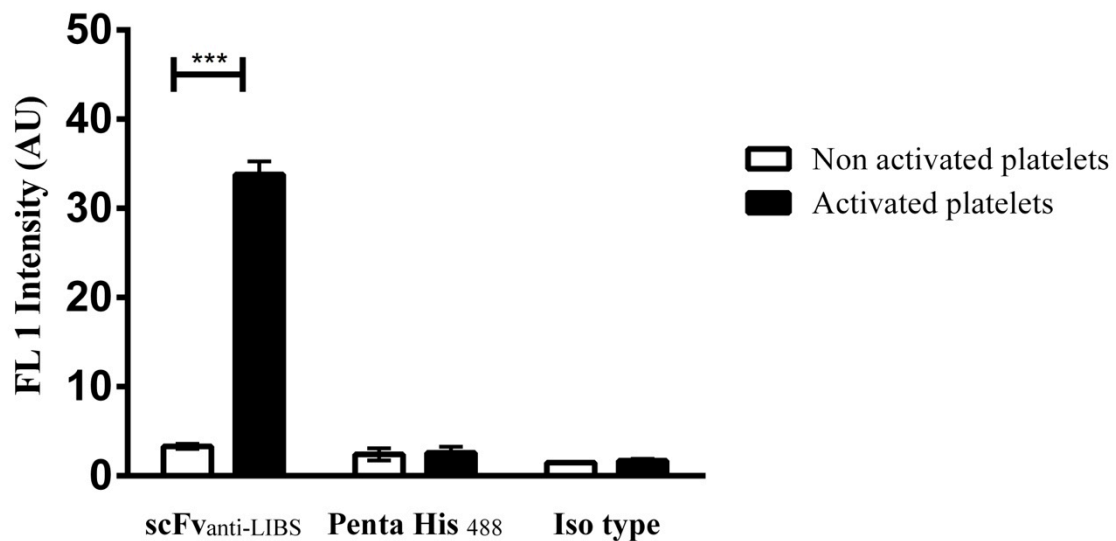


Figure 3-2: Binding of scFv_{anti-LIBS} to activated platelets.

The single-chain antibody shows binding toward activated, rather than non-activated platelets ($3.310 \pm \text{SEM}$ vs. $33.80 \pm \text{SEM}$, $***p < 0.001$, $n=3$). The Iso type control ($1.467 \pm \text{SEM}$ vs. $1.693 \pm \text{SEM}$, ns, $n=3$), as well as the Alexa Penta His 488 ($2.420 \pm \text{SEM}$ vs. $2.593 \pm \text{SEM}$, ns, $n=3$) control, did not show binding to non-activated nor activated platelets. Statistical analysis was performed with the mean fluorescence in FL-1 channel. The secondary antibody-target was the terminal His-tag on the single chain.



Figure 3-3: Binding of scFv_{anti-LIBS} to activated platelets.

The single-chain antibody shows binding toward activated, rather than non-activated platelets ($2.877 \pm \text{SEM}$ vs. $37.40 \pm \text{SEM}$, $**p < 0.01$, $n=3$). The Iso type control ($2.757 \pm \text{SEM}$ vs. $3.140 \pm \text{SEM}$, ns, $n=3$), as well as R-Phycoerythrin Streptavidin control ($3.370 \pm \text{SEM}$ vs. $3.733 \pm \text{SEM}$, ns, $n=3$), did not show binding to non-activated, nor activated platelets. Statistical analysis was performed with the mean fluorescence in FL-2 channel. The secondary antibody-target was the terminal biotin on the single chain.

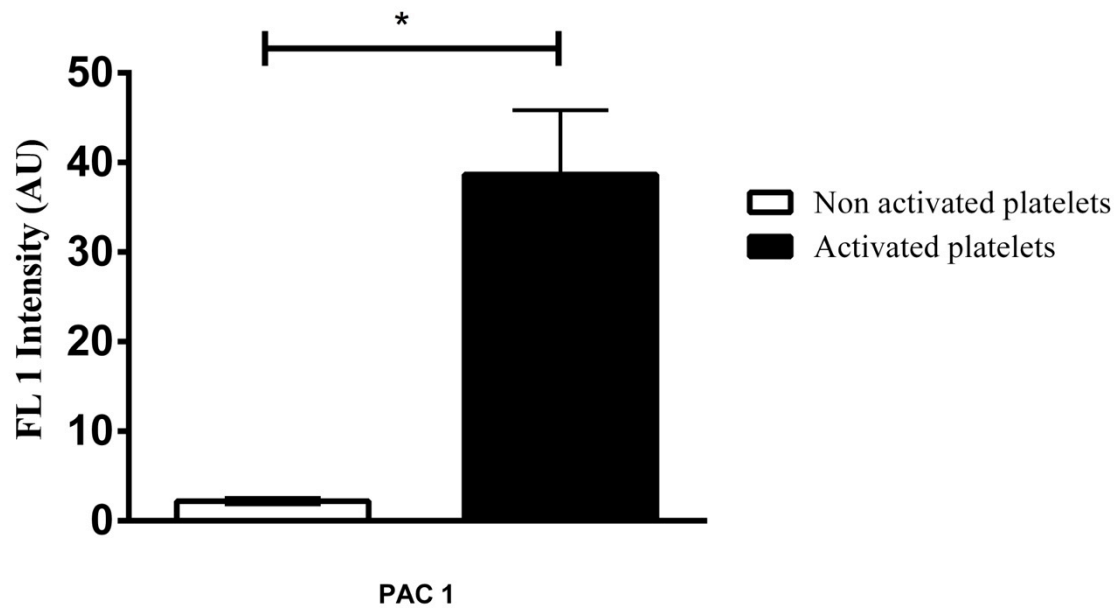


Figure 3-4: Proving platelet activation with PAC-1.

PAC-1 serves as a control for the commercial antibody, targeting activated platelets. The commercially available antibody presents a higher affinity to platelets, activated by ADP, than to normal, non-stimulated platelets (mean of difference $36.45 \pm \text{SEM}$, $*p < 0.05$, $n=3$).

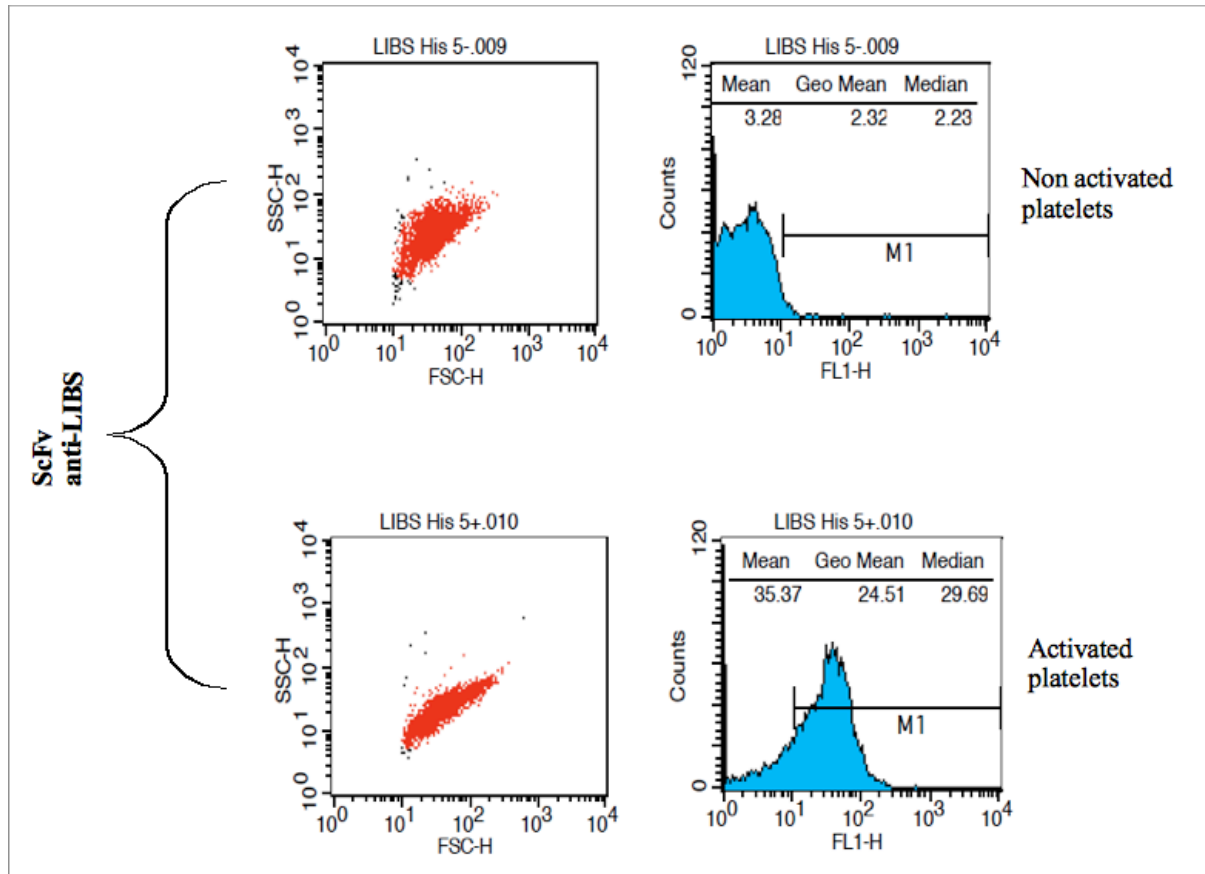


Figure 3-5: Histograms demonstrating binding of scFv_{anti-LIBS}.

Elongation in forward and side scatter of dot plot below was an indication for successful platelet stimulation. A clear shift in FL1-channel is achieved when incubating the scFv_{anti-LIBS} with activated platelets. Raw mean, geo mean and median values of all gated events are displayed above the blue histograms. Statistical analysis was performed on the means. M1 was set for orientation.

3.2 *In vitro* analysis of scuPA constructs:

3.2.1 Production and purification of scuPA (with LPETG tag) and biotinylated scuPA

The final urokinase on the TT-MB was biotinylated scuPA. Firstly, however scuPA with a LPETG tag was produced and then converted enzymatically to biotinylated scuPA. The DNA of scuPA (with a LPETG aminoacid ending to allow for consequent enzymatic biotinylation) was cloned successfully in the pSecTag2A for high expression in human embryonic kidney cells (HEK cells) (Figure 3-6, A-B). After the production and purification process the scuPA protein could be visualised with a 6x His tag antibody (Figure 3-6, C). After biotinylation a streptavidin HRP indicated the successful introduction of biotin to the end of the protein (Figure 3-6, C).

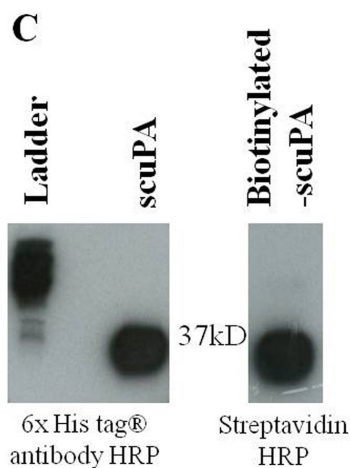
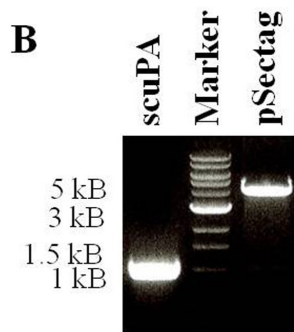
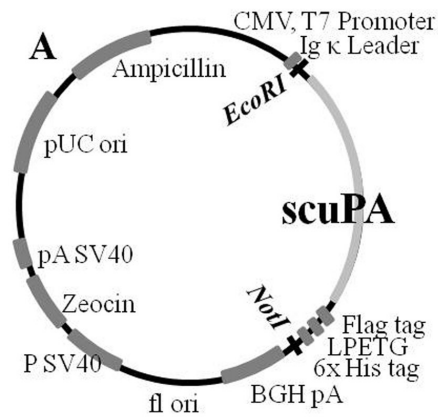


Figure 3-6: Vector map and gene work of scuPA as well as indication of successful biotinylation.

(A) Vector map of scuPA (with a lpetg tag) to allow for enzymatic sortase conjugation of biotin
 (B) The scuPA vector and the psectag expression vector on an agarose gel at their expected heights. (C) On the left a Western blot analysis with an HRP coupled 6x His tag antibody. scuPA is expected at the height of around 37kD. The sortase reaction lead to the product (biotinylated scuPA) and a loss of the terminal His tag. Thus, on the right, a Western blot was performed with horseradish peroxidase (HRP) streptavidin antibody directed against biotin.

3.2.2 Evaluation of functionality with S2251 substrate assay

Biotinylated scuPA was plotted against standards of commercial urokinase in a light transmission assay (enzymatic conversion of a particular substrate to yellow colour). More exactly, the mean of the slope around the iso 50 was plotted. Derived from the standard curve of the slope ($R^2 = 0.97$, Figure 3-7, C) enzymatic units per nmol of produced protein could be calculated. 10nmol of the biotinylated scuPA production were worth 0.7 enzymatic units.

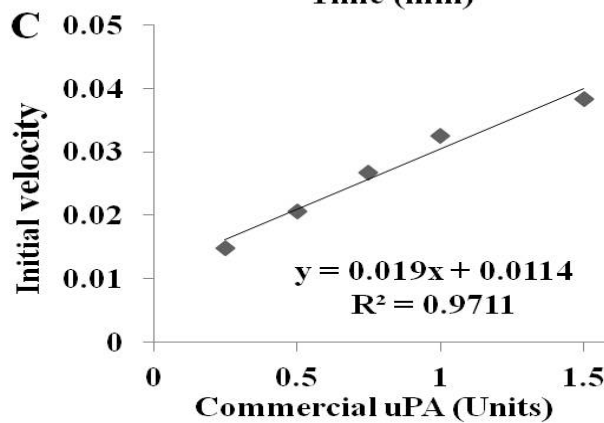
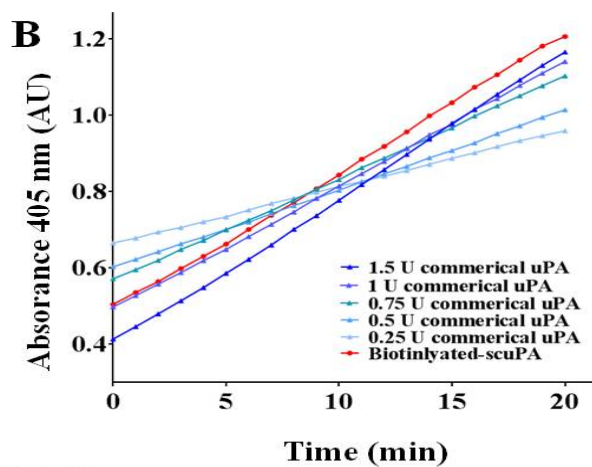
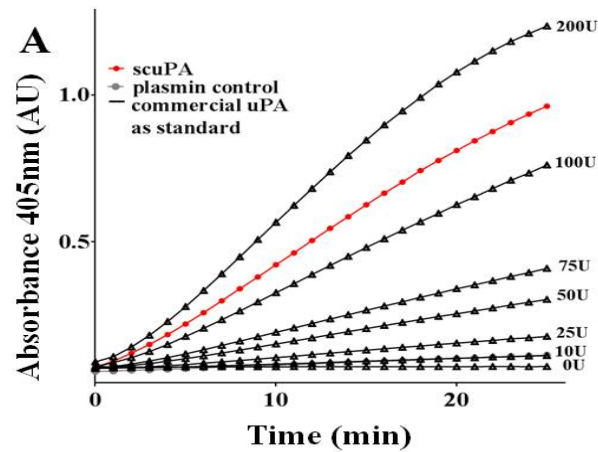


Figure 3-7: Assessment of amidolytic activity of the scuPA/biotinylated scuPA in light transmission assay (96 well plate).

(A) Measurement of activity in the light transmission assay by increase of absorption in the 405 nm wave length every minute over a period of 40 mins. The scuPA and commercial scuPA at different concentrations exhibit linear activity over time. (B) The conversion of plasminogen to plasmin was monitored with the S2251 assay. Biotinylated scuPA at 10nmol/L was compared against standards of commercial urokinase at different concentration. (C) Activity of biotinylated scuPA was calculated from the initial velocities obtained from lines fitted to data of time versus plasmin generated for the standards at a range of 0 to 1.5 units commercial urokinase.

3.2.3 Evaluation of fibrinolysis in microthrombi

Platelet rich plasma was stimulated to aggregate in a 96 well plate. Commercial scuPA and biotinylated scuPA were added to lyse the clot in vitro. Different concentration of commercial uPA and biotinylated scuPA showed thrombolytic activities. Time points 30 and 45 mins were chosen to compare fibrinolysis of the biotinylated scuPA construct against PBS control with a significant difference ($***p < 0.001$, SEM, $n = 5$). 200 U/ml commercial uPA and 400 U/ml were also tested as a control. They exhibit strong fibrinolytic potential as expected (Figure 3-8).

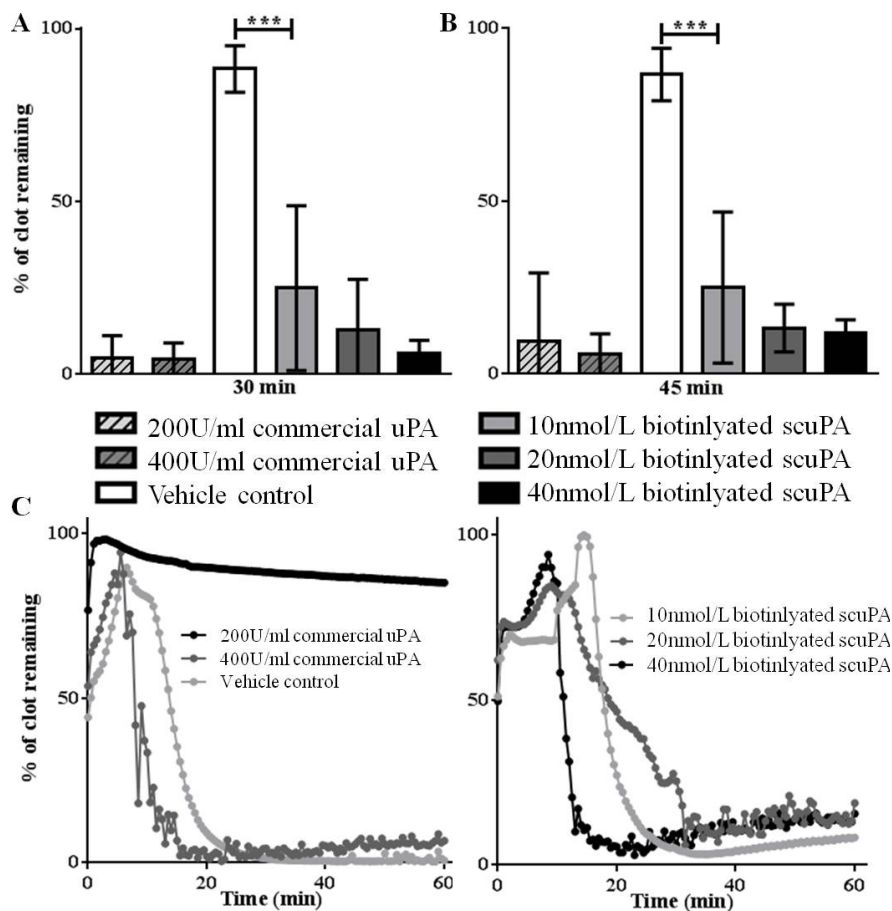


Figure 3-8: Fibrinolysis assay in a 96-well plate demonstrating successful thrombolysis with biotinylated scuPA.

(A) Bar chart showing % of clot remaining after 30 min of fibrinolysis. Commercial uPA at 200U/ml and 400U/ml showed strong fibrinolysis of clots as opposed to the control, which did not show any fibrinolysis ($n = 5$; $***p < 0.001$). The biotinylated scuPA at 10nmol/L, 20nmol/L and 40nmol/L also showed strong fibrinolysis as compared to the vehicle control ($n = 5$; $***p < 0.001$). (B) Bar chart showing % of clot remaining after 45 min of fibrinolysis with similar results to the 30 min time point. (C) Representative figures of the fibrinolysis assays are shown.

3.3 Testing of targeted theranostic microbubbles *in vitro* and *in vivo*:

3.3.1 Evaluation of adhesion in flow chamber

TT-MBs (coated with the biotinylated scuPA and scFv_{anti-LIBS} in a 1:1 ratio) bind to platelet aggregates under flow conditions (shear rate: 50s^{-1}) and stay attached during the time course of the experiment (at least 45 minutes) (Figure 3-9).

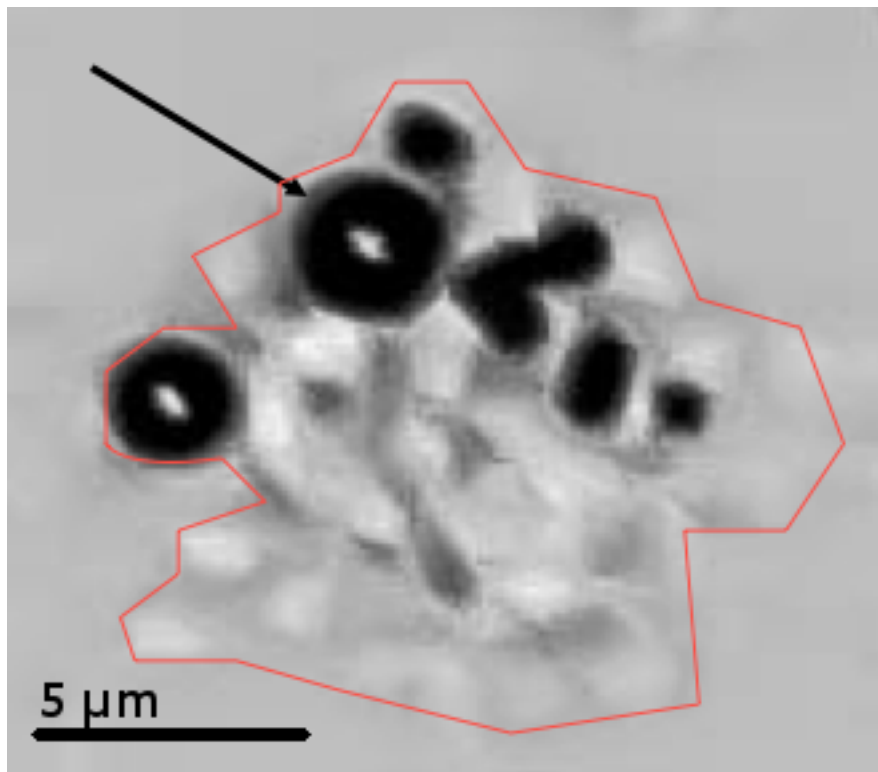


Figure 3-9: TT-MB adhesion to platelet aggregate.

Representative picture of flow chamber experiment at a shear rate of 50s^{-1} . The red line outlines the platelet aggregate and the black arrow is pointing to one microbubble (DIC, 32x magnification, Olympus IX81 Microscope).

3.3.2 Molecular ultrasound imaging of thrombolysis

Here, TT-MBs exhibit thrombolytic activity *in vivo*. They attach to the thrombus in the carotid artery of the mouse, increasing its visibility and allowing for the local reduction in thrombus size. A significant difference can be seen between the TT-MBs, using the targeted delivering strategy (red) and a separate infusion of a low concentration of commercial urokinase (75U/g) (** $p < 0.001$, SEM, $n \geq 3$) (Figure 3-10). LIBS-MB are infused at the same time to the application of low scuPA concentration to visualize the clot. In a similar regime, the high commercial urokinase concentration (500U/g) exhibit efficient fibrinolysis.

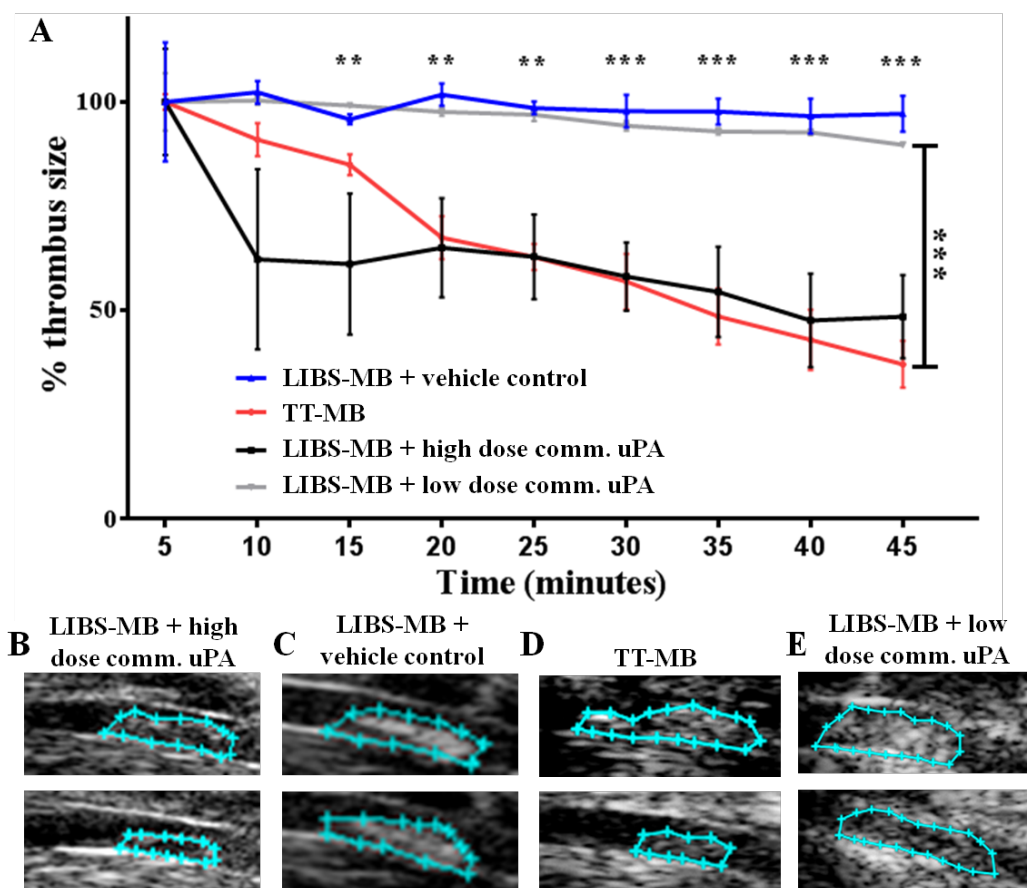


Figure 3-10: In vivo thrombolysis under ultrasound control.

(A) The reduction of thrombus size over time is displayed according to traced thrombus as shown in (B). Only high doses of commercial uPA (500U/g, black) achieve the same reduction as our TT-MB. The differences are caused due to the clot-localised fibrinolysis due to the targeting of our TT-MB. A significant difference (** $p < 0.001$, SEM, $n \geq 3$) can be seen between the controls and low dose commercial uPA regime (75U/g) (blue and grey) and the TT-MBs (red).

3.3.3 Assessment of bleeding time

High doses of commercial uPA increase the bleeding time in comparison with our TT-MBs. The bleeding risk is thus significantly lower with our new TT-MBs (Figure 3-11).

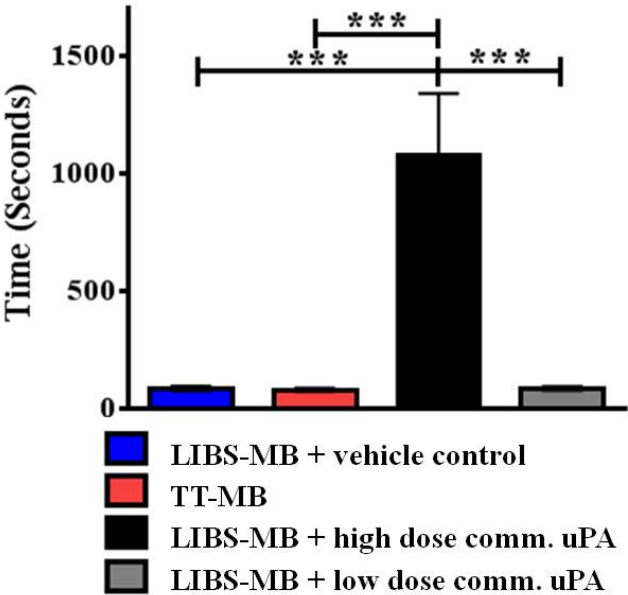


Figure 3-11: Assessment of bleeding risk of TT-MBs.

The TT-MB depict a similar bleeding time as a low dose uPA at 75U/g or negative control, where no uPA was added. The high dose commercial uPA at 500U/g exhibits a high bleeding risk (***) $p < 0.001$, SEM, $n=4$).

Chapter 4. Discussion

In this proof-of-concept study we demonstrated that our TT-MB attach to acute arterial thrombosis in an in vivo mouse model and lyse a thrombus simultaneously, importantly without an increased bleeding risk. Thus, we evolved the lab's previously published targeted diagnostic ultrasound approach (Wang et al., 2014) to a theranostic level. This new highly attractive approach implies a specific thrombus visualisation and direct therapeutic intervention, guaranteeing efficiency when a timely medical response is called for. The theranostic approach has attracted major attention in the recent years, as it led to the development of single agents with both diagnostic and therapeutic capabilities, promising individualised therapy with fewer side-effects. It allows for simultaneous diagnosis and treatment, and is a reliable and convenient method of monitoring the treatment outcome. We have applied the theranostic concept to the widely available, easy-to-use, non-invasive and affordable ultrasound method, which can be used in various clinical settings and would be therefore helpful for a great number of patients. The ultrasound signal enhancing MBs are for this transitionally attractive theranostic approach coated with a fibrinolytic agent and an activation specific single chain targeting antibody (scFv_{anti-LIBS}), forming TT-MBs. With the innovative scFv_{anti-LIBS}, TT-MB attachment merely occurs on *activated* platelets. Upon activation ligand induced binding sites are exposed on the most abundant platelet receptor (GPIIb/IIIa), to which the single chain selectively binds. Low-cost production, no expected immunogenicity due to lacking of Fc fragment, fast clearance from circulation and denser MB packing, due to its small size, warrant the use of the innovative single chain. Visualisation and monitoring of thrombus size is established by targeting the MBs, the clot-localised thrombolysis is subsequently initiated by the fibrinolytic agent (biotinylated scuPA), also conjugated on the surface of the ultrasound contrast-enhancing MB.

The ultrasound method has developed dramatically from a simple two-dimensional image to an advanced high-resolution 3D imaging platform. For further enhancement of the technique the MBs have been approved by the FDA in the US, as well as Europe and Canada for a number of echocardiographic and radiological indications (Unger et al., 2014). The employment of MBs as a vehicle became the basis for targeted ultrasound imaging, e.g. for functional characterisation of malignant angiogenesis without the need of invasive biopsy (Pysz et al., 2010). In particular, atherosclerotic lesions and expression of receptor profiles were studied by pioneering groups with this

technique (Kaufmann et al., 2010, Takalkar et al., 2004). Acknowledging the rapid development in ultrasound technology, the here-described, inherently real-time theranostic approach, without radiation risk, presents an alternative to other imaging platforms. In an aging population and financially burdened health care system with increasing costs, the theranostic approach could be valuable, as it could allow for an inexpensive and rapid diagnosis and treatment of acute thrombosis (occurring e.g. in myocardial infarction and stroke).

It is clear that thrombolysis is a beneficial therapy for many patients (Collen and Lijnen, 2009). However, a major drawback is the bleeding complication (Goldenberg et al., 2003). For a considerably large number of patients, this valuable therapy can therefore not be administered. The need for efficient novel reperfusion strategies has prompted the development and/or refinement of several approaches, including sonothrombolysis (Alexandrov et al., 2004; Molina et al., 2006; Nacu et al., 2015; Pagola et al., 2007; Tachibana and Tachibana, 1995; Xie et al., 2009a, 2009c) and targeted delivering therapy (Greineder et al., 2013; Hohmann et al., 2013; Wang et al., 2014; Zaitsev et al., 2010).

In 1995, Tachibana et al. presented first evidence of MBs accelerating thrombolysis (Tachibana and Tachibana, 1995). In a ground breaking Clotbust trial with 126 patients, Alexandrov et al. brought the approach to a clinical stroke setting, augmenting t-PA induced middle cerebral arterial recanalisation with transcranial Doppler ultrasound and MB infusion (Alexandrov et al., 2004). Molina et al. (Molina et al., 2006) and Pagola et al. (Pagola et al., 2007) reported enhanced thrombolysis in acute stroke patients with a similar approach. Recent study protocols aim to establish a safe procedure, and assess the effect of a pragmatic approach to t-PA therapy and additional MB Infusion with diagnostic ultrasound (Nacu et al., 2015).

Sonothrombolysis, incorporating the destruction of MBs through application of high mechanical indices and, in turn, highly negative peak pressures (sonoporation), achieve high patency rates e.g. in arterial thrombi in a preclinical study by Xie et al. (Xie et al., 2009a). In another excellent study, F. Xie et al. (Xie et al., 2009c) developed the usage of targeted MBs against GPIIb/IIIa on platelets, sonoporation and the consecutive infusion of urokinase following acute thrombotic coronary occlusions in swine with highly successful reperfusion. However, they did not investigate the safety in regards to the bleeding risks. Additionally, concerns about bio effects have been

raised concerning application of high mechanical indices, (Kutty et al., 2012) as undertaken in this study.

More recently, Hua et al. investigated targeted MBs with internal t-PA loading (Hua et al., 2014). This research group was able to reduce the amount of the fibrinolytic drug administered while still achieving sufficient thrombolysis with their clever method. The targeting agent a simple RGDS aminoacid sequence lacks in specificity. More importantly, the microbubbles must be shattered for drug release (sonoporation), consequently losing the ability to monitor the process.

Our unique approach, on the other hand, assembles the targeting and fibrinolytic agent on the surface of the microbubble, enabling clinicians to assess the therapeutic success or failure. Secondly, this new theranostic method is not dependant on high mechanical indices and the bursting of the bubbles (sonoporation), which has been regarded as a safety issue in the past. Thirdly, our highly specific single chain antibody selectively binds to activated platelets in contrast to other targeting strategies, for example RGDS and abicixmab (Alonso et al., 2007) which, on top of unspecific binding, can even lead to paradoxical platelet activation (Quinn et al., 2002).

Our TT-MBs could be used in various clinical settings. The most impact could certainly be achieved in myocardial infarction. A technique to rapidly diagnose coronary thrombi and safe thrombolysis has the potential to alter the outcome for MI patients. Furthermore, a timely decision on a therapeutic conversion to an angioplasty and stenting could be executed with the knowledge of the success or failure of the therapy. With an extensive availability of the ultrasound method, even in rural areas and ambulances, the theranostic microbubbles can potentially be administered easily in remote areas and early in the rescue chain.

4.1 Limitations

The coupling technique to the MBs with biotin-streptavidin incorporates an immunogenic potential. However, recently a drug using the streptavidin-biotin coupling strategy has been approved (Equinox Investigators, 2011). This method is convenient and adequate for this proof of concept study, however could, if needed, be replaced by other, non-immunogenic coupling techniques e.g. a sortase reaction or click chemistry (Moses and Moorhouse 2007).

Background clearance of unbound MBs commonly requires 5-10 minutes (Shim and Lindner 2014), but this is not a problem in our experimental settings. Additionally, actual real-time imaging is possible with “image-push-image” (Zhao et al., 2007).

The scFv_{anti-LIBS} antibody used in this study was successfully checked for cross reactivity (data not shown) in human blood clots and in vivo non-human primates, establishing a good basis for further transitional investigations.

Chapter 5. Summary

Thrombosis, leading to myocardial infarction and stroke, accounts for a large number of deaths and premature disability worldwide. Effective, systemically administered fibrinolysis comes with the major drawback of bleeding complications, hampering its broader use. To date, no non-invasive imaging technology for a rapid diagnosis of acute thrombosis exists, despite a significant medical need for a timely therapy.

In this preclinical proof of concept study, the aim was to combine diagnosis and bleeding-free therapy for thrombosis in a single 'theranostic' agent for a non-invasive, easy to use, radiation-free ultrasound setting.

We have produced targeted theranostic microbubbles (TT-MB) which comprise of ultrasound contrast enhancing agents (MB), single chain antibodies which specifically target activated platelets (scFV_{anti-LIBS}) and a fibrinolytic agent (biotinylated scuPA), the two latter of which are conjugated onto the surface of the bubble. After thorough, *in vitro* testing of the separate functionality of the single chain antibody and the fibrinolytic agent, TT-MBs were created. They bound to microthrombi, in an *in vitro* flow adhesion assay, showing successful adherence under shear stress. Additionally, we successfully proved that the TT-MB bind to ferric-chloride-induced thrombi in the carotid artery of the mouse *in vivo*, initiating therapeutic thrombolysis while enabling real time monitoring of the success or failure of thrombolysis via ultrasound B-mode imaging. The antibody mediated attachment allows for an efficient clot localised fibrinolysis. The localised potency of the fibrinolytic agent at the clot, and the subsequently low systemic concentration, notably prevented an increase in the overall bleeding risk in the *in vivo* mouse tail-bleed model, compared to a systemically administered, non-targeted fibrinolytic agent.

Overall, we have developed a unique agent for ultrasound, which is able to diagnose acute thrombosis and allow targeted thrombolytic treatment simultaneously, as well as to provide the opportunity to monitor its treatment in real time. This technology holds promise for a new technique in rapid diagnosis and bleeding-free thrombolysis, thereby potentially preventing the often devastating consequences of thrombotic disease in many patients. Therefore, this approach has the potential to be translated into clinical application.

The research findings have been published in Theranostic 2016 (impact factor 8.854), where I was equally contributing first author (see supplements).

5.1 Zusammenfassung

Thrombosen/Thrombembolien, die zum Myokardinfarkt oder Schlaganfall führen, sind weltweit für eine bedeutende Zahl von Todesfällen und vorzeitiger Behinderung verantwortlich. Vorhandene effektive, systemisch applizierte Fibrinolyse hat als erheblichen Nachteil Blutungskomplikationen, die einen häufigeren Gebrauch verhindern. Trotz des Bedarfs für eine zeitnahe Therapieeinleitung existiert bis heute keine nicht-invasive Bildgebung zur schnellen Diagnose einer akuten Thrombose/Thrombemboli.

In dieser präklinischen ‚Proof of Concept‘-Arbeit bestand die Zielsetzung darin, eine Kombination von Diagnose und blutungsfreier Therapie einer Thrombose durch einen alleinigen ‚theranostischen‘ Partikel in einem nicht-invasiven, einfach zu handhabenden Ultraschall-Setting ohne Strahlenbelastung zu erreichen.

Wir stellten ‚targeted theranostic Microbubbles (TT-MB)‘ her, die aus den ultraschallkontrastverstärkenden Partikeln (MB), scFv-Antikörperfragmenten, welche spezifisch aktivierte Thrombozyten binden (scFv_{anti-LIBS}) und einem fibrinolytischen Protein (biotinylierte scuPA) bestanden, wobei die beiden Letztgenannten auf die Hülle der MB konjugiert wurden. Nach gründlicher *in vitro* Testung der separaten Funktion des scFv-Antikörperfragments und des fibrinolytischen Proteins produzierten wir TT-MB. Diese banden an Mikrothromben in einem *in vitro* Fließ-Bindungs-Test, sodass eine erfolgreiche Bindung unter anliegenden Scherkräften gezeigt werden konnte. Darüber hinaus bewiesen wir, dass die TT-MB an Eisen-Chlorid-induzierten Thromben in der A. carotis der Maus *in vivo* binden, therapeutische Thrombolyse initiieren und eine gleichzeitige Beurteilung über Erfolg oder Misserfolg der Thrombolyse über das Ultraschall B-Bild erlauben. Die Antikörperfragment-vermittelte Bindung ermöglichte eine effiziente Thrombus-lokalisierte Fibrinolyse. Die lokalisierte Wirksamkeit des fibrinolytischen Agens an dem Thrombus und die dadurch geringe systemische Konzentration verhinderten insbesondere das Blutungsrisiko in dem *in vivo* Mausschwanz-Blutungsmodell im Vergleich zu der systemisch applizierten, nicht zielgerichteten Fibrinolyse.

Zusammenfassend haben wir also einen einzigartigen Partikel für den Ultraschall geschaffen, der es uns ermöglicht, eine akute Thrombose zu diagnostizieren und

simultan eine zielgerichtete thrombolytische Therapie einzuleiten. Dabei gibt der Partikel uns die Möglichkeit, die Behandlung zeitgleich zu überwachen. Die Technologie verspricht eine schnelle Diagnose und blutungsfreie Thrombolyse, infolgedessen könnten potentiell, oft schwerwiegende Konsequenzen einer Thrombosierung bei vielen Patienten verhindert werden. Deswegen kann unser Ansatz auch für eine klinische Anwendung in Betracht gezogen werden.

Diese wissenschaftlichen Ergebnisse wurden 2016 im *Theranostic Journal* (Impact Faktor 8,854) veröffentlicht. Dabei war ich geteilter Erstautor (siehe ‚supplements‘).

Chapter 6. List of abbreviations

Table 6-1: List of abbreviations.

5-HT	serotonin
ACS	acute coronary syndrome
ADP	adenosine diphosphate
aPTT	activated partial thromboplastin time
amp	ampicillin
AMREP	Alfred Medical Research and Education Precinct
Avb3	alpha-v beta-3
BBB	blood brain barrier
BCA	bicinchoninic acid
B-mode	brightness mode
bp	base pair
BSA	bovine serum albumin
CD	cluster of differentiation
CD62P	P-selection
CEA	carcinoembryonic antigen
CHD	coronary heart disease
COPD	chronic obstructive pulmonary disease
CT	computed tomography
CVD	cardiovascular disease
cys	cysteine
dB	decibel
ddH2O	double-distilled Milli-Q®-filtered water
DNA	deoxyribonucleic acid
ECM	extra cellular membrane
E. coli	Escherichia coli
e.g.	exempli gratia (lat.) = for example
et al.	et alii (lat.) = and other
Fab	fragment antigen-binding
FACS	fluorescence-activated cell sorting
Fc	fragment crystallisable constant
FDA	Food and Drug Administration
Fv	variable fragment
FITC	fluorescein isothiocyanate
FPLC	fast protein liquid chromatography
FSC	forward scatter
FXa	factor Xa
G-protein	guanine nucleotide binding protein
GP	glycoprotein
HCC	hepato cellular carcinoma
HEK293	human embryonic kidney 293 cells
His tag	hexahistidyl-tag
HIV	human immunodeficiency virus
HRP	horseradish peroxidase
Hz	hertz
Ig	immunoglobulins

IHD	ischemic heart disease
Il	Interleukin
Ile	Isoleucine
IMAC	immobilized metal chelate affinity chromatography
INR	international normalized ratio
IU	intensity unit
kb	kilo base
kD	kilo daltons
L	litre
LB	luria broth
LIBS	ligand-induced binding sites
LPS	lipopolysaccharides
Lys	lysine
MB	microbubbles
MFI	mean intensity fluorescence
MI	myocardial infarction
Mi	mechanical index
MPa	mega pascal
MRI	magnetic resonance imaging
mHz	megahertz
mm	millimetre
MWCO	molecular weight cut off
nm	nanometre
OD	optical density
oxLDL	oxidised LDL
P2Y	purinergic G protein-coupled
PAC-1	first procaspase activating compound
PAF	platelet activating factor
PAI	plasminogen activator inhibitor
PAR	proteinase-activated receptor
PBS	phosphate buffered saline
PCI	percutaneous coronary intervention
PCR	polymerase chain reaction
PE	phycoerythrin
PEG	polyethylene glycol
PEI	polyethylenimine
PET	positron emission tomography
PF-4	platelet derived factor 4
PGH ₂	prostaglandin H ₂
PRP	platelet-rich-plasma
RGD	arginine-glycine-aspartic acid
RGDS	arginine-glycine-aspartic-serine acid
RF	radiofrequency
rpm	rotations per minute
RF	radiofrequency
rpm	rotations per minute
RT	room temperature
SD	standard deviation
scFv	single-chain antibodies

scFv _{anti-LIBS}	LIBS binding scFv
scFv _{SCE5}	GP1Ib/IIIa blocking scFv
scuPA	single chain urokinase plasminogen activator
SDS-PAGE	sodium dodecyl sulfate polyacrylamide gel electrophoresis
SEM	standard error of the mean
SOB	super optimal broth
SOC	super optimal broth with catabolite repression
SSC	side scatter
TACE	transcatheter arterial chemoembolisation
TAFI	thrombin activatable fibrinolysis inhibitor
TAP	tick anticoagulant peptide
Taq	Thermococcus thermoquaticus
TF	tissue factor
THY	tryptone, yeast and HEPES
T _m	melting temperature
TNF α	tumour necrosis factor α
TT-MB	targeted theranostic Microbubbles
TVR	target vessel revascularisation
TXA ₂	thromboxane A ₂
μ g	microgram
μ l	microliter
μ m	micrometre
UI	uncertainty interval
UPA	urokinase plasminogen activator
u-PAR	urokinase plasminogen activator receptor
UV	ultraviolet
VCAM-1	vascular cell adhesion molecule-1
VEGFR-2	vascular endothelial growth factor receptor type-2
VH	variable heavy chain
VL	variable light chain
vWF	von Willebrand factor
w/v	weight per volume
WHO	world health organization

Chapter 7. Bibliography

Scientific papers:

- Adams, R.L., Bird, R.J., 2009**, Review article: Coagulation cascade and therapeutics update: relevance to nephrology. Part1: Overview of coagulation, thrombophilias and history of anticoagulants. *Nephrology (Carlton)* 14, 462-70.
- Ahmad, Z.A., Yeap, S.K., Ali, A.M., Ho, W.Y., Alitheen, N.B.M., Hamid, M., 2012.** scFv antibody: principles and clinical application. *Clin. Dev. Immunol.* 2012, 980250.
- Alberelli, M.A., De Candia, E., 2014.** Functional role of protease activated receptors in vascular biology. *Vascul. Pharmacol.* 62, 72–81.
- Alexandrov, A.V., Molina, C.A., Grotta, J.C., Garami, Z., Ford, S.R., Alvarez-Sabin, J., Montaner, J., Saqqur, M., Demchuk, A.M., Moyé, L.A., Hill, M.D., Wojner, A.W., CLOTBUST Investigators, 2004.** Ultrasound-enhanced systemic thrombolysis for acute ischemic stroke. *N. Engl. J. Med.* 351, 2170–2178.
- Alonso, A., Della Martina, A., Stroick, M., Fatar, M., Griebe, M., Pochon, S., Schneider, M., Hennerici, M., Allémann, E., Meairs, S., 2007.** Molecular imaging of human thrombus with novel abciximab immunobubbles and ultrasound. *Stroke* 38, 1508–1514.
- Alt, K., Paterson, B.M., Ardipradja, K., Schieber, C., Buncic, G., Lim, B., Poniger, S.S., Jakoby, B., Wang, X., O’Keefe, G.J., Tochon-Danguy, H.J., Scott, A.M., Ackermann, U., Peter, K., Donnelly, P.S., Hagemeyer, C.E., 2014.** Single-chain antibody conjugated to a cage amine chelator and labeled with positron-emitting copper-64 for diagnostic imaging of activated platelets. *Mol. Pharm.* 11, 2855–2863.
- Alzaraa, A., Gravante, G., Chung, W.Y., Al-Leswas, D., Bruno, M., Dennison, A.R., Lloyd, D.M., 2012.** Targeted microbubbles in the experimental and clinical setting. *Am. J. Surg.* 204, 355–366.
- Barnett, S.B., Ter Haar, G.R., Ziskin, M.C., Rott, H.D., Duck, F.A., Maeda, K., 2000.** International recommendations and guidelines for the safe use of diagnostic ultrasound in medicine. *Ultrasound Med. Biol.* 26, 355–366.
- Batra, S.K., Jain, M., Wittel, U.A., Chauhan, S.C., Colcher, D., 2002.** Pharmacokinetics and biodistribution of genetically engineered antibodies. *Curr. Opin. Biotechnol.* 13, 603–608.
- Beaton, C., Cochlin, D., Kumar, N., 2010.** Contrast enhanced ultrasound should be the initial radiological investigation to characterise focal liver lesions. *Eur. J. Surg. Oncol. J. Eur. Soc. Surg. Oncol. Br. Assoc. Surg. Oncol.* 36, 43–46.
- Behrens, M.A., Botkjaer, K.A., Goswami, S., Oliveira, C.L.P., Jensen, J.K., Schar, C.R., Declerck, P.J., Peterson, C.B., Andreasen, P.A., Pedersen, J.S., 2011.** Activation of the zymogen to urokinase-type plasminogen activator is associated with increased interdomain flexibility. *J. Mol. Biol.* 411, 417–429.

- Berger, D.H., 2002.** Plasmin/plasminogen system in colorectal cancer. *World J. Surg.* 26, 767–771.
- Borden, M.A., Sarantos, M.R., Stieger, S.M., Simon, S.I., Ferrara, K.W., Dayton, P.A., 2006.** Ultrasound radiation force modulates ligand availability on targeted contrast agents. *Mol. Imaging* 5, 139–147.
- Cesarman-Maus, G., Hajjar, K.A., 2005.** Molecular mechanisms of fibrinolysis. *Br. J. Haematol.* 129, 307–321.
- Chadderdon, S.M., Belcik, J.T., Bader, L., Kirigiti, M.A., Peters, D.M., Kievit, P., Grove, K.L., Lindner, J.R., 2014.** Proinflammatory endothelial activation detected by molecular imaging in obese nonhuman primates coincides with onset of insulin resistance and progressively increases with duration of insulin resistance. *Circulation* 129, 471–478.
- Chiang, C.W., Lin, F.C., Fu, M., Fang, B.R., Hsu, T.S., Lee, Y.S., 1986.** Importance of adequate gas-mixing in contrast echocardiography. *Chest* 89, 723–726.
- Collen, D., Lijnen, H.R., 2009.** The tissue-type plasminogen activator story. *Arterioscler. Thromb. Vasc. Biol.* 29, 1151–1155.
- Cosgrove, D., Harvey, C., 2009.** Clinical uses of microbubbles in diagnosis and treatment. *Med. Biol. Eng. Comput.* 47, 813–826.
- Culp, W.C., Porter, T.R., Lowery, J., Xie, F., Roberson, P.K., Marky, L., 2004.** Intracranial clot lysis with intravenous microbubbles and transcranial ultrasound in swine. *Stroke J. Cereb. Circ.* 35, 2407–2411.
- Del Maschio, A., Corvazier, E., Maillet, F., Kazatchkine, M.D., Maclouf, J., 1989.** Platelet-dependent induction and amplification of polymorphonuclear leucocyte lysosomal enzyme release. *Br. J. Haematol.* 72, 329–335.
- Del Maschio, A., Evangelista, V., Rajtar, G., Chen, Z.M., Cerletti, C., De Gaetano, G., 1990.** Platelet activation by polymorphonuclear leukocytes exposed to chemotactic agents. *Am. J. Physiol.* 258, H870-879.
- Duncan, P.B., Needham, D., 2004.** Test of the Epstein-Plesset model for gas microparticle dissolution in aqueous media: effect of surface tension and gas undersaturation in solution. *Langmuir ACS J. Surf. Colloids* 20, 2567–2578.
- Ellegala, D.B., Leong-Poi, H., Carpenter, J.E., Klibanov, A.L., Kaul, S., Shaffrey, M.E., Sklenar, J., Lindner, J.R., 2003.** Imaging tumor angiogenesis with contrast ultrasound and microbubbles targeted to alpha(v)beta3. *Circulation* 108, 336–341.
- Equinox Investigators, 2011.** Efficacy and safety of once weekly subcutaneous idrabiotaparinux in the treatment of patients with symptomatic deep venous thrombosis. *J. Thromb. Haemost. JTH* 9, 92–99.

- European Association For The Study Of The Liver**, European Organisation For Research And Treatment Of Cancer, 2012. EASL-EORTC clinical practice guidelines: management of hepatocellular carcinoma. *J. Hepatol.* 56, 908–943.
- Ferrara, K.**, Pollard, R., Borden, M., 2007. Ultrasound microbubble contrast agents: fundamentals and application to gene and drug delivery. *Annu. Rev. Biomed. Eng.* 9, 415–447.
- Friedman, G.**, Jankowski, S., Shahla, M., Goldman, M., Rose, R.M., Kahn, R.J., Vincent, J.L., 1996. Administration of an antibody to E-selectin in patients with septic shock. *Crit. Care Med.* 24, 229–233.
- Gessner, R.**, Dayton, P.A., 2010. Advances in molecular imaging with ultrasound. *Mol. Imaging* 9, 117–127.
- Go, A.S.**, Mozaffarian, D., Roger, V.L., Benjamin, E.J., Berry, J.D., Blaha, M.J., Dai, S., Ford, E.S., Fox, C.S., Franco, S., Fullerton, H.J., Gillespie, C., Hailpern, S.M., Heit, J.A., Howard, V.J., Huffman, M.D., Judd, S.E., Kissela, B.M., Kittner, S.J., Lackland, D.T., Lichtman, J.H., Lisabeth, L.D., Mackey, R.H., Magid, D.J., Marcus, G.M., Marelli, A., Matchar, D.B., McGuire, D.K., Mohler, E.R., Moy, C.S., Mussolino, M.E., Neumar, R.W., Nichol, G., Pandey, D.K., Paynter, N.P., Reeves, M.J., Sorlie, P.D., Stein, J., Towfighi, A., Turan, T.N., Virani, S.S., Wong, N.D., Woo, D., Turner, M.B., American Heart Association Statistics Committee and Stroke Statistics Subcommittee, 2014. Heart disease and stroke statistics--2014 update: a report from the American Heart Association. *Circulation* 129, e28–e292.
- Goldenberg, I.**, Matetzky, S., Halkin, A., Roth, A., Di Segni, E., Freimark, D., Elian, D., Agranat, O., Har Zahav, Y., Guetta, V., Hod, H., 2003. Primary angioplasty with routine stenting compared with thrombolytic therapy in elderly patients with acute myocardial infarction. *Am. Heart J.* 145, 862–867.
- Graham, F.L.**, Smiley, J., Russell, W.C., Nairn, R., 1977. Characteristics of a Human Cell Line Transformed by DNA from Human Adenovirus Type 5. *J. Gen. Virol.* 36, 59–72.
- Gramiak, R.**, Shah, P.M., 1968. Echocardiography of the aortic root. *Invest. Radiol.* 3, 356–366.
- Greco, N.J.**, Jamieson, G.A., 1991. High and moderate affinity pathways for alpha-thrombin-induced platelet activation. *Proc. Soc. Exp. Biol. Med. Soc. Exp. Biol. Med. N. Y.* N 198, 792–799.
- Greineder, C.F.**, Howard, M.D., Carnemolla, R., Cines, D.B., Muzykantov, V.R., 2013. Advanced drug delivery systems for antithrombotic agents. *Blood* 122, 1565–1575.
- Hagay, Y.**, Lahav, J., Levanon, A., Varon, D., Brill, A., Panet, A., 2006. Molecular characterization of an human monoclonal antibody that interacts with a

sulfated tyrosine-containing epitope of the GPIIb receptor and inhibits platelet functions. *Mol. Immunol.* 43, 443–453.

- Hagemeyer, C.E.**, Tomic, I., Jaminet, P., Weirich, U., Bassler, N., Schwarz, M., Runge, M.S., Bode, C., Peter, K., 2004. Fibrin-targeted direct factor Xa inhibition: construction and characterization of a recombinant factor Xa inhibitor composed of an anti-fibrin single-chain antibody and tick anticoagulant peptide. *Thromb. Haemost.* 92, 47–53.
- Hagemeyer, C.E.**, von Zur Muhlen, C., von Elverfeldt, D., Peter, K., 2009. Single-chain antibodies as diagnostic tools and therapeutic agents. *Thromb. Haemost.* 101, 1012–1019.
- Hansson, G.K.**, Libby, P., 2006. The immune response in atherosclerosis: a double-edged sword. *Nat. Rev. Immunol.* 6, 508–519.
- Hohmann, J.D.**, Wang, X., Krajewski, S., Selan, C., Haller, C.A., Straub, A., Chaikof, E.L., Nandurkar, H.H., Hagemeyer, C.E., Peter, K., 2013. Delayed targeting of CD39 to activated platelet GPIIb/IIIa via a single-chain antibody: breaking the link between antithrombotic potency and bleeding? *Blood* 121, 3067–3075.
- Hu, S.**, Shively, L., Raubitschek, A., Sherman, M., Williams, L.E., Wong, J.Y.C., Shively, J.E., Wu, A.M., 1996. Minibody: A Novel Engineered Anti-Carcinoembryonic Antigen Antibody Fragment (Single-Chain Fv-CH3) Which Exhibits Rapid, High-Level Targeting of Xenografts. *Cancer Res.* 56, 3055–3061.
- Hua, X.**, Zhou, L., Liu, P., He, Y., Tan, K., Chen, Q., Gao, Y., Gao, Y., 2014. In vivo thrombolysis with targeted microbubbles loading tissue plasminogen activator in a rabbit femoral artery thrombus model. *J. Thromb. Thrombolysis* 38, 57–64.
- Huo, Y.**, Schober, A., Forlow, S.B., Smith, D.F., Hyman, M.C., Jung, S., Littman, D.R., Weber, C., Ley, K., 2003. Circulating activated platelets exacerbate atherosclerosis in mice deficient in apolipoprotein E. *Nat Med* 9, 61–67.
- Idée, J.-M.**, Guiu, B., 2013. Use of Lipiodol as a drug-delivery system for transcatheter arterial chemoembolization of hepatocellular carcinoma: a review. *Crit. Rev. Oncol. Hematol.* 88, 530–549.
- Idee, J.-M.**, Louguet, S., Ballet, S., Corot, C., 2013. Theranostics and contrast-agents for medical imaging: a pharmaceutical company viewpoint. *Quant. Imaging Med. Surg.* 3, 292–297.
- Kastrati, A.**, Mehilli, J., Schühlen, H., Dirschinger, J., Dotzer, F., ten Berg, J.M., Neumann, F.-J., Bollwein, H., Volmer, C., Gawaz, M., Berger, P.B., Schömig, A., 2004. A Clinical Trial of Abciximab in Elective Percutaneous Coronary Intervention after Pretreatment with Clopidogrel. *N. Engl. J. Med.* 350, 232–238.

- Kaufmann, B.A.**, Carr, C.L., Belcik, J.T., Xie, A., Yue, Q., Chadderdon, S., Caplan, E.S., Khangura, J., Bullens, S., Bunting, S., Lindner, J.R., 2010. Molecular imaging of the initial inflammatory response in atherosclerosis: implications for early detection of disease. *Arterioscler. Thromb. Vasc. Biol.* 30, 54–59.
- Kelkar, S.S.**, Reineke, T.M., 2011. Theranostics: Combining Imaging and Therapy. *Bioconjug. Chem.* 22, 1879–1903.
- Killeen, S.D.**, Wang, J.H., Andrews, E.J., Redmond, H.P., 2009. Bacterial endotoxin enhances colorectal cancer cell adhesion and invasion through TLR-4 and NF-kappaB-dependent activation of the urokinase plasminogen activator system. *Br. J. Cancer* 100, 1589–1602.
- Klibanov, A.L.**, 2005. Ligand-carrying gas-filled microbubbles: ultrasound contrast agents for targeted molecular imaging. *Bioconjug. Chem.* 16, 9–17.
- Kruithof, E.K.**, Tran-Thang, C., Ransijn, A., Bachmann, F., 1984. Demonstration of a fast-acting inhibitor of plasminogen activators in human plasma. *Blood* 64, 907–913.
- Kutty, S.**, Wu, J., Hammel, J.M., Xie, F., Gao, S., Drvol, L.K., Lof, J., Radio, S.J., Therrien, S.L., Danford, D.A., Porter, T.R., 2012. Microbubble mediated thrombus dissolution with diagnostic ultrasound for the treatment of chronic venous thrombi. *PloS One* 7, e51453.
- Labinaz, M.**, Ho, C., Banerjee, S., Martin, J., Chen, S., Mensinkai, S., 2007. Meta-analysis of clinical efficacy and bleeding risk with intravenous glycoprotein IIb/IIIa antagonists for percutaneous coronary intervention. *Can. J. Cardiol.* 23, 963–970.
- Libby, P.**, 2002. Inflammation in atherosclerosis. *Nature* 420, 868–874.
- Lijnen, H.R.**, 2001. Elements of the fibrinolytic system. *Ann. N. Y. Acad. Sci.* 936, 226–236.
- Lindemann, S.**, Tolley, N.D., Dixon, D.A., McIntyre, T.M., Prescott, S.M., Zimmerman, G.A., Weyrich, A.S., 2001. Activated platelets mediate inflammatory signaling by regulated interleukin 1beta synthesis. *J. Cell Biol.* 154, 485–490.
- Linden, M.D.**, Frelinger, A.L., Barnard, M.R., Przyklenk, K., Furman, M.I., Michelson, A.D., 2004. Application of Flow Cytometry to Platelet Disorders. *Semin. Thromb. Hemost.* 30, 501–511.
- Lindner, J.R.**, 2009. Contrast ultrasound molecular imaging of inflammation in cardiovascular disease. *Cardiovasc. Res.* 84, 182–189.
- Lindner, J.R.**, 2004. Microbubbles in medical imaging: current applications and future directions. *Nat. Rev. Drug Discov.* 3, 527–532.

- Lindner, J.R.**, Song, J., Jayaweera, A.R., Sklenar, J., Kaul, S., 2002. Microvascular rheology of Definity microbubbles after intra-arterial and intravenous administration. *J. Am. Soc. Echocardiogr. Off. Publ. Am. Soc. Echocardiogr.* 15, 396–403.
- Mahaffey, K.W.**, Van de Werf, F., Shernan, S.K., Granger, C.B., Verrier, E.D., Filloon, T.G., Todaro, T.G., Adams, P.X., Levy, J.H., Hasselblad, V., Armstrong, P.W., 2006. Effect of pexelizumab on mortality in patients with acute myocardial infarction or undergoing coronary artery bypass surgery: a systematic overview. *Am. Heart J.* 152, 291–296.
- Mann, K.G.**, Brummel, K., Butenas, S., 2003. What is all that thrombin for? *J. Thromb. Haemost. JTH* 1, 1504–1514.
- Mann, K.G.**, Brummel-Ziedins, K., Orfeo, T., Butenas, S., 2006. Models of blood coagulation. *Blood Cells. Mol. Dis.* 36, 108–117.
- Martin, M.J.**, Chung, E.M.L., Goodall, A.H., Della Martina, A., Ramnarine, K.V., Fan, L., Hainsworth, S.V., Naylor, A.R., Evans, D.H., 2007. Enhanced detection of thromboemboli with the use of targeted microbubbles. *Stroke J. Cereb. Circ.* 38, 2726–2732.
- Massberg, S.**, Brand, K., Grüner, S., Page, S., Müller, E., Müller, I., Bergmeier, W., Richter, T., Lorenz, M., Konrad, I., Nieswandt, B., Gawaz, M., 2002. A Critical Role of Platelet Adhesion in the Initiation of Atherosclerotic Lesion Formation. *J. Exp. Med.* 196, 887–896.
- McEver, R.P.**, 2001. Adhesive interactions of leukocytes, platelets, and the vessel wall during hemostasis and inflammation. *Thromb. Haemost.* 86, 746–756.
- Molina, C.A.**, Ribo, M., Rubiera, M., Montaner, J., Santamarina, E., Delgado-Mederos, R., Arenillas, J.F., Huertas, R., Purroy, F., Delgado, P., Alvarez-Sabín, J., 2006. Microbubble administration accelerates clot lysis during continuous 2-MHz ultrasound monitoring in stroke patients treated with intravenous tissue plasminogen activator. *Stroke J. Cereb. Circ.* 37, 425–429.
- Moses, J.E., Moorhouse, A.D.**, 2007. The growing applications of click chemistry. *Chem Soc Rev.* 36, 1249–62.
- Nacu, A.**, Kvistad, C.E., Logallo, N., Naess, H., Waje-Andreassen, U., Aamodt, A.H., Solhoff, R., Lund, C., Tobro, H., Rønning, O.M., Salvesen, R., Idicula, T.T., Thomassen, L., 2015. A pragmatic approach to sonothrombolysis in acute ischaemic stroke: the Norwegian randomised controlled sonothrombolysis in acute stroke study (NOR-SASS). *BMC Neurol.* 15.
- Nassar, T.**, Sachais, B.S., Akkawi, S. 'ed, Kowalska, M.A., Bdeir, K., Leitersdorf, E., Hiss, E., Ziporen, L., Aviram, M., Cines, D., Poncz, M., Higazi, A.A.-R., 2003. Platelet factor 4 enhances the binding of oxidized low-density lipoprotein to vascular wall cells. *J. Biol. Chem.* 278, 6187–6193.

- Nurden, A.T.**, Nurden, P., 2014. Congenital platelet disorders and understanding of platelet function. *Br. J. Haematol.* 165, 165–178.
- Owen, W.G.**, Bichler, J., Ericson, D., Wysokinski, W., 1995. Gating of thrombin in platelet aggregates by pO₂-linked lowering of extracellular Ca²⁺ concentration. *Biochemistry (Mosc.)* 34, 9277–9281.
- Pagola, J.**, Ribo, M., Alvarez-Sabín, J., Lange, M., Rubiera, M., Molina, C.A., 2007. Timing of recanalization after microbubble-enhanced intravenous thrombolysis in basilar artery occlusion. *Stroke J. Cereb. Circ.* 38, 2931–2934.
- Pérez-Gómez, F., Bover R.**, 2007. The new coagulation cascade and its possible influence on the delicate balance between thrombosis and hemorrhage. *Rev. Esp. Cardiol.* 60:1217-9.
- Pysz, M.A.**, Foygel, K., Rosenberg, J., Gambhir, S.S., Schneider, M., Willmann, J.K., 2010. Antiangiogenic Cancer Therapy: Monitoring with Molecular US and a Clinically Translatable Contrast Agent (BR55)1. *Radiology* 256, 519–527.
- Quinn, M.J.**, Plow, E.F., Topol, E.J., 2002. Platelet glycoprotein IIb/IIIa inhibitors: recognition of a two-edged sword? *Circulation* 106, 379–385.
- Rijken, D.C., Lijnen, H.R.**, 2009. New insights into the molecular mechanisms of the fibrinolytic system. *J. Thromb. Haemost. JTH* 7, 4–13.
- Roffi, M.**, Mukherjee, D., 2008. Platelet glycoprotein IIb/IIIa receptor inhibitors--end of an era? *Eur. Heart J.* 29, 429–431.
- Roth, G.J.**, 1991. Developing relationships: arterial platelet adhesion, glycoprotein Ib, and leucine-rich glycoproteins. *Blood* 77, 5–19.
- Rychak, J.J.**, Klibanov, A.L., Ley, K.F., Hossack, J.A., 2007. Enhanced targeting of ultrasound contrast agents using acoustic radiation force. *Ultrasound Med. Biol.* 33, 1132–1139.
- Savage, B.**, Saldívar, E., Ruggeri, Z.M., 1996. Initiation of platelet adhesion by arrest onto fibrinogen or translocation on von Willebrand factor. *Cell* 84, 289–297.
- Schumann, P.A.**, Christiansen, J.P., Quigley, R.M., McCreery, T.P., Sweitzer, R.H., Unger, E.C., Lindner, J.R., Matsunaga, T.O., 2002. Targeted-microbubble binding selectively to GPIIb IIIa receptors of platelet thrombi. *Invest. Radiol.* 37, 587–593.
- Schwarz, M.**, Meade, G., Stoll, P., Ylanne, J., Bassler, N., Chen, Y.C., Hagemeyer, C.E., Ahrens, I., Moran, N., Kenny, D., Fitzgerald, D., Bode, C., Peter, K., 2006. Conformation-Specific Blockade of the Integrin GPIIb/IIIa A Novel Antiplatelet Strategy That Selectively Targets Activated Platelets. *Circ. Res.* 99, 25–33.
- Schwarz, M.**, Röttgen, P., Takada, Y., Gall, F.L., Knackmuss, S., Bassler, N., Büttner, C., Little, M., Bode, C., Peter, K., 2004. Single-chain antibodies for the

- conformation-specific blockade of activated platelet integrin $\alpha\text{IIb}\beta\text{3}$ designed by subtractive selection from naive human phage libraries. *FASEB J.* 18, 1704–1706.
- Shattil, S.J.**, Hoxie, J.A., Cunningham, M., Brass, L.F., 1985. Changes in the platelet membrane glycoprotein IIb/IIIa complex during platelet activation. *J. Biol. Chem.* 260, 11107–11114.
- Shi, H.**, Fu, C., Wang, W., Li, Y., Du, S., Cao, R., Chen, J., Sun, D., Zhang, Z., Wang, X., Zhu, X., 2014. The FGF-1-specific single-chain antibody scFv1C9 effectively inhibits breast cancer tumour growth and metastasis. *J. Cell. Mol. Med.*
- Shung, K.K.**, 2010. Ultrasound: Past, Present and Future, in: Toi, V.V., Khoa, T.Q.D. (Eds.), *The Third International Conference on the Development of Biomedical Engineering in Vietnam, IFMBE Proceedings*. Springer Berlin Heidelberg, pp. 10–13.
- Skyba, D.M.**, Price, R.J., Linka, A.Z., Skalak, T.C., Kaul, S., 1998. Direct in vivo visualization of intravascular destruction of microbubbles by ultrasound and its local effects on tissue. *Circulation* 98, 290–293.
- Shim, C.Y.**, **Lindner, J.R.**, 2014. Cardiovascular molecular imaging with contrast ultrasound: principles and applications. *Korean Circ J.* 44, 1-9.
- Smith, G.P.**, 1985. Filamentous fusion phage: novel expression vectors that display cloned antigens on the virion surface. *Science* 228, 1315–1317.
- Spraggon, G.**, Phillips, C., Nowak, U.K., Ponting, C.P., Saunders, D., Dobson, C.M., Stuart, D.I., Jones, E.Y., 1995. The crystal structure of the catalytic domain of human urokinase-type plasminogen activator. *Struct. Lond. Engl.* 1993 3, 681–691.
- Stone, G.W.**, Grines, C.L., Cox, D.A., Garcia, E., Tcheng, J.E., Griffin, J.J., Guagliumi, G., Stuckey, T., Turco, M., Carroll, J.D., Rutherford, B.D., Lansky, A.J., 2002. Comparison of Angioplasty with Stenting, with or without Abciximab, in Acute Myocardial Infarction. *N. Engl. J. Med.* 346, 957–966.
- Swers, J.S.**, Widom, A., Phan, U., Springer, T.A., Wittrup, K.D., 2006. A high affinity human antibody antagonist of P-selectin mediated rolling. *Biochem. Biophys. Res. Commun.* 350, 508–513.
- Szűjártó, C.**, Rossi, S., Waton, G., Krafft, M.P., 2012. Effects of perfluorocarbon gases on the size and stability characteristics of phospholipid-coated microbubbles: osmotic effect versus interfacial film stabilization. *Langmuir ACS J. Surf. Colloids* 28, 1182–1189.
- Tachibana, K.**, Tachibana, S., 1995. Albumin microbubble echo-contrast material as an enhancer for ultrasound accelerated thrombolysis. *Circulation* 92, 1148–1150.

- Takalkar, A.M.**, Klibanov, A.L., Rychak, J.J., Lindner, J.R., Ley, K., 2004. Binding and detachment dynamics of microbubbles targeted to P-selectin under controlled shear flow. *J. Control. Release Off. J. Control. Release Soc.* 96, 473–482.
- Tardy, I.**, Pochon, S., Theraulaz, M., Nanjappan, P., Schneider, M., 2002. In vivo ultrasound imaging of thrombi using a target-specific contrast agent. *Acad. Radiol.* 9 Suppl 2, S294-296.
- Thérroux, P.**, Armstrong, P.W., Mahaffey, K.W., Hochman, J.S., Malloy, K.J., Rollins, S., Nicolau, J.C., Lavoie, J., Luong, T.M., Burchenal, J., Granger, C.B., 2005. Prognostic significance of blood markers of inflammation in patients with ST-segment elevation myocardial infarction undergoing primary angioplasty and effects of pexelizumab, a C5 inhibitor: a substudy of the COMMA trial. *Eur. Heart J.* 26, 1964–1970.
- Thomas, P.**, Smart, T.G., 2005. HEK293 cell line: A vehicle for the expression of recombinant proteins. *J. Pharmacol. Toxicol. Methods, Electrophysiological Methods in Neuropharmacology* 51, 187–200.
- Turitto, V.T.**, Muggli, R., Baumgartner, H.R., 1977. Physical Factors Influencing Platelet Deposition on Subendothelium: Importance of Blood Shear Rate*. *Ann. N. Y. Acad. Sci.* 283, 284–292.
- Unger, E.**, Porter, T., Lindner, J., Grayburn, P., 2014. Cardiovascular drug delivery with ultrasound and microbubbles. *Adv. Drug Deliv. Rev.* 72, 110–126.
- von Elverfeldt, D.**, Maier, A., Duerschmied, D., Braig, M., Witsch, T., Wang, X., Mauler, M., Neudorfer, I., Menza, M., Idzko, M., Zirlik, A., Heidt, T., Bronsert, P., Bode, C., Peter, K., von Zur Muhlen, C., 2014. Dual-contrast molecular imaging allows noninvasive characterization of myocardial ischemia/reperfusion injury after coronary vessel occlusion in mice by magnetic resonance imaging. *Circulation* 130, 676–687.
- Wang, X.**, Hagemeyer, C.E., Hohmann, J.D., Leitner, E., Armstrong, P.C., Jia, F., Olschewski, M., Needles, A., Peter, K., Ahrens, I., 2012. Novel single-chain antibody-targeted microbubbles for molecular ultrasound imaging of thrombosis: validation of a unique noninvasive method for rapid and sensitive detection of thrombi and monitoring of success or failure of thrombolysis in mice. *Circulation* 125, 3117–3126.
- Wang, X.**, Palasubramaniam, J., Gkanatsas, Y., Hohmann, J.D., Westein, E., Kanojia, R., Alt, K., Huang, D., Jia, F., Ahrens, I., Medcalf, R.L., Peter, K., Hagemeyer, C.E., 2014. Towards effective and safe thrombolysis and thromboprophylaxis: preclinical testing of a novel antibody-targeted recombinant plasminogen activator directed against activated platelets. *Circ. Res.* 114, 1083–1093.
- Weber, C.**, Noels, H., 2011. Atherosclerosis: current pathogenesis and therapeutic options. *Nat. Med.* 17, 1410–1422.

- Weyrich, A.S.**, McIntyre, T.M., McEver, R.P., Prescott, S.M., Zimmerman, G.A., 1995. Monocyte tethering by P-selectin regulates monocyte chemotactic protein-1 and tumor necrosis factor-alpha secretion. Signal integration and NF-kappa B translocation. *J. Clin. Invest.* 95, 2297–2303.
- Wiman, B.**, Collen, D., 1978. Molecular mechanism of physiological fibrinolysis. *Nature* 272, 549–550.
- Wu, Y.**, Unger, E.C., McCreery, T.P., Sweitzer, R.H., Shen, D., Wu, G., Vielhauer, M.D., 1998. Binding and lysing of blood clots using MRX-408. *Invest. Radiol.* 33, 880–885.
- Xie, F.**, Lof, J., Everbach, C., He, A., Bennett, R.M., Matsunaga, T., Johanning, J., Porter, T.R., 2009a. Treatment of acute intravascular thrombi with diagnostic ultrasound and intravenous microbubbles. *JACC Cardiovasc. Imaging* 2, 511–518.
- Xie, F.**, Lof, J., Matsunaga, T., Zutshi, R., Porter, T.R., 2009b. Diagnostic ultrasound combined with glycoprotein IIb/IIIa-targeted microbubbles improves microvascular recovery after acute coronary thrombotic occlusions. *Circulation* 119, 1378–1385.
- Xie, F.**, Lof, J., Matsunaga, T., Zutshi, R., Porter, T.R., 2009c. Diagnostic Ultrasound Combined with Glycoprotein 2b/3a Targeted Microbubbles Improve Microvascular Recovery Following Acute Coronary Thrombotic Occlusions. *Circulation* 119, 1378–1385.
- Xiong, R.**, Soenen, S.J., Braeckmans, K., Skirtach, A.G., 2013. Towards Theranostic Multicompartment Microcapsules: in-situ Diagnostics and Laser-induced Treatment. *Theranostics* 3, 141–151.
- Yan, H.-L.**, Sun, S.-H., Wang, W.-T., Ding, F.-X., Mei, Q., Xue, G., 2007. Design and characterization of a platelet-targeted plasminogen activator with enhanced thrombolytic and antithrombotic potency. *Biotechnol. Appl. Biochem.* 46, 115–125.
- Yan, P.**, Chen, K.-J., Wu, J., Sun, L., Sung, H.-W., Weisel, R.D., Xie, J., Li, R.-K., 2014. The use of MMP2 antibody-conjugated cationic microbubble to target the ischemic myocardium, enhance Timp3 gene transfection and improve cardiac function. *Biomaterials* 35, 1063–1073.
- Yang, L.**, Sajja, H.K., Cao, Z., Qian, W., Bender, L., Marcus, A.I., Lipowska, M., Wood, W.C., Wang, Y.A., 2013. uPAR-targeted Optical Imaging Contrasts as Theranostic Agents for Tumor Margin Detection. *Theranostics* 4, 106–118.
- Zaitsev, S.**, Spitzer, D., Murciano, J.-C., Ding, B.-S., Tliba, S., Kowalska, M.A., Marcos-Contreras, O.A., Kuo, A., Stepanova, V., Atkinson, J.P., Poncz, M., Cines, D.B., Muzykantov, V.R., 2010. Sustained thromboprophylaxis mediated by an RBC-targeted pro-urokinase zymogen activated at the site of clot formation. *Blood* 115, 5241–5248.

Zhao, S., Kruse, D.E., Ferrara, K.W., Dayton P.A., 2007. Selective imaging of adherent targeted ultrasound contrast agents. *Phys Med Biol.* 52, 2055-72.

Monographs:

Maniatis T., Frisch, E.F., Sambrook, J., 1982. *Molecular cloning: a laboratory manual*, Cold Spring Harbor, New York.

Bhatt, D.L., 2008. *Platelets in Cardiovascular Disease*, Imperial College Press, London

Chapter 8. Acknowledgment

I want to thank a number of people as I come to the end of this journey 'dissertation'. First and foremost, I am very grateful to have received great supervision from Dr. Xiaowei Wang and Professor Karlheinz Peter in Melbourne, Australia. Their support, guidance and advice - especially in the difficult hours – will not be forgotten and always be appreciated. Dr. Wang has not only been a very helpful teacher and mentor, but has become a valued friend. The same must be said for Jan David Hohmann, who I could always approach with difficult matters. A particular appreciation is to be conveyed to Professor Thomas Eschenhagen. He was ready to support my dissertation endeavours in a foreign country from the beginning and provided unquestioning help whenever needed. All colleagues and friends from the laboratory in the Baker IDI must be mentioned, especially our highly esteemed lab assistant Joy Yao. Many thanks to Dr. Jathushan Palasubramaniam, my bench work buddy, whose humour and ideas are still in good memory. Finally, I would like to thank my beautiful family - my parents and sister - for their never ending support, including - of course - my partner and best friend, Sarah Bryan, for her proof reading and outstanding advice.

Chapter 9. Curriculum vitae

Entfällt aus datenschutzrechtlichen Gründen.

Entfällt aus datenschutzrechtlichen Gründen.

Chapter 10. Eidesstattliche Erklärung

Ich versichere ausdrücklich, dass ich die Arbeit selbständig und ohne fremde Hilfe verfasst, andere als die von mir angegebenen Quellen und Hilfsmittel nicht benutzt und die aus den benutzten Werken wörtlich oder inhaltlich entnommenen Stellen einzeln nach Ausgabe (Auflage und Jahr des Erscheinens), Band und Seite des benutzten Werkes kenntlich gemacht habe.

Ferner versichere ich, dass ich die Dissertation bisher nicht einem Fachvertreter an einer anderen Hochschule zur Überprüfung vorgelegt oder mich anderweitig um Zulassung zur Promotion beworben habe.

Ich erkläre mich einverstanden, dass meine Dissertation vom Dekanat der Medizinischen Fakultät mit einer gängigen Software zur Erkennung von Plagiaten überprüft werden kann.

Unterschrift:

A handwritten signature in black ink, appearing to read 'Sven Gunkel', written over a dotted line.

Chapter 11. Supplements

A. List of publications

- Wang*, X., **Gkanatsas*, Y.**, Palasubramaniam, J., Hohmann, J.D., Chen, Y.C., Lim, B., Hagemeyer, C.E., Peter, K. 2016, Thrombus-Targeted Theranostic Microbubbles: A New Technology towards Concurrent Rapid Ultrasound Diagnosis and Bleeding-free Fibrinolytic Treatment of Thrombosis. *Theranostics*. 6(5): 726–738.
 - *shared first authors
 - <https://www.ncbi.nlm.nih.gov/pubmed/27022419>
- Wang, X., Palasubramaniam, J., **Gkanatsas, Y.**, Hohmann, J.D., Westein, E., Kanojia, R., Alt, K., Huang, D., Jia, F., Ahrens, I., Medcalf, R.L., Peter, K., Hagemeyer, C.E., 2014. Towards effective and safe thrombolysis and thromboprophylaxis: preclinical testing of a novel antibody-targeted recombinant plasminogen activator directed against activated platelets. *Circ. Res.* 114, 1083–1093.
 - <https://www.ncbi.nlm.nih.gov/pubmed/24508759>

B. Thrombus-Targeted Theranostic Microbubbles: A New Technology towards Concurrent Rapid Ultrasound Diagnosis and Bleeding-free Fibrinolytic Treatment of Thrombosis

Theranostics 2016, Vol. 6, Issue 5

726



Theranostics

2016; 6(5): 726-738. doi: 10.7150/thno.14514

Research Paper

Thrombus-Targeted Theranostic Microbubbles: A New Technology towards Concurrent Rapid Ultrasound Diagnosis and Bleeding-free Fibrinolytic Treatment of Thrombosis

Xiaowei Wang^{1,2,✉*}, Yannik Gkanatsas^{1,3,✉*}, Jathushan Palasubramaniam¹, Jan David Hohmann¹, Yung Chih Chen¹, Bock Lim¹, Christoph E Hagemeyer^{1,4}, Karlheinz Peter^{1,2,4}

1. Baker IDI Heart & Diabetes Institute, Melbourne, Australia.
2. Department of Medicine, Monash University, Melbourne, Australia.
3. Department of Experimental Pharmacology and Toxicology, University Medical Center Hamburg-Eppendorf, Hamburg, Germany;
4. Department of Immunology, Monash University, Melbourne, Australia.

*Equally contributing first authors.

✉ Corresponding authors: Dr Xiaowei Wang; Prof Karlheinz Peter, Atherothrombosis & Vascular Biology, Baker IDI Heart and Diabetes Institute, 75 Commercial Road, Melbourne VIC 3004 Australia. Fax: +61(0)385321100, Tel: +61(0)385321495 Email: xiaowei.wang@bakeridi.edu.au; karlheinz.peter@bakeridi.edu.au.

© Ivyspring International Publisher. Reproduction is permitted for personal, noncommercial use, provided that the article is in whole, unmodified, and properly cited. See <http://ivyspring.com/terms> for terms and conditions.

Received: 2015.11.24; Accepted: 2016.02.08; Published: 2016.03.20

Abstract

Rationale: Myocardial infarction and stroke are leading causes of morbidity/mortality. The typical underlying pathology is the formation of thrombi/emboli and subsequent vessel occlusion. Systemically administered fibrinolytic drugs are the most effective pharmacological therapy. However, bleeding complications are relatively common and this risk as such limits their broader use. Furthermore, a rapid non-invasive imaging technology is not available. Thereby, many thrombotic events are missed or only diagnosed when ischemic damage has already occurred.

Objective: Design and preclinical testing of a novel 'theranostic' technology for the rapid non-invasive diagnosis and effective, bleeding-free treatment of thrombosis.

Methods and Results: A newly created, innovative theranostic microbubble combines a recombinant fibrinolytic drug, an echo-enhancing microbubble and a recombinant thrombus-targeting device in form of an activated-platelet-specific single-chain antibody. After initial *in vitro* proof of functionality, we tested this theranostic microbubble both in ultrasound imaging and thrombolytic therapy using a mouse model of ferric-chloride-induced thrombosis in the carotid artery. We demonstrate the reliable highly sensitive detection of *in vivo* thrombi and the ability to monitor their size changes in real time. Furthermore, these theranostic microbubbles proved to be as effective in thrombolysis as commercial urokinase but without the prolongation of bleeding time as seen with urokinase.

Conclusions: We describe a novel theranostic technology enabling simultaneous diagnosis and treatment of thrombosis, as well as monitoring of success or failure of thrombolysis. This technology holds promise for major progress in rapid diagnosis and bleeding-free thrombolysis thereby potentially preventing the often devastating consequences of thrombotic disease in many patients.

Key words: platelets, theranostics, thrombolysis, glycoprotein IIb/IIIa, microbubbles.

<http://www.thno.org>

Introduction

Cardiovascular diseases such as myocardial infarction (MI) and stroke are leading causes of death worldwide. The typical underlying pathology is the formation of thrombi and vessel occlusion either at the origin of thrombosis or at sites of embolization. One key contributor to thrombosis, especially in the case of MI, is atherosclerosis, which is driven by an inflammatory response caused by mechanisms such as oxidation and accumulation of lipids in the artery wall^{1,2}. This results in adhesion of activated platelets and monocytes at the site of vascular inflammation^{1,2}.

Although chronic atherosclerotic lesions can significantly obstruct the vessel lumen and thus reduce blood flow, most acute cases of MI and many cases of stroke are caused by plaque rupture triggering the exposure of thrombogenic material and inducing the activation of the coagulation cascade, platelet activation/aggregation, and subsequent vessel blockage^{3,4}. Many other cases of stroke are caused by embolization of thrombotic material that originates from ruptured atherosclerotic lesions or heart chambers in the setting of atrial fibrillation. This ultimately leads to vessel occlusion, a medical emergency, which requires timely diagnosis and immediate action to reperfuse the affected vessels and salvage the ischemic tissue.

There is clearly a significant medical need for the rapid diagnosis of acute thrombosis as, for example, in the case of coronary thrombosis leading to MI. So far there is no non-invasive imaging technology available that allows the detection of coronary thrombi. Our current work provides a unique approach for diagnosis and targeted therapy based on molecular ultrasound imaging. Among all imaging modalities, ultrasound has several advantages that prompted us to use it for the development of a unique theranostic approach. It is non-invasive, carries no radiation-associated risk, has no side-effects, and is inherently real time. Ultrasound scanners are highly portable and are already available in most hospitals. Therefore molecular ultrasound imaging could provide a safe, rapid, and cost-effective technique for detection of thrombosis⁵.

Platelets play a pivotal role in thrombosis, and the most abundant receptor expressed on the platelet surface is the glycoprotein (GP) IIb/IIIa complex, also known as integrin α IIb β 3 (CD41/CD61), which is the main fibrinogen/fibrin receptor-mediating platelet aggregation^{6,7}. When platelets are activated, GPIIb/IIIa undergoes a conformational change from a low-affinity to a high-affinity state, allowing the binding of fibrinogen, which leads to platelet aggregation and thrombus formation^{6,7}. These

features make GPIIb/IIIa an ideal target for both molecular imaging of thrombosis and delivery of thrombolytic drugs. We have developed conformation-specific anti-GPIIb/IIIa single-chain antibodies (scFvs), which bind specifically to a ligand-induced binding site (LIBS) on activated GPIIb/IIIa⁶⁻⁸, and thereby constitute a unique targeting tool for molecular imaging and targeted therapy of thrombosis.

We have previously demonstrated the ability of scFV_{anti-LIBS} to detect activated platelets in MRI⁹⁻¹² and PET¹³ for thrombosis and inflammation. We have also developed a non-invasive molecular ultrasound imaging method for the diagnosis of thrombosis¹⁴ via the conjugation of scFV_{anti-LIBS} onto ultrasound-enhancing microbubbles (MBs). These targeted MBs bind to activated GPIIb/IIIa receptors on activated platelets, thereby allowing real-time imaging of thrombosis, as well as monitoring of success or failure of pharmacological thrombolysis¹⁴. The advantages of such a rapid and accurate diagnosis would be greatly enhanced if non-invasive targeted thrombolysis could be performed concurrently using activated-platelet-targeted and drug-loaded MBs.

Non-invasive thrombolytic reperfusion use of plasminogen activators (PAs), such as streptokinase, tissue plasminogen activators (tPA), and urokinase plasminogen activators (uPAs), is available in current clinical settings. While these drugs are beneficial¹⁵, side-effects such as bleeding complications and neurotoxicity (in the case of tPA) have been described, thereby hampering their wide clinical use¹⁶. Past and ongoing substantial research efforts have focused on identifying new strategies to eliminate such complications. We have recently developed a promising approach using single-chain antibodies to deliver drugs to evolving or established blood clots, enabling enhanced and localized therapy with no or reduced risk of bleeding^{17,18}. We have demonstrated that our recombinant single-chain urokinase plasminogen activators (scuPA) result in efficient thrombolysis¹⁸.

Here we present a non-invasive theranostic (simultaneously diagnostic and therapeutic) approach for the diagnosis of thrombi, as well as fibrinolytic treatment and monitoring of success or failure of thrombolysis. By dual conjugation of both scFV_{anti-LIBS} and scuPA to form targeted theranostic microbubbles (TT-MBs), we demonstrate that these TT-MBs are well suited for diagnosis in molecular ultrasound imaging and for thrombolytic therapy of thrombi *in vivo* in the carotid artery of mice. These theranostic MBs allow the detection of reduced thrombus size triggered by their therapeutic payload. Overall, the presented

targeted molecular imaging approach has strong potential to be translated to clinical application in humans.

Methods

A detailed description of the methods is provided in the online-only Supplementary material.

Single-chain antibodies and single-chain urokinase plasminogen activator

The scFV_{anti-LIBS} construct was generated, expressed, and purified as previously described¹⁴. Briefly, the recombinant scuPA with an LPETG peptide motif at the C-terminus was cloned into the pSecTag2A vector system for expression in human embryonic kidney cells (HEK293F). The purity of the recombinant proteins was analyzed using SDS-PAGE and Western blotting. The addition of the LPETG motif allowed coupling of a GGG-biotin peptide to the scuPA construct using the recombinantly produced *S. aureus* transpeptidase sortase A^{19,20}.

Flow cytometry

Platelet-rich plasma (PRP) was obtained from healthy volunteers. Binding of scFV_{anti-LIBS} constructs, to either non-activated or activated platelets, was assessed by an AlexaFluor 488-coupled anti-His-tag antibody using a FACS Calibur (BD Bioscience, USA).

Enzymatic activity assays

Urokinase activity was determined with the S2444 and the conversion of plasminogen to plasmin with the S2251 chromogenic substrate (both Chromogenix, Italy). Comparison between clinically used uPA (Medac GmbH, Germany) and scuPA was made on the basis of equal urokinase activity.

Flow-chamber adhesion assay

Whole blood was perfused through glass capillaries, which were coated overnight with 100 µg/ml collagen. scFV_{anti-LIBS} and scuPA were added to target-ready microbubbles (VisualSonics Inc., Canada), to form targeted theranostic microbubbles (TT-MBs).

In vivo ultrasound molecular imaging in mice

All experiments involving animals were approved by the Alfred Medical Research and Education Precinct Animal Ethics Committee (E/1406/2013/B). Ultrasound of mice was performed with a Vevo2100 high-resolution imaging system (VisualSonics Inc., Canada). Thrombi were induced in the left carotid artery with a 6% ferric-chloride injury.

Assessment of tail bleeding time

The mouse tail was transected 5mm from the tip

and submersed in saline at 37°C. Bleeding time was determined as the time needed for the cessation of a visible blood flow for at least 1 min.

Statistical analysis

Data is expressed as mean ± standard error of the mean (SEM), unless otherwise specified. Flow cytometry and thrombolysis data were analyzed with two-way ANOVA repeated measures analysis using Bonferroni's multiple-comparison post-test.

Results

Cloning, purification, and biotinylation of scuPA constructs

The generation of a scuPA construct suitable for bioconjugation to microbubbles was achieved by the addition of an LPETG tag at the C-terminus of scuPA (Figure 1A). This five amino acid tag serves as a recognition sequence for the recombinantly produced *S. aureus* transpeptidase Sortase, which catalyzes a peptide bond formation with GGG-Biotin to scuPA-LPETGGG-Biotin^{19,20}. The success of DNA amplification, purification, and restriction digest of scuPA fragments was evaluated by agar gel electrophoresis. The construct was visualized in comparison to a marker after amplification with PCR and restriction digest (Figure 1B). The pSectag2A plasmid was visualized at ~ 5kb after restriction digest. After the scuPA construct was cloned into the pSectag2A plasmid, transformed, and purified, gel electrophoresis was performed. The sequence of the scuPA construct was confirmed via DNA sequencing. After production of scuPA, Western blotting was used to demonstrate successful purification (Figure 1C). Western blotting was also used to demonstrate successful biotinylation of the scuPA construct (Figure 1C).

Cloning, purification, and biotinylation of scFV_{anti-LIBS}

The scFV_{anti-LIBS} construct was cloned into a vector to incorporate a C-terminal AviTagTM, a tag that encodes the protein avidin, which enables the scFv to bind to biotin (Figure 1D). The success of DNA amplification, purification, and restriction digest was evaluated by agarose gel electrophoresis (Figure 1E). After production of scFv, Western blotting was used to demonstrate successful purification and *in vivo* biotinylation of the recombinant protein (Figure 1F).

Proof of function of scuPA constructs

Urokinase activity was monitored by incubating scuPA with urokinase substrate S2444L (Figure 2A) in comparison with commercial uPA. The scuPA construct and standards using commercial uPA at

different concentrations resulted in linear enzymatic activity over 40 min. Conversion of plasminogen to plasmin was monitored using the S2251 amidolytic assay (Figure 2B). The activity of plasmin generation of 10nmol/L of scuPA-biotin was compared against standards using commercial uPA (0U-2000U/ml). The standards were plotted on a graph and fitted with a linear regression, from which we obtained the equation to calculate and convert the activity of scuPA-biotin (Figure 2C).

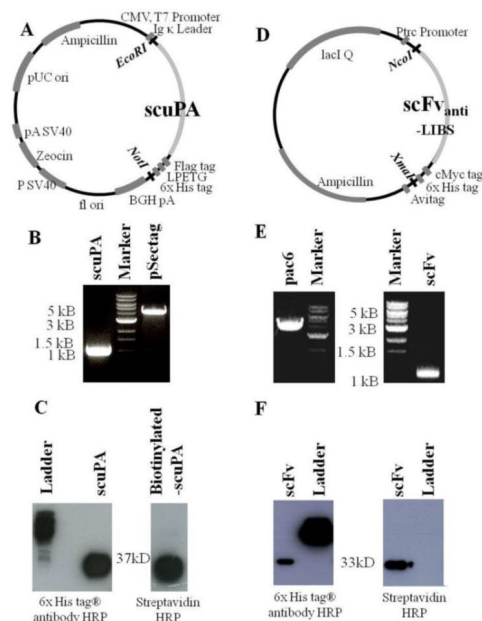


Figure 1: Vector-map, generation and purification of scuPA and scFv_{anti-LIBS} for microbubble conjugation. A. Gene-map of scuPA in pSectag2A vector for mammalian expression. The restriction enzymes used to insert the construct are EcoRI and NotI. B. Electrophoresis with 0.8% agarose gel: pSectag2A plasmid (5137bp) after double cut restriction digest, and scuPA (924bp) after polymerase chain reaction amplification. C. Western blot analysis of scuPA after protein purification detected with an HRP-coupled anti-6x His-tag antibody, and proof of successful biotinylation of scuPA via Sortase A enzyme as detected using streptavidin HRP. D. Gene-map of scFv_{anti-LIBS} in pAC6 vector for biotinylation. The restriction enzymes used to insert the construct are NcoI and XmaI. E. Electrophoresis with 0.8% agarose gel: pAC6 plasmid (4186bp) after double cut restriction digest, and scuPA (925bp) after polymerase chain reaction amplification. F. Western blot analysis of scFv_{anti-LIBS} after protein purification detected with an HRP-coupled anti-6x His-tag antibody and proof of biotin on the scFv_{anti-LIBS} as detected using streptavidin HRP.

In vitro proof of fibrinolytic potential of scuPA-biotin

Fibrinolysis in a 96-well plate assay was performed to determine the ability of the recombinant biotinylated scuPA to break down clots. Clot formation and clot breakdown were measured over 60

min (% of clot remaining). At 30 min, commercial uPA at 200U/ml and 400U/ml showed strong fibrinolysis of clots as compared to the vehicle control (Figure 3A; 4.839 ± 2.42 vs. 4.289 ± 1.7 vs. 88.32 ± 2.76, respectively; % clot remaining ± SEM; n=5; p<0.001). At 30 min, biotinylated scuPA at 10nmol/L, 20nmol/L, and 40nmol/L also showed strong fibrinolysis as compared to the vehicle control (Figure 3A; 25 ± 11.92 vs. 13.03 ± 5.89 vs. 6.125 ± 1.34; n=5; p<0.001). Similar results were obtained at 45 min (Figure 3B & 3C; n=5).

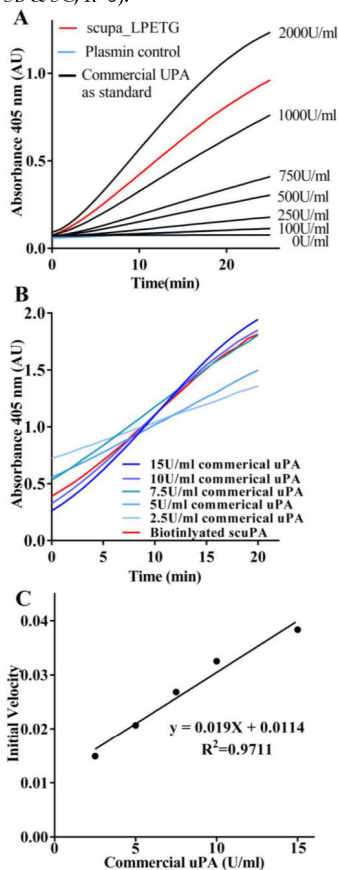


Figure 2: Proof of function of scuPA constructs. A. Urokinase activity assay of scuPA on 96-well plates using urokinase substrate S2444L. Increase of absorption at 405nm was measured over a 40 min period. ScuPA and standards using commercial uPA at different concentrations resulted in linear enzymatic activity. B. Plasminogen conversion assay of scuPA on 96-well plates using S2251 amidolytic assay. The conversion of plasminogen to plasmin was monitored with the S2251 amidolytic assay. Generation of plasmin for scuPA at 10nmol/L was compared against standards of commercial uPA at different concentration. Increase of absorption at 405nm was measured over a 40 min period. C. Activity of scuPA was calculated from the initial velocities obtained from lines fitted to data of time versus plasmin generated for the standards at a range of 0 to 15U/ml commercial uPA.

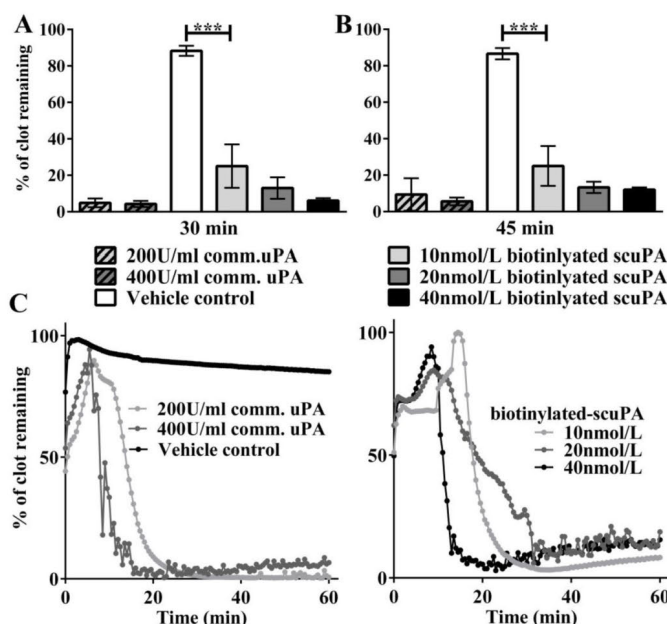


Figure 3: Fibrinolysis assay in a 96-well plate demonstrating successful thrombolysis with biotinylated scuPA. **A.** Bar chart showing % of clot remaining after 30 min of fibrinolysis. Commercial uPA at 200U/ml and 400U/ml showed strong fibrinolysis of clots as opposed to vehicle control, which did not show any fibrinolysis (n=5; p<0.001). Biotinylated-scuPA at 10nmol/L, 20nmol/L and 40nmol/L also showed strong fibrinolysis as compared to the vehicle control (n=5; ***p<0.001). **B.** Bar chart showing % of clot remaining after 45 min of fibrinolysis. Similar results were obtained. **C.** Representative traces of the fibrinolysis assays are shown.

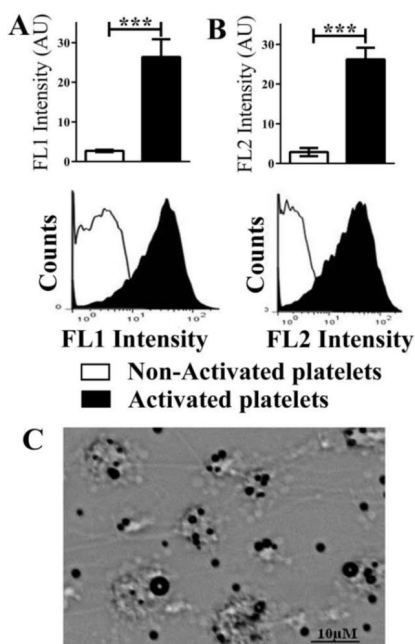


Figure 4: Flow cytometry demonstrating the functionality of scFv_{anti-LIBS} and efficiency of *in vivo* biotinylation. **A.** Functionality of scFv_{anti-LIBS} was proven with an AlexaFluor 488-coupled anti-Penta-His antibody in flow cytometry. Bar graphs depict the median fluorescence intensity values of five independent experiments. Representative fluorescence histograms are shown underneath the bar graphs. **B.** Functionality of scFv_{anti-LIBS} as well as the efficiency of *in vivo* biotinylation was evaluated using R-phycoerythrin streptavidin in flow cytometry (mean ± SD, ***p<0.001). These assays were analyzed using a paired t-test. **C.** Representative microscopy images of targeted-theranostic microbubbles (TT-MBs) attached to activated platelets on microthrombi in a flow chamber experiment.

In vitro binding of scFv_{anti-LIBS} constructs as assessed by flow cytometry

After the production of scFv_{anti-LIBS}, its binding capacity in relation to ADP-activated platelets was evaluated with an AlexaFluor 488-coupled anti-Penta-His antibody and R-phycoerythrin streptavidin in flow cytometry (Figure 4A & 4B). Incubation of ADP-activated platelets with scFv_{anti-LIBS} resulted in an increase in fluorescence intensity as compared to non-activated platelets (26.36 ± 4.46 vs 2.69 ± 0.29 AU; n=5; p<0.001) using an AlexaFluor 488-coupled anti-Penta-His antibody. Similar results were obtained when the efficiency of *in vivo* biotinylation and scFv functionality was determined using R-phycoerythrin streptavidin in flow cytometry (26.2 ± 2.95 vs 2.87 ± 1.05 AU; n=5; p<0.001). Dual

fluorescence staining for platelets using an anti-CD62P monoclonal antibody, and scFv_{anti-LIBS} using an AlexaFluor 488-coupled anti-Penta-His monoclonal antibody were performed to demonstrate the specific binding of scFv_{anti-LIBS} to activated platelets (Additional File 1: Supplemental Figure 1). In addition, dual fluorescence staining for platelets using PAC-1, and scFv_{anti-LIBS} using R-phycoerythrin streptavidin was performed to demonstrate the specific binding of scFv_{anti-LIBS} to activated GPIIb/IIIa receptors on activated platelets (Additional File 1: Supplemental Figure 1).

In vitro proof of attachment of targeted theranostic microbubbles to microthrombi

Flow-chamber adhesion assays were used to demonstrate the attachment of TT-MBs to microthrombi after the conjugation of scFv_{anti-LIBS} and scuPA to microbubbles (Figure 4C).

In vivo proof of theranostic molecular ultrasound imaging and simultaneous lysis of thrombi

Molecular ultrasound imaging was used to monitor thrombus size, particularly reduction in size. Ultrasound imaging of the mouse carotid artery on ultrasound typically shows luminal blood as black or dark grey, and microbubbles appear as a bright white color in the vessel lumen. Thrombi were visualized as white and bright signals after injection with platelet-targeted ultrasound contrast (LIBS-MB) on real-time ultrasound imaging. The baseline area, obtained 5 min after injection, was set to 100%. Imaging was performed every 5 min for 45 min and the thrombus area was calculated. Mice were injected with either LIBS-MB and a vehicle control using saline (n=3), TT-MB (n=4), LIBS-MB, and a high dose of commercial uPA (n=3), or LIBS-MB and a low dose of commercial uPA (n=4) (Figure 5).

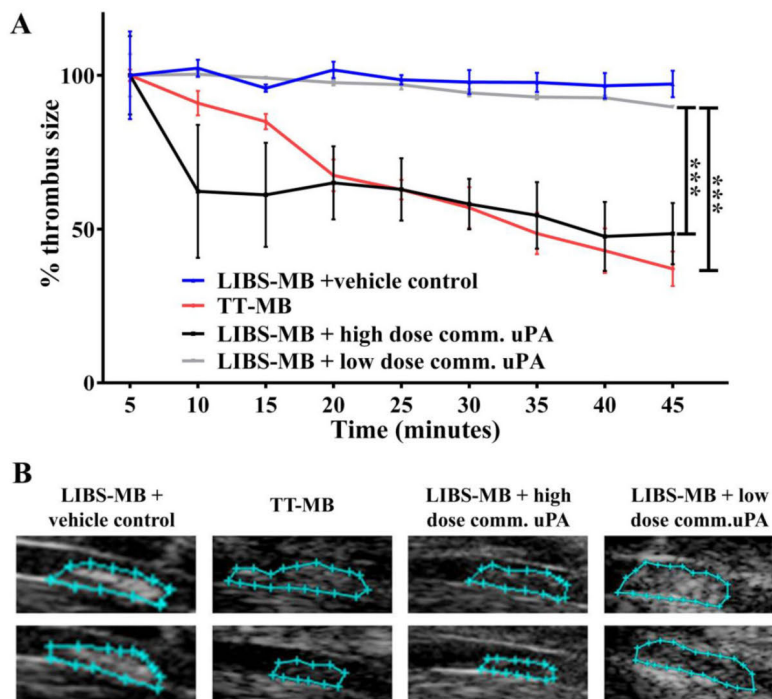


Figure 5: Monitoring of thrombolysis via molecular ultrasound imaging showed a theranostic effect and a reduction of thrombus size after the injection of TT-MB. A. A reduction of thrombus size was observed for animals administered with LIBS-MB and high dose of commercial uPA at 500U/g BVV (black line and B) as compared to LIBS-MB and saline (blue line and C) as vehicle control. A reduction of thrombus size was also observed with TT-MB (red line and D) as compared to LIBS-MB and low dose of commercial uPA at 75U/g BVV (light grey line and E). Baseline area was set to 100% and areas were calculated every 5 min for 45 min. Thrombus size was traced and calculated using VisualSonics software. Treatment groups were compared by use of repeated measures ANOVA over time with Bonferroni post tests at each time point (Mean % ± SEM; **p<0.01, ***p<0.001, n≥3 each).

Treatment with the TT-MBs significantly reduced thrombus size over the period 45 min, while no significant difference was observed in the LIBS-MB with saline vehicle control group (37.09 ± 5.6 vs. 97.16 ± 4.3 ; mean % \pm SEM; $p < 0.001$; $n > 3$) (Figure 5; Videos 1–4 in Additional file 2 - Additional file 5). Thrombolysis was observed via ultrasound imaging using LIBS-MB and a high dose of commercial uPA. The ability of TT-MBs to target and dissolve thrombi was compared to that of mice injected with LIBS-MB and a high dose of commercial uPA, but there were no significant differences over the period of 45 min (37.09 ± 5.6 vs. 48.53 ± 9.9 ; ns; $n \geq 3$).

The thrombolytic ability of TT-MBs was also compared with the LIBS-MB and a low dose of commercial uPA treatment group over 45 min. TT-MBs caused a reduction in thrombus size at 45 min post-administration compared to LIBS-MB and a low dose of commercial uPA (37.09 ± 5.6 vs. 89.72 ± 0.4 ; $p < 0.001$; $n \geq 3$). This LIBS-MB and low dose of commercial uPA treatment group was also compared against the LIBS-MB with saline vehicle control group. Administration of LIBS-MB and a low dose of commercial uPA showed no significant reduction in thrombus area compared to the saline group (89.72 ± 0.4 vs. 97.16 ± 4.3 ; ns; $n \geq 3$).

The comparison of the thrombus area measured at the start of the treatment and at the end of the treatment showed a significant decrease in thrombus size for animals injected with TT-MB ($p < 0.001$), as well as animals injected with LIBS-MB and treated with high dose of commercial uPA (positive control; $p < 0.001$; Additional File 1: Supplemental Figure 2).

No reduction in thrombus size was noted for animals injected with LIBS-MB and saline as negative controls or those treated with low dose of commercial uPA (NS)."

In addition to reduction in thrombus size, there was also a significant decrease in contrast intensity of the thrombus on molecular ultrasound imaging after treatment with TT-MB (Figure 6). The baselines of thrombus size and contrast intensity were set to 100% at the beginning of imaging. There was a significant reduction in the ultrasound contrast intensity for animals injected with TT-MB when compared to those injected with vehicle control (47.22 ± 4.2 vs. 82.25 ± 2.3 ; $p < 0.01$; $n \geq 3$). TT-MB treatment was as effective as a high dose of commercial uPA. The result in reduction of ultrasound contrast intensity is consistent with the data obtained in measuring reduction of thrombus size.

Histology of the carotid arteries from the four groups confirmed the sonographically observed differences in thrombus size (Figure 7).

Areas brighter than the reference image are presented in green after analysis with digital subtraction (ideos 1–4 in Additional file 2 - Additional file 5). Although thrombus identification and quantification using these B-mode images provide the necessary scientific and clinical information, digital subtraction and color highlighting were used for demonstration purposes and as an additional aid to facilitate immediate recognition of thrombi. Frames obtained before microbubble injection were subtracted from those obtained 45 min post-injection.

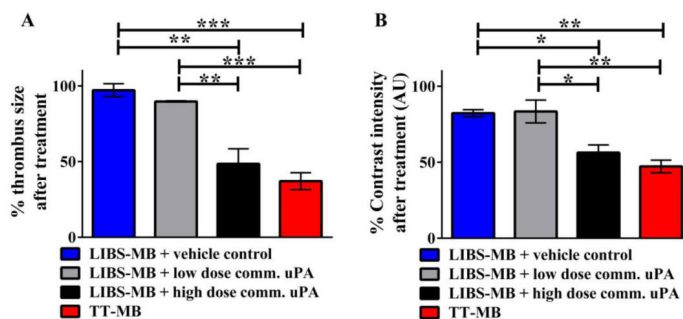


Figure 6: Quantitative measurement on molecular ultrasound imaging showing the reduction in both thrombus size and contrast intensity after treatment with TT-MB. A. Bar chart showing % of thrombus size at the end point of molecular ultrasound imaging. A reduction of thrombus size was observed for animals administered with LIBS-MB and high dose of commercial uPA at 500U/g BW (black) as compared to LIBS-MB and saline (blue) as vehicle control. The same significant reduction of thrombus size was also observed with TT-MB (red), but not with LIBS-MB and low dose of commercial uPA at 75U/g BW (light grey). B. Bar chart showing % contrast intensity at the end point of molecular ultrasound imaging. Results were similar to those of % thrombus size. Baseline area and contrast intensity was set to 100% and areas were measured at the start and end of imaging. Groups were compared by use of one-way ANOVA with Bonferroni post tests for multiple comparison (Mean \pm SEM, (* $p < 0.05$, ** $p < 0.01$, *** $p < 0.001$, $n \geq 3$ each).

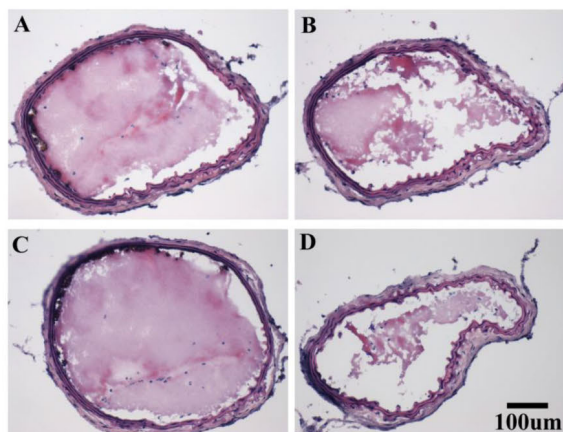


Figure 7: Representative images of hematoxylin and eosin stained thrombi in the carotid arteries of mice obtained after ultrasound imaging: A. after LIBS-MB and low dose commercial uPA, B. after TT-MB administration with a partially lysed thrombus, C. after LIBS-MB with saline as vehicle control and, D. after high dose commercial uPA with a partially lysed thrombus.

Effective targeted theranostic microbubbles do not cause bleeding time

Bleeding times were evaluated by surgical tail transection (Figure 8). LIBS-MB with a high dose of commercial uPA considerably prolonged bleeding compared to LIBS-MB with the saline vehicle control ($p < 0.001$; $n = 4$). In contrast, LIBS-MB with a low dose of commercial uPA and TT-MBs minimized bleeding time (ns ; $n = 4$). There was no difference between the bleeding times of animals given LIBS-MB with the vehicle control compared to TT-MBs (ns ; $n = 4$). Thus TT-MB has an anti-thrombotic effect without prolonging bleeding time.

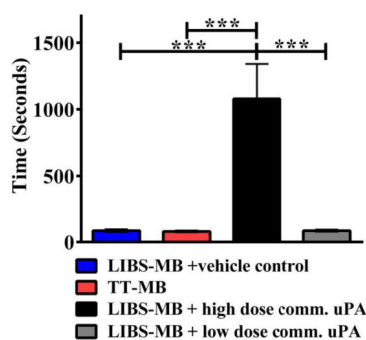


Figure 8: Bleeding time in mice determined by tail transection shows that there is no bleeding time prolongation at the effective dose of TT-MB. LIBS-MB with commercial uPA at 500U/g BW demonstrated considerably longer bleeding time as compared to LIBS-MB with saline vehicle control ($p < 0.001$, $n = 4$ each). TT-MB, LIBS-MB with low dose commercial uPA at 75U/g BW and saline control did not prolong bleeding time. These assays were analyzed with one-way repeated measures ANOVA with the Bonferroni post test.

Discussion

Theranostic approaches combining diagnostic and therapeutic capabilities in a single agent/imaging microbubble have attracted major attention, as they promise specific, individualized therapies with fewer side-effects for various diseases. The main benefit of theranostic approaches is the ability to provide simultaneous diagnosis and treatment, as well as the ability to reliably and conveniently monitor the treatment outcome. Particularly for thrombotic diseases, an ultrasound theranostic approach could be broadly used in various clinical settings and promises to provide major benefits for a large number of patients.

Aiming for such a translationally highly attractive approach, we conjugated recombinant scFvs, which are specific for the activated GPIIb/IIIa receptor on platelets, and scuPA, a clinically approved fibrinolytic drug, to microbubbles, which thereby became a thrombus-specific imaging tool and a drug-carrying vehicle in one. To the best of our knowledge, this is the first demonstration of a theranostic approach to thrombotic disease using molecular ultrasound imaging based on MBs, which are dually conjugated both with scFvs in order to visualize thrombosis, as well as with scuPA in order to lyse thrombi.

Our data demonstrates that these targeted theranostic microbubbles can selectively bind to thrombi, thereby allowing successful molecular ultrasound imaging of thrombosis. The binding of the TT-MBs at the site of the clot allows enrichment of the thrombolytic drug in order to break down the fibrin

network without systemic adverse effects such as prolongation of bleeding time. This data describes the unique concept of a non-invasive, inexpensive, and widely available technology simultaneously detecting thrombi, resolving vessel occlusion, and monitoring success or failure of thrombolysis.

We have used recombinant scFvs, a minimal form of a functional antibody, as targeting tools since scFvs exhibit several major advantages: 1) scFvs lack the Fc region, are small in size, and are therefore minimally immunogenic; 2) they can be easily modified using molecular biology techniques to add specific tags for detection and/or bioconjugation; 3) their cost of production is relatively low²¹. In addition, the use of phage display in the generation of single-chain antibodies allows the selection of function-specific antibodies²². Such a unique scFv, specific for the activated conformation of GPIIb/IIIa, was used for the targeting of our theranostic microbubbles¹⁴.

Ultrasound technology is an imaging modality that has evolved from a simple two-dimensional imaging tool used to assess crude anatomy to the current advanced three-dimensional, sensitive, high-resolution and sophisticated imaging platform. Employment of ultrasound contrast agents, such as microbubbles, provides the basis for molecular ultrasound imaging, which now exhibits a platform for functional characterization of diseased tissue without the necessity for surgical procedures or invasive biopsies^{23,24}. Following advances in scanner technology, particularly in relation to resolving of contrasts, the development of targeted molecular ultrasound contrast agents has been driven by several pioneering groups, also covering the diagnosis of atherosclerosis^{23,25-27}. In addition to its diagnostic use, ultrasound has been employed for therapeutic purposes. Given the rapidly improving technology of ultrasound scanners and the here-described development of contrast agents, theranostic ultrasound imaging offers an inexpensive, radiation-free, real-time, and portable alternative to MRI and nuclear imaging. With a growing ageing population and the consequent impact on healthcare costs, this new technology could be instrumental in allowing rapid and inexpensive diagnoses of MI and/or stroke, which would provide major benefits for a large number of patients.

There is no doubt that pharmacological thrombolysis can provide major benefits¹⁵. However, it comes with side-effects such as neurotoxicity and potentially fatal hemorrhagic complications¹⁶. In particular, the combination of anti-platelets and fibrinolytic agents shows a minimal improvement in mortality, safety, and efficacy, but results in increased

bleeding complications²⁸. Furthermore, many patients with MI or stroke are not given beneficial thrombolytic therapy because of their increased bleeding risk. Therefore, safety concerns have prompted research into more effective treatment in order to overcome the limitations associated with current pharmacological thrombolysis. As a consequence, there is a major need for novel reperfusion strategies; these include sonothrombolysis²⁹⁻³⁶ and targeted-drug delivery^{17,18,37-40}.

The clinical use of microbubbles for echocardiography has been approved by the FDA in the United States, and for both echocardiography and radiology indications in Europe and Canada⁴¹. Pioneering groups demonstrated that the mechanical response of microbubbles to ultrasound can promote extravasation, and, even without the use of thrombolytic agents, has proven to be an effective thrombolytic approach both *in vitro* and *in vivo*^{31,32,42}. Although these studies are mainly in the preclinical stage, they provide a strong basis for translation to clinical trials and offer a promising outlook for application in various cardiovascular diseases^{33,35}. Culp *et al.*³¹ demonstrated that infarct size decreases after treatment with sonothrombolysis using non-targeted MBs and Birnbaum *et al.*⁴³ observed recanalization of clots in the iliofemoral artery without significant side effects. Several clinical trials, such as the Combined Lysis of Thrombus in Brain Ischemia Using Transcranial Ultrasound and Systemic tPA (CLOTBUST)⁴⁴ and Transcranial Ultrasound in Clinical Sonothrombolysis (TUCSON)⁴⁵, examined the combination of non-targeted microbubbles, thrombolytic agents and ultrasound. These studies reported favorable results, such as improvement of recanalization rates and preservation of brain function. However, Molina *et al.*⁴⁵ in the TUCSON trial also reported an increased number of intracranial hemorrhages.

Other research groups further improved the combination of MB application and fibrinolytic drugs using elegant targeting strategies^{34,36,46,47}. Sonothrombolysis using targeted MBs allows the detection and localization of the thrombus. These studies looked into the feasibility of targeting the same integrin GPIIb/IIIa, using the arginine-glycine-aspartic acid (RGD) analog^{34,46,47}, and the non-activation-specific antibody fragment abciximab³⁶. However, the RGD analogs are ligand mimetics that bind to all circulating platelets (both resting and activated), but also bind to other cells on the basis of their cross-reactivity toward other RGD-ligand-recognizing integrins.

Xie *et al.*³⁴ observed that using diagnostic

ultrasound and MRX-802 (RDG-MBs) in combination with a half-dose of recombinant pro-urokinase, heparin, and aspirin for 30 min improved epicardial recanalization rates and microvascular recovery. In another excellent study, Alonso *et al.*³⁶ reported that the use of abciximab immunobubbles and continuous diagnostic ultrasound over 30 min induced thrombolysis in rats. Since abciximab is a clinically used drug for preventing/treating platelet aggregation and thrombus formation, such an approach seems easily translatable. However, like RGD, abciximab binds to all circulating platelets and has been shown to cross-react with other integrin receptors⁴⁸. An additional issue is that the binding of abciximab to non-activated GPIIb/IIIa receptors on circulating platelets results in an extended functional half life, and platelet inhibition over several days, thereby potentially increasing the risk of bleeding complications for a prolonged period⁴⁹.

Hua *et al.*⁴⁶ detailed in a recent publication that tPA-loaded RGD-MBs improved recanalization rates. These tPA-loaded RGD-MBs were given as a bolus followed by 30 min infusion, and ultrasound was performed on the site of interest over the time of infusion. The above studies infused the targeted or non-targeted microbubbles and thrombolytic agents, and sonoporated at various intensities or frequencies over time to obtain the desired thrombolysis or recanalization rate. However, safety concerns for patients in regard to the application of high-intensity, low-frequency ultrasound with microbubbles persist and have to be addressed in future studies.

Targeted drug delivery is another promising approach as a non-invasive pharmacological reperfusion strategy. In addition to platelet^{5,17,18} and fibrin targeting⁴⁰, other epitopes, such as platelet endothelial cell adhesion molecule 1 (PECAM-1)³⁹ and glycophorin A on erythrocytes³⁸ have been targeted. Although thrombolysis has been demonstrated for both PECAM-1 and erythrocyte-targeting, these targets are not exclusive for thrombi. We have previously shown that fusion of anti-platelet and/or thrombolytic drugs to activated-platelet-targeting antibodies can provide an effective and safe alternative, delivering a localized high concentration at the site of the thrombus, thereby providing therapy and at the same time allowing a low systemic concentration, and so preventing bleeding complications^{17,18}. In this study, we extend our previously successful therapeutic targeting to a successful targeted molecular theranostic approach with a single bolus injection for concurrent diagnosis and therapy of thrombotic diseases.

To avoid the safety concerns of sonoporation, we conjugated both the activated targeted scFvs and the

thrombolytic agents to the outside of the MBs. This dual conjugation allowed the TT-MBs to be directed and to bind to the blood clot, and for the scuPA on the surface to react with the thrombus, and for thrombolysis to occur. Although the use of sonoporation for sonothrombolysis might have the potential to enhance the degree of thrombolysis, our study has been designed to avoid the disadvantages associated with the bursting of microbubbles. Our approach allows us to have good visualization of the thrombi on real-time ultrasound imaging. In addition to making it possible to directly monitor the reduction in thrombus size, this approach also notably eliminates the potential hemorrhagic complication associated with sonothrombolysis as noted in several studies^{16,27}.

There are several clinical scenarios in which ultrasound imaging with targeted theranostic microbubbles could be useful. Of these, the most important is MI. A method with fast diagnosis of coronary thrombi, together with rapid and "safe" thrombolysis using the theranostic microbubbles, has enormous potential to change outcomes for patients with MI on a large scale. Furthermore, this theranostic technique could be used to determine the success or failure of the applied thrombolysis, allowing an early decision toward direct invasive coronary angiography with consequent angioplasty and stenting. With the general access to ultrasound machines, the described theranostic ultrasound microbubbles can potentially be administered quickly and easily in emergency departments, and even in ambulances and remote clinics. Further studies toward clinical implementation of such a strategy are highly warranted.

Limitations

In this proof of concept study, we have used biotin/streptavidin coupling to conjugate scFv and scuPA onto microbubbles. This conjugation method offers major advantages such as flexibility and rapid coupling. Although there have been concerns regarding the potential immunogenicity that may limit the use of this coupling approach in humans, biotinylated drugs and avidin-based reagents have been recently successfully introduced in the clinic^{50,51}. Nevertheless, as a potential alternative, our group has been developing novel enzymatic bioconjugation techniques for coupling, such as the use of the *S. aureus* transpeptidase sortase A, which can be adapted for use with our theranostic ultrasound molecular imaging approach^{14,19,20}.

Our study was conducted in a mouse model, which may not reflect thrombogenesis in humans in all aspects. Therefore further studies using bigger

animals and ultrasound scanners, as well as transducers typically used in patients, would facilitate further advancing this novel theranostic approach to clinical application. For this reason, we investigated additional cross-reactivity of our targeting single-chain antibody. We could show selective binding of the scFV_{anti-LIBS} to activated platelets of non-human primates (data not shown). Hence, the scFV_{anti-LIBS} not only shows cross-reactivity in humans and mice but also in non-human primates, which will facilitate translation of the newly described molecular ultrasound theranostic approach into clinical application in patients.

Conclusions

Our study demonstrates the successful generation of targeted theranostic microbubbles which bind specifically to activated platelets both *in vitro* and *in vivo*, thereby facilitating ultrasound molecular imaging of thrombi, as well as clot-localized enrichment of fibrinolytic activity. Thrombus size can be directly visualized in real time, offering unprecedented early diagnosis and monitoring of success or failure of thrombolytic therapy. Notably, single-chain antibody-mediated targeting allows enrichment at the thrombus site and at the same time a low systemic concentration of fibrinolytic activity, promising high thrombolytic efficacy without bleeding complications. This proof of concept study justifies further, particularly clinical, development and testing of this theranostic thrombolytic agent/ imaging microbubble for ultrasound diagnosis and targeted therapy of thrombotic disease in patients.

Supplementary Material

Additional File 1:

Supplemental Methods, Supplemental Results, Supplemental Figures 1-3.

<http://www.thno.org/v06p0726s1.pdf>

Additional File 2:

Video 1. <http://www.thno.org/v06p0726s2.avi>

Additional File 3:

Video 2. <http://www.thno.org/v06p0726s3.avi>

Additional File 4:

Video 3. <http://www.thno.org/v06p0726s4.avi>

Additional File 5:

Video 4. <http://www.thno.org/v06p0726s5.avi>

Acknowledgements

We would like to thank K. Alt and J. Yao for advice and technical support.

Sources of funding

This work was funded by the National Health

and Medical Research Council (NHMRC) project grant 1050018 (K.P.) and the National Heart Foundation (NHF) Grant-in-Aid G05M2134 (K.P.); an Australian Research Council Future Fellowship (K.P.), NHMRC Principal Research Fellowships (K.P.), NHF Career Development Fellowship (C.E.H) and a NHF Postdoctoral Fellowships (X.W. and Y.C.). Y.G was supported by a stipend from the Deutsche Herzstiftung. The study was supported in part by the Victorian Government's Operational Infrastructure Support Program.

Competing Interests

The authors have declared that no competing interest exists.

References

- Weber C, Noels H. Atherosclerosis: current pathogenesis and therapeutic options. *Nat Med.* 2011;17:1410-1422.
- Mackman N. Triggers, targets and treatments for thrombosis. *Nature.* 2008;451:914-918.
- Rader DJ, Daugherty A. Translating molecular discoveries into new therapies for atherosclerosis. *Nature.* 2008;451:904-913.
- Lindemann S, Krämer B, Seizer P, Gawaz M. Platelets, inflammation and atherosclerosis. *J Thromb Haemost TH.* 2007;5 Suppl 1:203-211.
- Lindner JR. Molecular imaging of thrombus: technology in evolution. *Circulation.* 2012;125:3057-3059.
- Schwarz M, Meade G, Stoll P, Ylänne J, Bassler N, Chen YC, Hagemeyer CE, Ahrens I, Moran N, Kenny D, Fitzgerald D, Bode C, Peter K. Conformation-specific blockade of the integrin GPIIb/IIIa: a novel antiplatelet strategy that selectively targets activated platelets. *Circ Res.* 2006;99:25-33.
- Armstrong PC, Peter K. GPIIb/IIIa inhibitors: from bench to bedside and back to bench again. *Thromb Haemost.* 2012;107:808-814.
- Stoll P, Bassler N, Hagemeyer CE, Eisenhardt SU, Chen YC, Schmidt R, Schwarz M, Ahrens I, Katagin Y, Pannen B, Bode C, Peter K. Targeting ligand-induced binding sites on GPIIb/IIIa via single-chain antibody allows effective anticoagulation without bleeding time prolongation. *Arterioscler Thromb Vasc Biol.* 2007;27:1206-1212.
- von Elverfeldt D, Maier A, Duerschmied D, Braig M, Witsch T, Wang X, Mauler M, Neudorfer I, Menza M, Idzko M, Zirk A, Heidt T, Bronsert P, Bode C, Peter K, von Zur Mühlen C. Dual-contrast molecular imaging allows noninvasive characterization of myocardial ischemia/reperfusion injury after coronary vessel occlusion in mice by magnetic resonance imaging. *Circulation.* 2014;130:676-687.
- von zur Mühlen C, von Elverfeldt D, Moeller JA, Choudhury RP, Paul D, Hagemeyer CE, Olschewski M, Becker A, Neudorfer I, Bassler N, Schwarz M, Bode C, Peter K. Magnetic resonance imaging contrast agent targeted toward activated platelets allows *in vivo* detection of thrombosis and monitoring of thrombolysis. *Circulation.* 2008;118:258-267.
- von zur Mühlen C, Peter K, Ali ZA, Schneider JE, McAteer MA, Neubauer S, Channon KM, Bode C, Choudhury RP. Visualization of activated platelets by targeted magnetic resonance imaging utilizing conformation-specific antibodies against glycoprotein IIb/IIIa. *J Vasc Res.* 2009;46:6-14.
- von Zur Mühlen C, Sibson NR, Peter K, Campbell SJ, Wilainam P, Grau GE, Bode C, Choudhury RP, Anthony DC. A contrast agent recognizing activated platelets reveals murine cerebral malaria pathology undetectable by conventional MRI. *J Clin Invest.* 2008;118:1198-1207.
- Alt K, Paterson BM, Ardipradja K, Schieber C, Buncic G, Lim B, Poniger SS, Jakob B, Wang X, O'Keefe GJ, Tochon-Danguy HJ, Scott AM, Ackermann U, Peter K, Donnelly PS, Hagemeyer CE. Single-chain antibody conjugated to a cage amine chelator and labeled with positron-emitting copper-64 for diagnostic imaging of activated platelets. *Mol Pharm.* 2014;11:285-293.
- Wang X, Hagemeyer CE, Hohmann JD, Leitner E, Armstrong PC, Jia F, Olschewski M, Needles A, Peter K, Ahrens I. Novel Single-Chain Antibody-Targeted Microbubbles for Molecular Ultrasound Imaging of Thrombosis: Validation of a Unique Noninvasive Method for Rapid and Sensitive Detection of Thrombi and Monitoring of Success or Failure of Thrombolysis in Mice. *Circulation.* 2012;125:3117-3126.
- Collen D, Lijnen HR. The tissue-type plasminogen activator story. *Arterioscler Thromb Vasc Biol.* 2009;29:1151-1155.
- Donnan GA, Davis SM, Parsons MW, Ma H, Dewey HM, Howells DW. How to make better use of thrombolytic therapy in acute ischemic stroke. *Nat Rev Neurol.* 2011;7:400-409.
- Hohmann JD, Wang X, Krajewski S, Selan C, Haller CA, Straub A, Chaikof EL, Nandurkar HH, Hagemeyer CE, Peter K. Delayed targeting of CD69 to activated platelet GPIIb/IIIa via a single-chain antibody: breaking the link between antithrombotic potency and bleeding? *Blood.* 2013;121:3067-3075.
- Wang X, Palasubramaniam J, Gkanatsas Y, Hohmann JD, Westein E, Kanojia R, Alt K, Huang D, Jia F, Ahrens I, Medcalf RL, Peter K, Hagemeyer CE. Towards effective and safe thrombolysis and thromboprophylaxis: preclinical testing of a novel antibody-targeted recombinant plasminogen activator directed against activated platelets. *Circ Res.* 2014;114:1083-1093.

19. Ta HT, Prabhu S, Leitner E, Jia F, von Elverfeldt D, Jackson KE, Heidt T, Nair AKN, Pearce H, von Zur Muhlen C, Wang X, Peter K, Hagemeyer CE. Enzymatic single-chain antibody tagging: a universal approach to targeted molecular imaging and cell homing in cardiovascular disease. *Circ Res*. 2011;109:365-373.
20. Hagemeyer CE, Alt K, Johnston APR, Such GK, Ta HT, Leung MKM, Prabhu S, Wang X, Caruso F, Peter K. Particle generation, functionalization and sortase A-mediated modification with targeting of single-chain antibodies for diagnostic and therapeutic use. *Nat Protoc*. 2014;10:90-105.
21. Hagemeyer CE, von Zur Muhlen C, von Elverfeldt D, Peter K. Single-chain antibodies as diagnostic tools and therapeutic agents. *Thromb Haemost*. 2009;101:1012-1019.
22. Eisenhardt SU, Schwarz M, Bassler N, Peter K. Subtractive single-chain antibody (scFv) phage-display: tailoring phage-display for high specificity against function-specific conformations of cell membrane molecules. *Nat Protoc*. 2007;2:3063-3073.
23. Leuschner F, Nahrendorf M. Molecular imaging of coronary atherosclerosis and myocardial infarction: Considerations for the bench and perspectives for the clinic. *Circ Res*. 2011;108:593-606.
24. Pysz MA, Foygel K, Rosenberg J, Gambhir SS, Schneider M, Willmann JK. Antiangiogenic Cancer Therapy: Monitoring with Molecular US and a Clinically Translatable Contrast Agent (ER55). *Radiology*. 2010;256:519-527.
25. Metzger K, Vogel S, Chatterjee M, Borst O, Seizer P, Schonberger T, Geisler T, Lang F, Langer H, Rheinlaender J, Schaffer TE, Gawaz M. High-frequency ultrasound-guided disruption of glycoprotein VI-targeted microbubbles targets atheroprogession in mice. *Biomaterials*. 2015;36:680-69.
26. Liu Y, Davidson EP, Yue Q, Belcik T, Xie A, Inaba Y, McCarty OJT, Tormoen GW, Zhao Y, Ruggen ZM, Kaufmann BA, Lindner JR. Molecular imaging of inflammation and platelet adhesion in advanced atherosclerosis: effects of antioxidant therapy with NADPH oxidase inhibition. *Circ Cardiovasc Imaging*. 2013;6:74-82.
27. McCarty OJT, Conley RB, Shentu W, Tormoen GW, Zha D, Xie A, Qi Y, Zhao Y, Carr C, Belcik T, Keene DR, de Groot FG, Lindner JR. Molecular imaging of activated von Willebrand factor to detect high-risk atherosclerotic phenotype. *JACC Cardiovasc Imaging*. 2010;3:947-955.
28. Reperfusion therapy for acute myocardial infarction with fibrinolytic therapy or combination reduced fibrinolytic therapy and platelet glycoprotein IIb/IIIa inhibition: the GUSTO V randomised trial. *The Lancet*. 2001;357:1905-1914.
29. de Saint Victor M, Crake C, Coussios C-C, Stride E. Properties, characteristics and applications of microbubbles for sonothrombolysis. *Expert Opin Drug Deliv*. 2014;11:187-209.
30. Tachibana K, Tachibana S. Albumin microbubble echo-contrast material as an enhancer for ultrasound accelerated thrombolysis. *Circulation*. 1995;92:1148-1150.
31. Culp WC, Flores R, Brown AT, Lowery JD, Roberson PK, Hennings LJ, Woods SD, Hatton JH, Culp BC, Skinner ED, Borrelli MI. Successful microbubble sonothrombolysis without tissue-type plasminogen activator in a rabbit model of acute ischemic stroke. *Stroke J Cereb Circ*. 2011;42:2280-2285.
32. Porter TR, LeVeen FF, Fox R, Kricfield A, Xie F. Thrombolytic enhancement with perfluorocarbon-exposed sonicated dextrose albumin microbubbles. *Am Heart J*. 1996;132:964-968.
33. Xie F, Slikkerveer J, Gao S, Lof J, Kamp O, Unger E, Radio S, Matsunaga T, Porter TR. Coronary and microvascular thrombolysis with guided diagnostic ultrasound and microbubbles in acute ST segment elevation myocardial infarction. *J Am Soc Echocardiogr*. 2011;24:1400-1406.
34. Xie F, Lof J, Matsunaga T, Zutshi R, Porter TR. Diagnostic ultrasound combined with glycoprotein IIb/IIIa-targeted microbubbles improves microvascular recovery after acute coronary thrombotic occlusions. *Circulation*. 2009;119:1378-1385.
35. Kutty S, Xie F, Gao S, Dvool LK, Lof J, Fletcher SE, Radio SJ, Danford DA, Hammel JM, Porter TR. Sonothrombolysis of intra-catheter aged venous thrombi using microbubble enhancement and guided three-dimensional ultrasound pulses. *J Am Soc Echocardiogr*. 2010;23:1001-1006.
36. Alonso A, Dempfle C-E, Martina A Della, Stroick M, Fatar M, Zohsel K, Allemann E, Hennrich MG, Meairs S. In vivo clot lysis of human thrombus with intravenous absciximab immunobubbles and ultrasound. *Thromb Res*. 2009;124:70-74.
37. Greineder CF, Howard MD, Carmemolla F, Cines DB, Muzykantor VR. Advanced drug delivery systems for antithrombotic agents. *Blood*. 2013;122:1565-1575.
38. Zaitsev S, Spitzer D, Murciano J-C, Ding B-S, Tibba S, Kowalska MA, Marcos-Contreras OA, Kuo A, Stepanova V, Atkinson JP, Poncz M, Cines DB, Muzykantor VR. Sustained thromboprophylaxis mediated by an RBC-targeted pro-urokinase zymogen activated at the site of clot formation. *Blood*. 2010;115:5241-5248.
39. Ding B-S, Hong N, Murciano J-C, Ganguly K, Gottstein C, Christofidou-Solomidou M, Albelda SM, Fisher AB, Cines DB, Muzykantor VR. Prophylactic thrombolysis by thrombin-activated latent pro-urokinase targeted to PECAM-1 in the pulmonary vasculature. *Blood*. 2008;111:1999-2006.
40. Peter K, Graeber J, Kipriyanov S, Zewe-Welsch M, Runge MS, Kubler W, Little M, Bode C. Construction and functional evaluation of a single-chain antibody fusion protein with fibrin targeting and thrombin inhibition after activation by factor Xa. *Circulation*. 2000;101:1158-1164.
41. Unger E, Porter T, Lindner J, Grayburn P. Cardiovascular drug delivery with ultrasound and microbubbles. *Adv Drug Deliv Rev*. 2014;72:110-126.
42. Nishioka T, Luo H, Fishbein MC, Cercek B, Forrester JS, Kim CJ, Berglund H, Siegel RJ. Dissolution of thrombotic arterial occlusion by high intensity, low frequency ultrasound and dodecafluoropentane emulsion: an in vitro and in vivo study. *J Am Coll Cardiol*. 1997;30:561-568.
43. Birnbaum Y, Luo H, Nagai T, Fishbein MC, Peterson TM, Li S, Knickfeld D, Porter TR, Siegel RJ. Noninvasive in vivo clot dissolution without a thrombolytic drug: recanalization of thrombosed iliofemoral arteries by transcatheter ultrasound combined with intravenous infusion of microbubbles. *Circulation*. 1996;97:130-134.
44. Alexandrov AV, Molina CA, Grotta JC, Garami Z, Ford SR, Alvarez-Sabin J, Montaner J, Saqqur M, Demchuk AM, Morys LA, Hill MD, Wojner AW. CLOTBUST Investigators. Ultrasound-enhanced systemic thrombolysis for acute ischemic stroke. *N Engl J Med*. 2004;351:2170-2178.
45. Molina CA, Barreto AD, Tsvigoulis G, Sierzenski P, Malkoff MD, Rubiera M, Gonzalez N, Mikulik R, Pate G, Ostrem J, Singleton W, Manvelian G, Unger EC, Grotta JC, Schellinger PD, Alexandrov AV. Transcranial ultrasound in clinical sonothrombolysis (TUCSON) trial. *Ann Neurol*. 2009;66:28-38.
46. Hua X, Zhou L, Liu P, He Y, Tan K, Chen Q, Gao Y, Gao Y. In vivo thrombolysis with targeted microbubbles loading tissue plasminogen activator in a rabbit femoral artery thrombus model. *J Thromb Thrombolysis*. 2014;38:57-64.
47. Hagiwara K, Nishioka T, Suzuki R, Maruyama K, Takase B, Ishihara M, Kurita A, Yoshimoto N, Nishida Y, Iida K, Luo H, Siegel RJ. Thrombus-targeted perfluorocarbon-containing liposomal bubbles for enhancement of ultrasonic thrombolysis: in vitro and in vivo study. *J Thromb Haemost*. 2013;11:1565-1573.
48. Schwarz M, Nordt T, Bode C, Peter K. The GP IIb/IIIa inhibitor abciximab (c7E3) inhibits the binding of various ligands to the leukocyte integrin Mac-1 (CD11b/CD18, alphaMbeta2). *Thromb Res*. 2002;107:121-128.
49. Peter K, Kohler E, Straub A, Ruef J, Moser M, Nordt T, Olschewski M, Ohman ME, Kubler W, Bode C. Flow cytometric monitoring of glycoprotein IIb/IIIa blockade and platelet function in patients with acute myocardial infarction receiving reteplase, abciximab, and ticlopidine: continuous platelet inhibition by the combination of abciximab and ticlopidine. *Circulation*. 2000;102:1490-1496.
50. Petronzelli F, Pelliccia A, Anastasi AM, Lindstedt E, Manganello S, Ferrari LE, Albertoni C, Leoni B, Rosi A, D'Alessio V, Deiana K, Paganelli G, De Santis R. Therapeutic use of avidin is not hampered by antiavidin antibodies in humans. *Cancer Biother Radiopharm*. 2010;25:563-570.
51. Equinox Investigators. Efficacy and safety of once weekly subcutaneous idrabiotaparinux in the treatment of patients with symptomatic deep venous thrombosis. *J Thromb Haemost JTH*. 2011;9:92-99.

Authors' Biography

Prof Karlheinz Peter MD, PhD, works as senior interventional cardiologist at the Alfred Hospital and as Associate Director and Head of the Atherothrombosis and Vascular Biology Program at Baker IDI Heart and Diabetes Institute, Melbourne, Australia. He is Professor of Medicine and Immunology at Monash University and is a NHMRC principal research fellow. He obtained his research and clinical training in at the Universities of Freiburg and Heidelberg in Germany and at Johns Hopkins Medical School and Scripps Research Institute in the US. His research is focused on the cellular mechanisms, prevention and novel therapeutic approaches in myocardial infarction, encompassing the role of platelets, coagulation and inflammation in atherosclerosis, as well as the mechanisms leading to the rupture of atherosclerotic plaques. Using recombinant antibody technologies he has developed novel biomarker and molecular imaging strategies using magnetic resonance imaging (MRI), positron emission tomography (PET)/CT, ultrasound and fluorescence imaging as well as novel antithrombotic and fibrinolytic approaches that are not associated with increased bleeding risks. Prof Peter has received numerous awards throughout his career, including the Ludwig Heilmeyer Prize of the University of Freiburg, the Oskar Lapp Prize of the German Cardiac Society, the Ross Hohnen award of the Australian Heart Foundation, and the RT Hall Prize of the Cardiac Society of Australia and New Zealand.

Dr Xiaowei Wang is a postdoctoral fellow at the Baker IDI Heart and Diabetes Institute, Melbourne, Australia. She was trained as a sonographer for echocardiography prior to her research career therefore Dr Wang's research has a strong focus on translational cardiovascular research in diagnostics, therapeutics and theranostics. Dr Wang was awarded

a Postdoctoral Fellowship and the Paul Korner Innovation Award by the National Heart Foundation. She has received numerous young investigator awards and travel grants for international conferences. Dr Wang is also one of the founding board members of the Australia Society of Molecular Imaging.